THE HUNAN OPERATOR AS AN OPTIMAL FILTER AND OPTIMAL CONTROLLER

Thesis for the Degree of Ph. D.
MICHIGAN STATE UNIVERSITY
RODNEY DAN WIERENGA
1968



This is to certify that the

thesis entitled

THE HUMAN OPERATOR AS AN OPTIMAL FILTER AND OPTIMAL CONTROLLER

presented by

Rodney Dan Wierenga

has been accepted towards fulfillment of the requirements for

Ph. D. degree in Elect. Engr.

Date __April 19, 1968__

ABSTRACT

THE HUMAN OPERATOR AS AN OPTIMAL FILTER AND OPTIMAL CONTROLLER

by Rodney Dan Wierenga

In this thesis, a mathematical model of the human operator in a control task is postulated and its validity is investigated. In the model that is suggested, an "augmented plant" is used which contains not only the plant that the human operator is controlling, but also the forcing functions and the operator's own time delay, neuromuscular lag, and noise characteristics.

An optimal time-varying linear filter and an optimal time-varying linear controller are utilized in the model. Consequently, because of the form of the augmented plant, the model develops estimates of the state variables of the plant, the forcing functions, and the man's own characteristics. As postulated, the augmented plant can be time varying.

The validity of the model is investigated in terms of a transfer function match with data available in the literature.

Also, in that the model is capable of prediction, this attribute is investigated by means of tracking experiments using a sine-wave forcing function.

A method for ordering the comparative values of displays in a control task is suggested. This method is investigated by means of experiments with human operators in a compensatory control task using two vastly different displays. The experimental results are matched with the model where the parameters needed for this match provide the method of ordering.

In general, the results are very good, and although a great amount of evaluation of other potential advantages of the model is still to be done, limited application of the model, as it stands, is justified.

THE HUMAN OPERATOR AS AN OPTIMAL FILTER AND OPTIMAL CONTROLLER

Ву

Rodney Dan Wierenga

A THESIS

Submitted to
Michigan State University
in partial fulfillment of the requirements
for the degree of

DOCTOR OF PHILOSOPHY

Department of Electrical Engineering

651553

ACKNOWLEDGEMENTS

The author wishes to thank his advisor, Dr. H. E. Koenig of the Michigan State University Electrical Engineering Department and Systems Science Group for his guidance and many helpful suggestions during the preparation of this thesis. The substantial assistance given by Dr. T. E. Perfitt, Dr. P. R. Fuller, Mr. G. E. Teachman, and Mr. U. Plate of the Lear Siegler, Inc. Instrument Division is also greatly appreciated.

In addition, the author expresses thanks to the Instrument Division for their financial support, for their sponsorship of the work done on this thesis, and for the use of their facilities, in particular, the analog and digital computers.

Sincere thanks are given to Miss Anna D'Angelo, Mrs. Emily Lotter, Mrs. Maryann Smith, and Mrs. Linda Richmond for the typing of the manuscript and its numerous revisions.

Finally, the author wishes to express his appreciation to his wife, Betty. Without her interest and encouragement this thesis would not have been possible.

TABLE OF CONTENTS

			Page
LIST	OF TA	BLES	ν
LIST	OF FI	GURES	νi
LIST	OF AP	PPENDICES	хi
1.	INTR	CODUCTION	1
	1.1	Statement of the Problem	1
	1.2	Manual Control System	2
	1.3	Characteristics of the Human Operator	6
	1.4	Brief Survey of Present Models	9
	1.5	Objectives of the Study	12
2.	THE	MODEL	14
	2.1	Basic Approach	14
	2.2	Structure of the Model	15
	2.3	Solution of the Model	20
	2.4	Basic Features	24
3.	VALI	DATION FOR TIME STATIONARY CONDITIONS	28
	3.1	Experimental Results of Other Investigators	28
	3.2	Model Solution	32
	3.3	Model Validation	42
	3.4	Sensitivity Studies	55

TABLE OF CONTENTS (cont)

			Page
4.	SINE	-WAVE TRACKING	74
	4.1	Experiments	75
	4.2	Tracking Model	80
	4.3	Model Validation	88
5.	DISP	LAY EFFECT	109
	5.1	Description of Experiments	109
	5.2	Parameter Evaluation	121
6.	CONC	LUSIONS AND RECOMMENDATIONS	135
LIST	OF RE	FERENCES	177

LIST OF TABLES

Table		Page
3.1	Forcing Function Magnitudes	31
3.2	Parameters for Model Validation	50
5.1	Display Study Forcing Function	115
5.2	Model Parameters for CRT Match	130
5.3	Model Parameters for DVM Match	133

LIST OF FIGURES

Figure		Page
1.1	Manual control system schematic diagram	3
1.2	Compensatory task block diagram	5
1.3	Pursuit task block diagram	6
1.4	Quasi-linear model block diagram	10
2.1	Manual control system basic block diagram	16
2.2	Basic block diagram with an augmented plant	17
2.3	Solution block diagram	22
2.4	Simplified block diagram with an augmented plant	24
3.1	Augmented plant for time stationary conditions	35
3.2	Forcing functions	38
3.3	Match for the constant gain plant	43
3.4	Match for the constant gain plant with a highly trained pilot	44
3.5	Match for the integrator plant	45
3.6	Match for the unstable plant	46
3.7	Model results as P converges	49
3.8	A comparison of the remnant with model noise	51
3.9	Unstable plant match human operator only	54
3.10	Effect of various T _N	56
3.11	Effect of the time delay	57
3.12	Effect of a precision neuromuscular lag	59
3.13	Effect of a second-order time delay	60

Figure		Page
3.14	Effect of the measurement noise	62
3.15	Effect of the cost associated with u	63
3.16	Effect of the forcing function variance	64
3.17	Effect of the drift	66
3.18	Effect of the forcing function corner frequency	67
3.19	Effect of the order of the forcing function bandlimit	69
3.20	Effect of the off diagonal elements of Q	70
4.1	Sine-wave tracking block diagram	74
4.2	CRT display used for sine-wave tracking	76
4.3	Controller used for sine-wave tracking	77
4.4	Complete sine-wave tracking run	78
4.5	Partial sine-wave tracking run	79
4.6	Sine-wave tracking with the eyes closed after 6 seconds	81
4.7	Augmented plant for sine-wave tracking	82
4.8	Block diagram for sine-wave tracking	82
4.9	Mean sine-wave tracking model response	89
4.10	Mean x and \hat{x}	90
4.11	Solution for P	91
4.12	Complete sine-wave tracking model run	92
4.13	Partial sine-wave tracking model run	93

Figure		Page
4.14	Solution for \hat{x} with noise	94
4.15	Model tracking with eyes closed after 6 seconds	95
4.16	Solution for P with the eyes closed after 6 seconds	96
4.17	Digital computer printout of P with the eyes closed after 6 seconds	100
4.18	Frequency response with P(10)	102
4.19	Frequency response with P(1)	104
4.20	Frequency response with P(35)	105
4.21	Sine-wave tracking model block diagram	106
4.22	Power spectral density match	108
5.1	Display study experimental equipment	110
5.2	Display study block diagram	109
5.3	CRT for the display study	111
5.4	DVM for the display study	111
5.5	Controller for the display study	113
5.6	Cross-spectral analyzer accuracy	117
5.7	Typical CRT run	119
5.8	Typical DVM run	120
5.9	CRT match operator 1	122
5.10	CRT match operator 2	123
5.11	CRT match operator 3	124

Figure		Page
5.12	CRT match operators 1, 2, and 3	125
5.13	DVM match operator 1	126
5.14	DVM match operator 2	127
5.15	DVM match operator 3	128
5.16	DVM match operators 1, 2, and 3	129
5.17	Effect of 2nd and 3rd order Padé approximations of the time delay	132
B.1	Basic flow chart for time stationary model solution	142
B.2	Example problem augmented plant	141
B.3	Expanded example problem block diagram	143
B.4	Input data	144
B.5	Solution for K	147
B.6	Solution for P	149
B.7	Filter and controller model	152
B.8	Constituent idempotents	153
B.9	Filter and controller transfer function	154
B.10	Man-plant transfer function	155
B.11	Man-plant frequency response data	156
B.12	Example problem Bode plot	165
D.1	The basic operations to find the cross-spectral density at ω_n	169

Figure		Page
D.2	Frequency shift and filter combined	170
D.3	Simplified block diagram for $\phi_{xv}(\omega_n)$	175

LIST OF APPENDICES

Appendix		Page
Α	Man-plant Transfer Function in Terms of $e^{\hat{A}t}$	138
В	Solution for the Time Stationary Model	141
С	Effects of $\frac{M}{n}$ and $\frac{Q}{r}$ on the Model	166
D	Cross-spectral Analyzer	168

1. INTRODUCTION

1.1 STATEMENT OF THE PROBLEM

In the design of manually controlled systems, it is highly desirable to have a mathematical description of what the human operator does in performing his tasks. This description must reflect the effects of the plant on the man. It must be accurate and practical to generate without having to perform elaborate experiments each time the plant configuration or parameters are modified.

In general, an adequate model should characterize a "representative" operator, yet with appropriate modification in parameters, it should be possible to characterize a broad range of operators. It should serve as a "building block" in the analysis of a complete system, or any part of one.

For a model of the human operator to be of practical value in design, it must be capable of handling multi-axis problems, account for noise, include prediction, and, in many cases, be timevarying and nonlinear. It must handle the effects of side task loading and task difficulty, and reflect the effects of different types of displays and manipulators.

Models presently available are useful only under restricted conditions. They are for particular very simple plants, such as $Y_c = \frac{1}{s^2}$, and they are linear, time stationary, not capable of

prediction, and do not include the effects of stress and the inputoutput devices. The multi-axis case is handled only by extrapolation from the single axis case. Given a model for the operator when controlling one plant, it is difficult to determine the manmodel when controlling another slightly different plant.

Large-scale simulators and human operators are used at present to design and evaluate vehicles, control systems, and instruments. The simulation system includes a cockpit mock-up with instruments along with a computer simulation of the vehicle and control system. Such a system is necessary whether it is required to evaluate a whole vehicle or any part of it -- such as an instrument. From a statistical evaluation point of view, many operators and a large number of runs are needed along with a great amount of data reduction to evaluate a given design.

1.2 MANUAL CONTROL SYSTEM

1.2.1 The general System

In its broadest sense, a manual control system is one in which a human operator attempts to control a plant by varying selected control variables of the plant given information about the system state or outputs from various sensor inputs. This function is shown schematically in Figure 1.1. The control variable inputs to the plant are provided by manipulators, as for example, a steering wheel, foot pedals or a control stick, and the sensory inputs are provided by displays which give information about the condition of the plant and/or about the input forcing functions. The displays are usually visual, as for example, the visual field of an automobile drive or the altimeter in an airplane, but they might also

be of an auditory or tactile nature [1]. In addition to displayed information, the operator can also in many cases sense the condition or state of the plant by means of his vestibular receptors, and the condition of a manipulator and the limb controlling it by means of joint, skin, spindle, and tendon receptors [2,3].

The plant may have external random forcing functions in the form of disturbances such as a gust on an airplane. The operator may also generate his own forcing function, as for example, the path a pilot desires to follow while approaching the runway when landing an airplane.

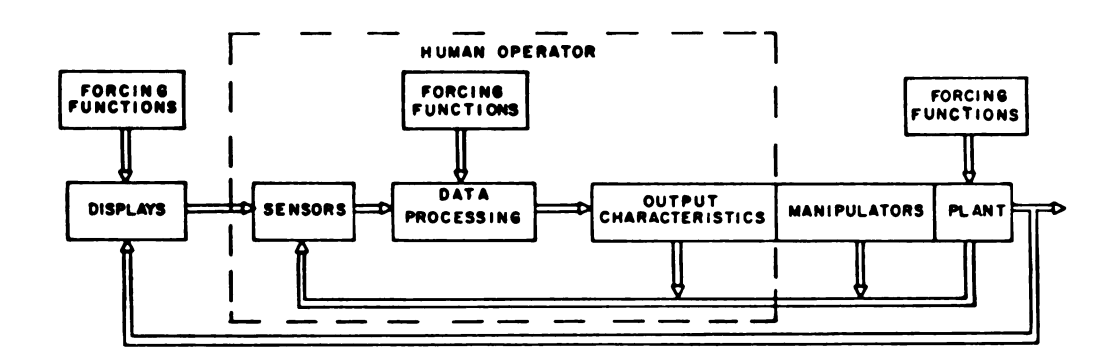


Figure 1.1. Manual control system schematic diagram.

The output characteristics (such as the arm or leg dynamics), the manipulator, and the plant may all be integrally related so that input-output equations for each cannot be expressed separately as a no load transfer characteristic. For example, the control stick of an airplane represents a load on the arm of the pilot. This load, in the form of a reaction force, is sometimes referred to as "feel." It reflects, for some aircraft, the

aerodynamics of the control surface. The "load" is sensed by the operator and may actually aid him in controlling the plant. A simple spring-mass-damper system cannot, in general, be used to represent this reaction force since it is determined by the dynamics of the whole system.

A given set of variables may be sensed by the operator in two or more different ways. For example, the angular acceleration of an airplane may be visually displayed to the pilot by instruments but he may also sense it directly by means of his semi-circular canals. (Note, however, that pilots are trained to selectively ignore information sensed by their vestibular receptors and thus this feedback path is not significant.)

The remaining parts of the human operator as outlined in Figure 1.1 are lumped into the data processing block. This block includes such things as the transformation of the sensed information into a usable form so that it can be used in the control task (e.g., perception). It provides the feedback paths involved in the arm dynamics, and it includes the compensation that the man provides in an attempt to cause the man-machine system to perform as desired (e.g., so that it is stable with minimum error).

1.2.2 Two Important Classes of Manual Control Systems

Most of the research work in manual control has been restricted to systems that have a single manipulator and a single visual display showing the error between some input forcing function and an output of the plant. This is known as a "compensatory task." As shown in Figure 1.2, the difference between the forcing

function i(t) and the plant output m(t) is displayed to the operator. His task is to keep the error e(t) as small as possible using the manipulator with output c(t). The manipulator is usually constructed so that it reflects no "feel" of the plant and often so that the dynamics of the arm and manipulator are minimized.

The compensatory task system is not as synthetic as it might at first appear. Many tasks in flying an airplane, for example, are basically of this type. Such tasks as landing with glide slope

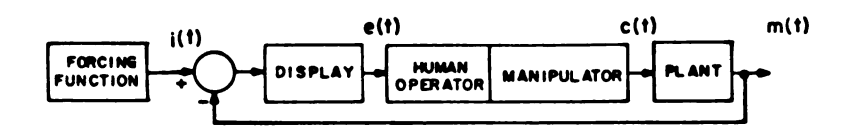


Figure 1.2. Compensatory task block diagram.

and localizer needles, or flying at a constant altitude or pitch attitude can be considered compensatory tasks in which the object is to maintain zero error.

Some work has been done on the multi-axis compensatory task involving, for example, two displays and two input controls to the plant. There may or may not be cross-coupling in the plant between the two inputs and the two displays. In general, the models that have been developed are extrapolations of the models found adequate for the single axis task.

A second class of manual control problems that have been considered is the "pursuit task." As shown in Figure 1.3, both the

forcing function and the plant output are displayed separately (usually with the same type of display or on the same display, e.g., a dual beam CRT) where the task is to keep the difference between the displayed variables as small as possible by controlling a single plant input c(t). More information is available to the operator in the pursuit task since he can see the characteristics of the forcing function and the plant output in addition to the error.

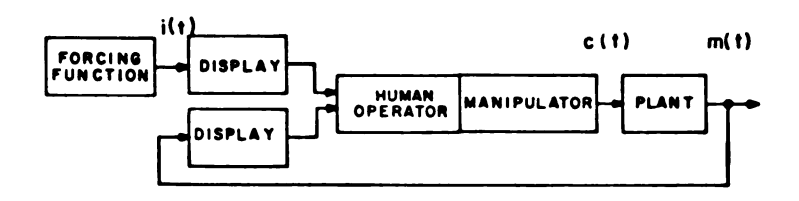


Figure 1.3. Pursuit task block diagram.

1.3 CHARACTERISTICS OF THE HUMAN OPERATOR

The human operator characteristics can be grouped under the overlapping headings, "General Characteristics," "Remnant Characteristics," and "Physiological Characteristics."

1.3.1 General Characteristics

The general characteristics include three important features as follows:

1) Adaptability - When confronted with a new set of circumstances, or a change of environment, the human operator will adapt or change his performance so that he accomplishes his task "better" with time.

- 2) <u>Learning</u> All external factors remaining the same, the human operator will improve his performance with experience.
- operator does the "best" he can in a control task as measured by some cost function. The particular cost function he uses and the way he accesses it is not known. Many investigators have hypothesized that in compensatory tracking tasks the RMS error is minimized [4,5,6].

1.3.2 Remnant Characteristics

Only part of the output power spectrum of the human operator can be linearly correlated with his input. The part that is left over is referred to as the "Remnant." This remnant is usually subdivided into nonstationarity, nonlinearity, and noise.

- 1) Nonstationarity During the execution of a task, the performance of the human operator changes with time.

 This is not only the case from run-to-run but during each run itself. Some of the factors that apparently contribute to it are attention, motivation, adaption, and learning. McRuer et al. [5] state that nonstationarity is a major source of the remnant.
- Nonlinearity Such characteristics as sensory thresholds, controller displacement limits, force limits, intermittency, and indifference thresholds are known contributions to nonlinearities in the input-output

characteristics of a human operator. McRuer et al. [5] indicate, however, that nonlinearity is not a major source of the remnant.

operator is not known and its importance is considered to be small [7]. However, as stated by Pew et al. [8], "Analysis of the error power spectra establishes the presence of a stable source of noise power in the operator's output that has implications for deriving models of manual tracking performance."

1.3.3 Physiological Characteristics

There are certain physiological characteristics of the human operator that have been investigated and, at least by deduction, have been characterized in terms of control theory.

- 1) Time Delay The response of a human operator exhibits a pure time delay that is generally attributed "to sensor excitation, nerve conduction, computational lags, and other processing activities in the central nervous system" [5]. Time delays of from 0.1 to 0.2 seconds are used [5].
- 2) Neuromuscular Lag The dynamics of the limb of an operator in response to "commands from the brain" is frequently described by a transfer function with a lagging characteristic. Descriptions and justifications for such a model are given in [2,3,5, and 10].

 A first-order lag with a time constant of from 0.1 to

0.6 seconds [5] is the simplest and most used form, but up to fourth-order models have been defined.

1.4 BRIEF SURVEY OF PRESENT MODELS

There have been many approaches and methods used in an attempt to model the human operator in a control task. The techniques used almost invariably reflect the most recently available tools. As stated by Muckler [11], "those who work in manual control theory have been very quickly responsive to changes in general control theory." However, Muckler adds a note of caution, "Bandwagons can be a useful mode of travel -- provided the band is going down the right street." He also points out that there are literally thousands of articles that have been published which list and describe the more significant work that has been done [10 through 14]. In addition, bibliographies of the more significant contributions have been compiled as given by [15,16].

Some models attempt to simulate on a computer the various "black boxes" in a conceived structure of the human operator. In some of these attempts [17,18] such things as sensory thresholds, rate limits, and dither are included.

There are some who say, because the human operator has an intermittent output, he acts like a sampled data system and should be modeled as such. Although it is generally agreed that the human operator does not act like a <u>periodic</u> sampler, useful results have been obtained with this concept. Note in particular the work of Bekey [14,19]. A lack of adequate control theory to handle the aperiodic problem is in part responsible for the limited work based on the sampling concept.

Others have said that the human operator can be modeled as an adaptive mechanism. To quote Shinners [13], "Most of the work done in this area recognizes the problems involved and provides, instead of exact solutions, guidelines, hypotheses, and constraints to be considered in the formulating of a representative model." The work described by Young and Stark [10] is an example.

By far the most tested and applied model is the quasi-linear describing function model as developed by McRuer et al. [4,5]. This model as shown in Figure 1.4 consists of a "describing function" and a "remnant." The describing function gives the output of man that is linearly correlated with the input. The remnant gives the

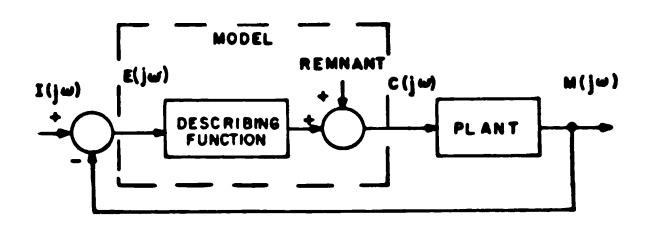


Figure 1.4. Quasi-linear model block diagram.

power at those frequencies of the total output power spectrum that are not given by the describing function. The describing function and remnant depend on the plant that is being controlled and upon the input forcing function. McRuer et al. [4,5] base this model on experiments using several basic types of plants $\left(K_c, K_c/s, K_c/(s-\lambda), K_c/s^2, \text{ and } K_c/[s(s-\lambda)]\right)$ and have devised basic model forms and a set of rules to be used for determining the operator's

describing function. The most complete form of this model, referred to as the "precision" model in [5], is

$$Y_{p} = K_{p}e^{-j\omega\tau} d\underbrace{\begin{pmatrix} T_{L}^{j\omega+1} \\ T_{I}^{j\omega+1} \end{pmatrix} \begin{pmatrix} T_{K}^{j\omega+1} \\ T_{K}^{j\omega+1} \end{pmatrix} \begin{pmatrix} T_{N}^{j\omega+1} \\ T_{N}^{j\omega+1} \end{pmatrix} \begin{pmatrix} 1 \\ T_{N}^{j\omega+1} \end{pmatrix} \begin{pmatrix} \frac{1}{(T_{N}^{j\omega+1})^{2} + \frac{2\zeta_{N}^{j\omega}}{\omega_{N}} + 1} \end{pmatrix}}_{\text{Neuromuscular Characteristic}}$$

The neuromuscular characteristic has been deduced using physiological considerations and feedback control theory [2,3]. The time delay is attributed to sensor excitation time (e.g., the retina of the eye), and nerve conduction time. The gain and equalization are the characteristics which are added by the human operator to provide the complete closed loop man-machine system with good stability and response.

There are simplified versions of the "precision" model in [5] which are referred to as the "crossover" model, the "first approximation," and the "second approximation."

The crossover model is the simplest and as the name implies, on an open loop Bode diagram, the model fits the data best at the frequency where the gain crosses the zero db line. This model includes the plant that is controlled and is expressed by

$$Y_{p}Y_{c} = \frac{\omega_{c} e^{-j\omega\tau} e}{j\omega}$$
 (1.2)

where

 $Y_{\mathbf{p}}$ is the pilot transfer function

 Y_c is the plant transfer function

 $\boldsymbol{\omega}_{\boldsymbol{c}}$ is the crossover frequency

 $\boldsymbol{\tau}_{\textbf{p}}$ is the effective time delay

The choice of the parameters to be used in each of McRuer's models is an art, where this choice is made using a knowledge of the plant, the input function, and a set of rules. These rules are based on feedback control theory and the results of the experiments using the five plants as defined above.

The first application of modern optimal control theory to the manual control problem was done by Thomas [20]. Obermeyer and Muckler in [21] give a general discussion on manual control in the context of modern control theory. Topics such as the Maximum Principle, Dynamic Programming, and adaptive control systems as given by Kalman et al. [28] are briefly described and related to the manual control problem. More recently, Obermeyer and Muckler [9] have turned the problem around, concerning themselves with the "inverse optimal control problem." That is, assuming that the operator performs in an optimal way, what performance index does he optimize? They restrict themselves to a quadratic cost function and as reported in [9], the results so far have been inconclusive.

1.5 OBJECTIVES OF THE STUDY

The primary objectives of this research are to postulate and demonstrate the validity of a mathematical model of the human

operator in a control task. It is to be shown that this model agrees with certain data available in the literature, and, in addition, that it exhibits characteristics heretofore not adequately included in a model. A method for ordering the relative values of displays in a control task is also suggested and evaluated.

2. THE MODEL

2.1 BASIC APPROACH

It is generally agreed that noise is present in the human operator in a control task [5,8]. Whether this noise exists at his input or output, or both, has not been established [13]. Many modellers have considered the human operator as a controller, but none have given serious attention to the perception mechanism at the interface between the displayed information and the control operation.

A model of this mechanism is required to transform the raw displayed information into a usable form. It is therefore postulated in this thesis that in a control task, this transformation is performed in the presence of noise, as an optimal time-varying linear filter (a Kalman filter). It is further postulated that in performing the control function, man uses the resultant estimates of the state of the system as an optimal time-varying linear controller. The data processing block in Figure 1.1 accordingly includes an optimal filter and an optimal controller.

It is assumed, in general, that optimal estimates are made of <u>all</u> of the state variables of the system including those of the plant being controlled, those associated with the forcing functions, and those associated with the man's own sensor and output characteristics. (This is not a necessary assumption and further research may prove this not to be the case, but it is assumed to be valid in this thesis.)

Regarding the human operator as having "optimal" characteristics is not to say that he performs perfectly, but only that he attempts to operate that way. The performance of the model is degraded by the filter as influenced by the noise. Therefore, the performance of the model, in general, is suboptimal as compared to an optimal controller by itself.

Modern control theory with state-space techniques [22] are used to provide the conceptual framework for systematically dealing with this large scale multi-variable multi-axis system. The model is therefore formulated as a set of state equations using parameters that may vary somewhat from one operator to another. Consequently, once the model is programmed, a variety of solutions are obtained by inserting the appropriate parameters.

By formulating the problem in terms of a state model, it is not intended to imply that the actual human operator thinks in terms of a particular set of state variables; only that his performance can be so characterized. A differential equation model implies that the human operator is characterizable as a continuous system. This, however, is not fundamental to the development since the human operator can also be regarded as a sampled data system if desired. The optimal filter and optimal controller in this case are characterized by difference equations.

2.2 STRUCTURE OF THE MODEL

As shown in Figure 2.1, it is postulated that in a control task, the human operator consists of a Kalman or optimal time-varying linear filter, an optimal time-varying linear controller, sensor and output characteristics with noise inputs $\,v\,$ and $\,w_{\,c}\,$, and internal forcing functions.

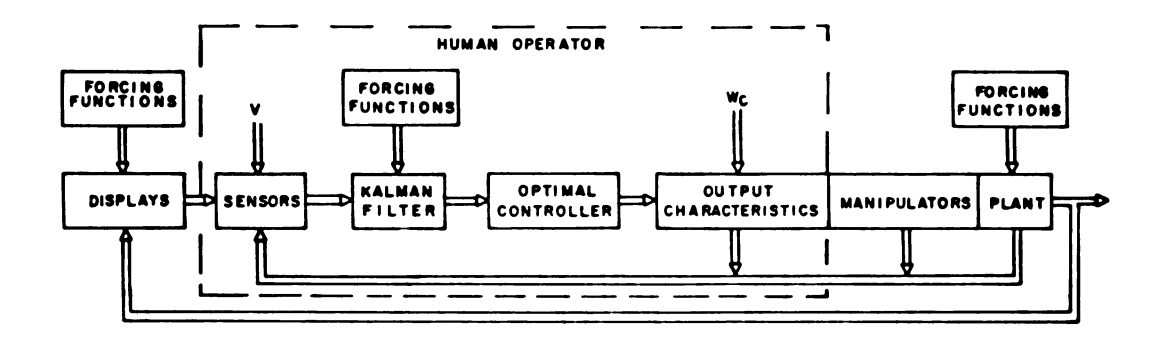


Figure 2.1. Manual control system basic block diagram.

To solve for the Kalman filter and the optimal controller, the system is rearranged into two overlapping parts as shown in Figure 2.2. The human operator part remains the same as in Figure 2.1, while the augmented plant contains everything but the filter and controller. With this rearrangement, the filter and controller can be found given all the characteristics of the augmented plant. However the model of the augmented plant must be in the form of linear, possibly time-varying, differential and algebraic equations. Statistically defined inputs (w and/or forcing functions) are included by "shaping" of white gaussian noise through a filter modeled by a set of linear, possibly time-varying, differential equais assumed to be additive white The "measurement noise" v gaussian noise and all components of v are assumed to be present. These restrictions on v can be relaxed somewhat by using the techniques given by Bryson and Johansen [23]. In addition, the linearity restrictions can be removed if the augmented plant can be quasi-linearized [24,47].

The augmented plant process equations are

$$\dot{x} = Ax + Bu + Dw, \qquad x(0) = x_0$$
 (2.1)

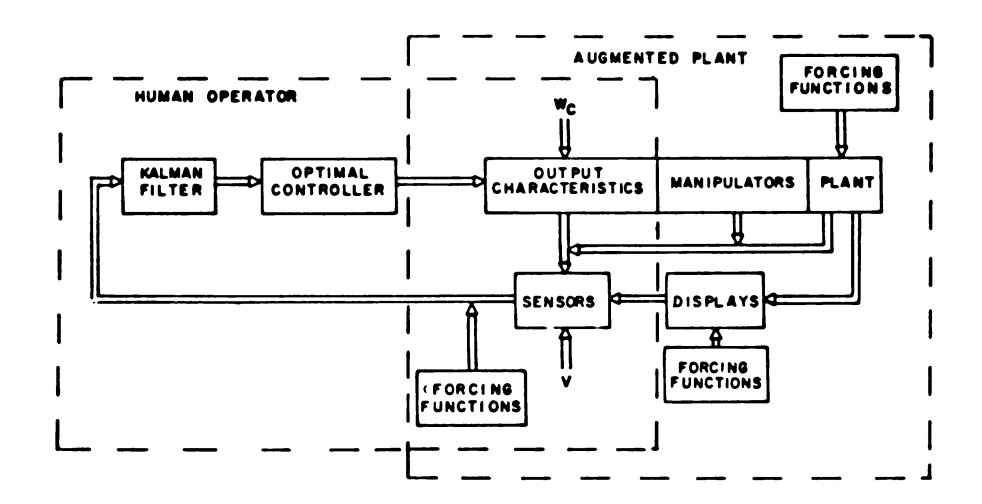


Figure 2.2. Basic block diagram with an augmented plant. and the measurement vector is

$$y = Cx + y (2.2)$$

where

$$E\{v(t)\} = E\{w(t)\} = E\{x_0\} = 0$$
 (2.3)

$$E\{v(t + \tau) v^{T}(t)\} = N\delta(\tau)$$
 (2.4)

$$E\{w(t + \tau) w^{T}(t)\} = M\delta(\tau)$$
 (2.5)

and

x is the augmented plant internal state vector of
 dimension n

 \boldsymbol{u} is the optimal controller output of dimension \boldsymbol{m}

y is the measurement vector of dimension ℓ

v, w are uncorrelated gaussian white noise vectors

 ${\bf x}$ is a gaussian random vector uncorrelated with ${\bf v}$ and ${\bf w}$

A, B, C, D, M, N are, in general, time-varying matrices $\delta\left(\tau\right) \text{ is the unit impulse function}$

The scalar cost function J to be minimized by both the filter and by the controller is a quadratic function of the form,

$$J = E \left\{ \frac{1}{2} \int_{0}^{t} f \left(x^{T} Q x + u^{T} R u \right) dt \right\}$$
 (2.6)

where

- E is the expected value operator
- Q is a constant square symmetric positive semi-definite matrix
- R is a constant square symmetric positive definite matrix
- t_{f} is the final time

As shown in [25,26] for the discrete case, the Kalman filtering problem and the optimum controller problem can be solved separately.

First, consider the optimum linear filter as developed by Kalman [27 through 31]. The Kalman filter, in general, is a minimum variance estimator. It is an optimum <u>linear</u> estimator if the white noise is non-gaussian and is <u>the</u> optimum estimator if the noise is gaussian [25]. It will be assumed, however, that the noise is gaussian.

The cost function that is minimized is $E\{(x - \hat{x})^T(x - \hat{x})\}$ where $\hat{x}(t)$ is the optimum estimate of x(t) given the observations

 $y(\tau)$, 0 < τ < t . The estimate of the plant state vector as given in [27 through 31] is

$$\hat{\hat{x}} = (A - \hat{K}C - BR^{-1}B^{T}K)\hat{x} + \hat{K}y, \qquad \hat{x}(0) = \hat{x}_{0}$$
(2.7)

where

 $\boldsymbol{\hat{K}}$ is the optimum linear filter gain matrix

and

K is the optimum linear controller gain matrix

As given by Kalman, \hat{K} is expressed by

$$\hat{K} = PC^{T}N^{-1} \tag{2.8}$$

where P(t) is the covariance of $[x(t) - \hat{x}(t)]$ given $y(\tau)$, $0 \le \tau \le t$, and is determined by solution of the matrix Riccati equation

$$\dot{P} = AP + PA^{T} - PC^{T}N^{-1}CP + DMD^{T}$$
 (2.9)

where the initial condition is

$$P(0) = E \left\{ \left(x_o - \hat{x}_o \right) \left(x_o - \hat{x}_o \right)^T \right\}$$
 (2.10)

The output of the Kalman filter is the optimal linear estimate of the augmented plant state vector and is used as the input to the optimal controller. Given the state vector as input, the optimal control problem reduces to the regulator problem. Using Pontryagin's maximum principle (see for example [32], [33]) the optimal control is

$$\mathbf{u} = -\mathbf{R}^{-1}\mathbf{B}^{\mathrm{T}}\mathbf{K}\hat{\mathbf{x}} \tag{2.11}$$

where K is obtained as the solution of

$$\dot{K} + KA + A^{T}K - KBR^{-1}B^{T}K + Q = 0$$
 (2.12)

Since $x(t_f)$ is arbitrary, the final condition can be taken as

$$K(t_f) = 0 (2.13)$$

2.3 SOLUTION OF THE MODEL

2.3.1 General Solutions

The complete system model can be solved on a digital, analog, or hybrid computer using (2.1) through (2.13). The optimal controller gain matrix as a function of time is first found by solving (2.12) backwards from $K(t_f) = 0$ to K(0). Then the following matrices are solved for simultaneously from t = 0 to $t = t_f$:

- 1) the optimal controller gain matrix K(t) defined by (2.12) using the initial condition K(0)
- 2) the covariance matrix P(t) defined by (2.4), (2.5), (2.9), and (2.10)

- 3) the Kalman gain matrix $\hat{K}(t)$ by (2.8)
- 4) the optimal linear estimate of the state vector $\hat{x}(t)$ defined by (2.7)
- 5) the optimal control law u(t) by (2.11)
- 6) the augmented plant response y(t) defined by
 (2.1) and (2.2)

Note that if the augmented plant is time stationary, then for t_f very large the optimal controller gain matrix can be taken as a constant with K(t) = K(0) over the time interval of interest, say from t = 0 to t = t'. The time t_f is sufficiently large, if, when (2.12) is solved backwards, the solution converges to a constant before time t' is reached.

If the beginning period of time, in addition to the end period of time, is not significant, the resultant model for the man is time stationary. In other words, the model is time stationary if sufficient time is allowed at the beginning for the solution of P to converge to a constant, and sufficient time is allowed at the end so that K remains constant.

For the time stationary case, the man-model can be written as a transfer function matrix

$$U_{c}(s) = H(s) Y(s)$$
 (2.14)

where

- $\mathbf{U}_{\mathbf{c}}(\mathbf{s})$ is the s-domain output vector of the human operator
- H(s) is the s-domain transfer function matrix
- Y(s) is the s-domain measurement vector

The case when $U_c(s)$ and U(s) are of dimension one is considered in Chapter 3.

A block diagram illustrating the solutions of the augmented plant, the Kalman filter, and optimal controller is given in Figure 2.3. As indicated, it is postulated that the human operator formulates a model that is nearly the same as the augmented plant that he is trying to control. The basic difference lies in the inclusion of \hat{K} and K.

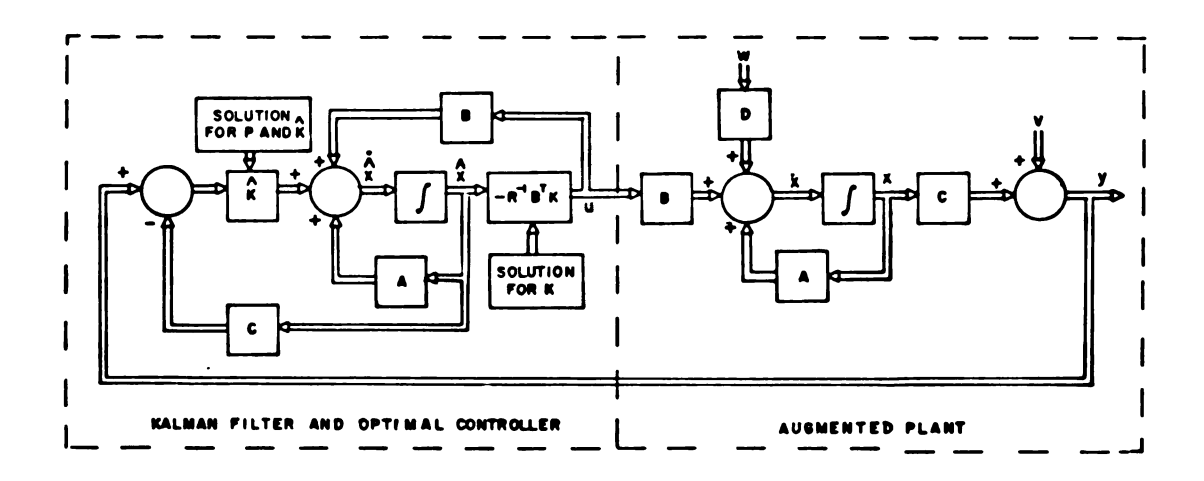


Figure 2.3. Solution block diagram.

The first part of the model -- the time-varying filter -- uses the sensed variables y which are corrupted by noise, and operates on them in such a way as to produce time-varying estimates of all of

the state variables of the augmented plant. These estimates are optimal estimates (if the noise is gaussian), in the sense that the variance of the estimation error is minimized.

With this formulation of the problem, compensatory as well as pursuit displays can be handled. In the compensatory task, the value of the displayed error as sensed by the human operator appears as a single variable in y. In the pursuit task, the forcing function and plant output, as sensed by the human operator, each appear as a variable in the vector y. The difference between them, or error, is determined in the controller using estimates of each variable as given by the filter.

2.3.2 A Simplified Form

The formulation as given above is very general and provides a framework for including factors in the human operator about which very little is known. So that the model can be studied in terms of available data and in terms of some of the general characteristics of the human operator that have already been established, it is reduced to that shown in Figure 2.4. This model is used in the remainder of the study. As indicated, a compensator task is used where the display characteristics are ignored. The operator sensor (except for the noise) and output characteristics are lumped into a time delay and neuromuscular lag. Also included in the neuromuscular lag are the manipulator characteristics which are assumed to be independent of the plant. (A detailed investigation using pressure, free-moving, and spring restrained manipulators is given in [34].) The noise inputs v and w₁ are included to represent man's

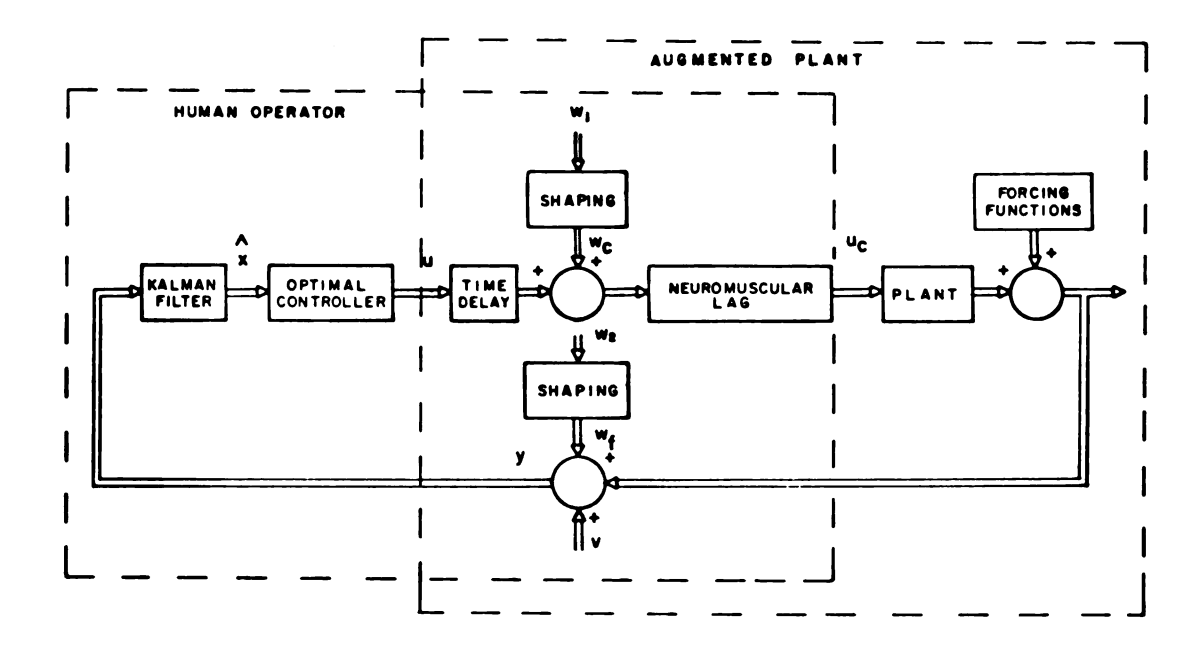


Figure 2.4. Simplified block diagram with an augmented plant.

measurement and output noise, respectively. The noise input \mathbf{w}_2 , as explained more fully in a later section, is included to represent an internal forcing function.

2.4 BASIC FEATURES

There are many potential advantages of the model given here over other models presently available. Some of these possible advantages, as indicated below, are investigated in this research.

2.4.1 Precognition

The model is capable of handling the precognition problem since the filter and controller part of the model (Figure 2.3), contains a model of the plant, the forcing functions, and the man's own physiological characteristics. The model "knows" the augmented plant and can predict its performance. Precognition of a forcing function is studied in Chapter 4 with sine-wave tracking.

2.4.2 Noise

The noise contribution is included in the model by v and w. Since v and w are white noise, high frequency components are present and indeed provide the means for introducing high frequency outputs in the operator. If required, the form of these inputs can be shaped in the augmented plant by combinations of leading and lagging characteristics. The variables v and w are vectors and can be used, if desired, to inject noise at several points internal to the operator as provided by the augmented plant. The amount of noise and the shaping required to give a good model for the man remain to be determined. It is noted that the amount and character of the noise is very important because it has a significant effect, as shown later, on the filtering characteristics and thus on the model that is generated for the man. This, of course, is in addition to the noise itself. Such factors as task difficulty and loading, stress and fatigue, and the effects of different displays might be considered in terms of noise inputs. The effect of two vastly different displays is considered in this way in Chapter 5.

2.4.3 Nonlinearity

The present state-of-the-art in optimal linear filtering and control theory extends to nonlinear plants that can be quasi-linearized. In such cases the first variation of the nonlinear model is used. This will not be considered here but solutions with nonlinear plants are entirely possible.

2.4.4 Nonstationarity

Assuming a stationary augmented plant, nonstationarity of

the man is accounted for by the time-varying filter. This time variation corresponds to a time-varying estimate of the augmented plant state vector. For example, with a step input, the operator has a preconception of the variance of the step and the other state variables. This information is contained in the initial value of P as given by (2.10). Subsequent to the application of the step, the variance of the operator's estimation error of the state vector changes with time, eventually approaching a steady-state value. Beyond this time the operator's estimate of the state variables will not improve substantially. How good the estimates are depends on the variances of the noise vectors v and w that are present.

Since the sensor and output characteristics are included in the augmented plant, any time variations of the parameters of the corresponding model contribute to nonstationarity. Also, the noise might be time-varying, giving rise to a time-varying filter with no "steady-state." The observed intermittency characteristics of man [19] might possibly be included in this way.

2.4.5 Multiple Inputs and Outputs

The number of inputs to the plant to be controlled theoretically can be any number (e.g., roll, pitch, and yaw) since ucis a vector. Similarly, the number of inputs to the operator is theoretically unlimited since the input y, representing sensed measurements, is a vector. The coupling between axes of a plant is automatically included in the model since, as shown in Figure 2.3, the operator "contains" a model of the plant which, of course, includes the coupling. The effect of a multi-axis task on single-

axis performance might possibly be included by the addition of noise at appropriate points in the model.

The noise inputs might be of a time-varying nature when multiple tasks are being performed on a part time basis. Thus, when another task is taking much of the operator's time, the noise would be large; when the operator is paying more attention to the central task of interest, the noise would be small. This would give a time-varying characteristic to the filter and thus to the model of the man.

2.5.6 Forcing Function Characteristics

The model includes the forcing function characteristics.

The type of forcing function -- whether generated externally or not, as for example, band-limited white gaussian noise, or a sine-wave -- is automatically included in the model of the man since it is in the augmented plant.

3. VALIDATION FOR TIME STATIONARY CONDITIONS

The objective of this chapter is to validate the model by showing how well the model results match data generated experimentally by others in a single-axis compensatory task. The experimental data are in the form of Bode plots for the linearly correlated portion of the response. Power spectral density plots for the remaining power (the remnant) are also considered.

McRuer et al. state in [5] that nonstationarity is a large part of the remnant. Their Bode plots, however, are obtained by time averaging over a complete run and therefore the nonstationarity during the run is ignored. Assuming the model can properly include this characteristic, an "average" of the time response is required to obtain a time stationary Bode plot. It is assumed in the results presented here that the noise can be selected so that the P matrix reaches a steady-state condition which corresponds to "the average" Bode plot.

3.1 EXPERIMENTAL RESULTS OF OTHER INVESTIGATORS

The data given by McRuer and Krendel in [4], those given by McRuer, Graham, Krendel and Reisener in [5], and those given by Wasicho, McRuer and Magdaleno in [41] are used. These data were selected because they appear to be very reliable. They are in general agreement with the data of others (e.g., Elkind in [40]), and they are in a form that is readily applied to investigate

the model. Since the data in each case were generated for the purpose of matching quasi-linear describing functions, they are given in the form of open loop frequency response plots (Bode plots) along with power spectral density plots of the remnant. The data given in [5] are used primarily and the experiments that were performed are described briefly below. The differences between [5] and the other references are pointed out when the other references are used.

McRuer et al. in [5] obtained their data using nine different pilots in a compensatory task (see Figure 1.2) with five different plants to control. They used the sum of ten sine-waves as a forcing function. The display was a six inch CRT and the manipulator was a hand operated stick with motion restricted to the roll axis. The stick was a low inertia, low damped spring restrained device. With a constant gain plant ($Y_c = 1$), the display motion was one inch per six degrees of stick motion. The force gradient was 2.21 oz/deg at a four inch moment arm.

Their data were generated using a cross-spectral analyzer where the cross-spectral density at each of the ten forcing function frequencies was measured and averaged over a four minute period. An initial 10-15 second transient period was allowed for the operator to reach a stable tracking condition. Prior to taking the data, each pilot was given a sufficient number of two minute trial runs to minimize variability due to practice effects. It was assumed that this point was reached when his RMS error reduced to a relatively constant value from run-to-run and usually took from ten to twenty trial runs.

The ten forcing function frequencies were uniformly spaced over the frequencies of interest. Also, the frequencies were picked so that there would be no overlapping harmonics, and so that there would be an integral number of cycles over the four minute run. The sum of sine-waves produces a "random appearing" input that is easily generated, and, in addition, the sine-waves are mathematically tractable in the cross-spectral analyzer. Since the selected forcing function is random appearing, the operator cannot "learn" it.

McRuer et al. in [5] show that the sum of ten sine-waves that they selected is gaussian with a Chi-squared test at the 0.05 level. As shown in [39] as few as five appropriately chosen sine-waves are nearly gaussian.

The one-sided power spectrum of the sum of sine-waves is

$$\Phi_{ii}(\omega) = \pi \sum_{n=1}^{N} \phi_{i}^{2}(\omega_{n}) \delta(\omega - \omega_{n})$$
 (3.1)

where $\phi_{\textbf{i}}(\omega_n)$ is the half-amplitude of the nth sine-wave. The variance or mean-squared value is

$$\sigma_{i}^{2} = \frac{1}{2\pi} \int_{0}^{\infty} \Phi_{ii}(\omega) d\omega \qquad (3.2)$$

$$= \frac{1}{2} \sum_{n=1}^{N} \phi_{i}^{2} (\omega_{n})$$
 (3.3)

Most of the data in [5] were taken with a display variance of

$$\sigma_i^2 = 0.25 \text{ in}^2$$
 (3.4)

Table 3.1 shows the frequencies and magnitudes of the three forcing functions, denoted by $F_{1.5}$, $F_{2.5}$, and F_4 , used by McRuer et al. in [5]. Note that in $F_{1.5}$, $F_{2.5}$, and F_4 the first six, seven, and eight frequencies, respectively, are at one power level while the power at the remaining frequencies are 20 db lower. The subscript refers to the frequency of the last sine-wave at the higher power level.

Table 3.1. Forcing function magnitudes.

	$\phi_{i}^{2}(\omega_{n})$ - Power db		
ω _n -Rad/Sec	F _{1.5}	F _{2.5}	F ₄
$\omega_1 = 0.157$	-10.8	-11.5	-12.0
$\omega_2 = 0.262$	-10.8	-11.5	-12.0
$\omega_3 = 0.393$	-10.8	-11.5	-12.0
$\omega_4 = 0.602$	-10.8	-11.5	-12.0
$\omega_5 = 0.969$	-10.8	-11.5	-12.0
$\omega_6 = 1.49$	-10.8	-11.5	-12.0
ω ₇ = 2.54	-30.8	-11.5	-12.0
$\omega_8 = 4.03$	-30.8	-31.5	-12.0
ω ₉ = 7.57	-30.8	-31.5	-32.0
$\omega_{10} = 13.8$	-30.8	-31.5	-32.0

The experimental data, given in the form of \pm 1σ ranges about the mean, are superimposed on the corresponding results obtained from the model and are given in later sections.

3.2 MODEL SOLUTION

As indicated in Chapter 2, a time stationary model results when:

- 1) the augmented plant is time stationary
- 2) the noise is time stationary
- 3) the initial time period required for the P matrix to reach an essentially constant value is ignored so that the filter gain matrix \hat{K} can be considered to be a constant
- 4) the final time period required for the control matrix

 K to reach an essentially constant value (when solved backwards) is ignored.

Under these conditions, the time stationary model for the filter and controller parts of the human operator given in (2.7) and (2.11) become

$$\hat{\hat{x}} = \hat{A}\hat{x} + \hat{K}y \tag{3.5}$$

$$u = \hat{C}\hat{x} \tag{3.6}$$

where

$$\hat{A} = A - \hat{K}C - BR^{-1}B^{T}K$$
 (3.7)

$$\hat{C} = -R^{-1}B^{T}K \tag{3.8}$$

and \hat{A} , \hat{C} , and \hat{K} are constant matrices.

For a single-axis compensatory task u and y are scalars. As shown in Appendix A, the transfer function for the man without the physiological characteristics is

$$\frac{U(s)}{Y(s)} = \hat{C} \left\{ e^{\hat{A}t} \right\} \hat{K}$$
 (3.9)

The available experimental data are for a complete system, including the human operator and the plant he is controlling. The transfer function for the complete man-plant combination, including the physiological characteristics is obtained by multiplying the transfer function in (3.9) by the transfer functions for the plant and the physiological characteristics.

Bode plots for the time-stationary model of the human operator and plant so obtained are generated by a digital computer program as described in detail in Appendix B. The inputs required by the program are the matrices A, B, C, and D from the augmented plant as given by (2.1) and (2.2), the matrices M and N which define the covariances of v and w as given by (2.4) and (2.5), the

matrices Q and R from the cost function as given by (2.6), and the transfer functions for the physiological characteristics and the plant. The program gives the steady-state optimal controller gain matrix K, the steady-state optimal filter gain matrix \hat{K} , the state model for the optimal filter and optimal controller, the transfer function for the optimal filter and optimal controller, the transfer function for the man-plant combination, and a Bode plot for the man-plant combination.

The particular model used for the augmented plant is shown schematically in Figure 3.1. Three of the five plant transfer functions Y_{c} presented by McRuer et al. in [5] are investigated. They are:

1) the constant gain plant

$$Y_{c} = 1$$
 (3.10)

2) the integrator plant

$$Y_{c} = \frac{1}{s} \tag{3.11}$$

3) the first order unstable plant

$$Y_{c} = \frac{5}{s-2}$$
 (3.12)

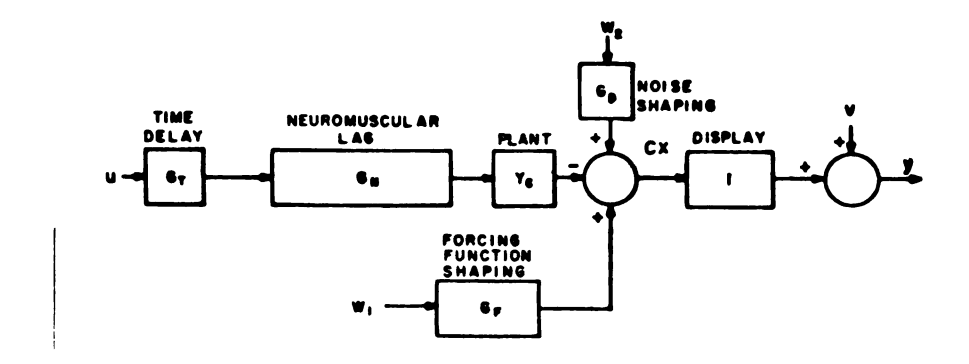


Figure 3.1. Augmented plant for time stationary conditions.

The neuromuscular lag is nominally approximated by a first-order lag

$$G_N(s) = \frac{1}{T_N s + 1}$$
 (3.13)

where T_N is taken to be 0.3 seconds. The time delay is nominally approximated by a first-order Padé approximation [35]

$$G_{T}(s) = \frac{-\frac{\tau}{2} s+1}{\frac{\tau}{2} s+1}$$
 (3.14)

where τ is taken to be 0.1 seconds. This time delay is assumed to be due to physiological characteristics only (conduction, etc.) and as given by McRuer et al. [5] ranges from 0.05 seconds to 0.1 seconds. Ranges of T_N from 0.1 to 0.6 seconds and ranges of τ from 0.06 to 0.15 second are considered in Section 3.4. A precision neuromuscular lag and a second-order time delay are also considered in Section 3.4.

As shown in Figure 3.1, there are three gaussian white noise inputs. The measurement noise v is a single dimensional input defined by (2.3) and (2.4) while process noise terms w_1 and w_2 form the two dimensional vector w defined by (2.3) and (2.5). The variables v, w_1 , and w_2 are orthogonal with

$$R_{VV}(\tau) = N\delta(\tau) = n\delta(\tau)$$
 (3.15)

$$R_{WW}(\tau) = M\delta(\tau) = \begin{bmatrix} m_{11} & 0 \\ & & \\ 0 & m_{22} \end{bmatrix} \delta(\tau)$$
 (3.16)

$$R_{VW}(\tau) = 0 \tag{3.17}$$

McRuer et al. considered one-sided power spectrums where

$$\Phi_{\mathbf{X}\mathbf{X}}(\omega) = 4 \int_{0}^{\infty} R_{\mathbf{X}\mathbf{X}}(\tau) \cos\omega\tau d\tau \qquad (3.18)$$

$$= 2 \int_{-\infty}^{\infty} R_{xx}(\tau) \cos\omega \tau d\tau \qquad (3.19)$$

Since by definition

$$\int_{-\infty}^{\infty} \delta(\tau) \cos \omega \tau d\tau = 1$$
 (3.20)

the one-sided power spectrums of v and w become

$$\Phi_{VV}(\omega) = 2n \tag{3.21}$$

$$\Phi_{WW}(\omega) = \begin{bmatrix} 2m_{11} & 0 \\ & & \\ 0 & 2m_{22} \end{bmatrix}$$
 (3.22)

The forcing functions given in Table 3.1 are approximated by gaussian white noise band-limited by a third-order lag filter with corner frequencies centered around the last sine-wave at the higher power level. For the forcing function $F_{2.5}$ the shaping is

$$G_{F}(s) = \frac{1}{\left(\frac{s}{2.4} + 1\right)\left(\frac{s}{2.5} + 1\right)\left(\frac{s}{2.6} + 1\right)}$$
(3.23)

Figure 3.2 shows the magnitudes squared of each of the sinusoidal components of the forcing function $F_{2.5}$ superimposed on the shaping function G_F . To illustrate the fit of the approximation, the low frequency portion of G_F is made to coincide with the lower frequencies of the given forcing function. The variance of the model forcing function $g_F^*w_1$ is adjusted by m_{11} in (3.16) so that it is the same as that used by McRuer et al. in [5] for $F_{2.5}$. The variance of $g_F^*w_1$ by (3.2) is

$$\sigma_{\dot{\mathbf{i}}}^{2} = \frac{1}{2\pi} \int_{0}^{\infty} \frac{\Phi_{\mathbf{w}_{1}\mathbf{w}_{1}}(\omega) d\omega}{\left| \left(\frac{\mathbf{j}\omega}{\mathbf{a}} + 1 \right) \left(\frac{\mathbf{j}\omega}{\mathbf{b}} + 1 \right) \left(\frac{\mathbf{j}\omega}{\mathbf{c}} + 1 \right) \right|^{2}}$$
(3.24)

$$= \frac{m_{11} \text{ abc}}{2} \left[\frac{(b^2-c^2)bc-(a^2-c^2)ac+(a^2-b^2)ab}{(a^2-b^2)(a^2-c^2)(b^2-c^2)} \right]$$
(3.25)

Taking a = 2.4, b = 2.5, and c = 2.6, the variance is

$$\sigma_i^2 = 0.468 \, m_{11}$$
 (3.26)

and the required value for m11 using (3.4) is

$$m_{11} = \frac{0.25}{0.468} = 0.534$$
 (3.27)

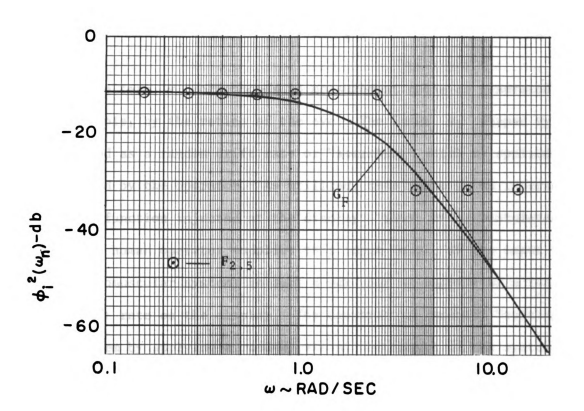


Figure 3.2. Forcing functions.

Experimental results in [4] for a constant gain plant show that the sum of sine-waves with power levels arranged along the curve of a third-order lag, and, the rectangular arrangement used in [5] (Table 3.1) both yield essentially the same transfer function for the operator. The experimental differences between third-order shaping and the rectangular shaping for other plants are not given in [4] and are assumed to be small. (They may not be, however.)

Referring to Figure 3.1, the noise inputs to the measurement y consist of a pure gaussian white noise term $\,v\,$ and a gaussian white noise term $\,w_2\,$ shaped by a pure integrator of the form

$$G_{D}(s) = \frac{1}{s}$$
 (3.28)

The noise term $\, \, v \, \,$ corresponds to measurement noise as generated, for example, by the retina of the eye. The input $\, w_2 \, \,$ shaped by $\, G_D \,$ is viewed as a random drift rate or "searching" which is applied and estimated by the operator. As utilized, this input is an internal forcing function injected at the display. Thus, it is postulated that the human operator supplies this input (e.g., at the input to his neuromuscular system) in such a way that it appears as a random drift rate on the display. The operator is randomly "testing" the system by applying a random rate at the output of the system. (In some respects this input is like "dither," although "dither" is usually considered to be at one frequency.)

Since the white noise inputs $\,v\,$ and $\,w_2\,$ are orthogonal

by (3.17) for all values of τ , the output of the noise shaping, call it w_{2S} , is also orthogonal to v. Indeed, for all t

$$R_{VW_{2S}}(\tau) = E \left\{ v(t+\tau)w_{2S}(t) \right\}$$
 (3.29)

$$= E \left\{ v(t+\tau) \int_{0}^{t} w_{2}(\alpha) d\alpha \right\}$$
 (3.30)

$$= \int_{0}^{t} E \left\{ v(t+\tau)w_{2}(\alpha) \right\} d\alpha \qquad (3.31)$$

$$= \int_{0}^{t} R_{VW_2}(t+\tau-\alpha) d\alpha = 0 \qquad (3.32)$$

Since ν and $w_{2\,S}$ are orthogonal, the power spectrum of the sum is

$$\Phi_{V+W_{2S}}(\omega) = \Phi_{VV}(\omega) + \frac{1}{\omega^2} \Phi_{W_2W_2}(\omega)$$
 (3.33)

From (3.21 and (3.22))

$$\Phi_{V+W_{2S}}(\omega) = 2\left(n + \frac{m_{22}}{\omega^2}\right) \qquad (3.34)$$

$$= 2n \left| \frac{j\omega + \sqrt{\frac{m_{22}}{n}}}{j\omega} \right|^2$$
 (3.35)

Normalizing by the variance of the forcing function given by (3.26), (3.35) yields

$$\frac{\Phi_{V+W_{2S}}(\omega)}{\sigma_{i}^{2}} = \frac{2n}{0.468 \, m_{11}} \left| \frac{j\omega + \sqrt{\frac{m_{22}}{n}}}{j\omega} \right|^{2}$$
 (3.36)

$$= 4.27 \frac{n}{m_{11}} \left| \frac{j_{\omega} + \sqrt{\frac{m_{22}}{n}}}{j_{\omega}} \right|^{2}$$
 (3.37)

Note that (3.37) only depends on the ratio of $\frac{M}{n}$, and as shown in Appendix D for a slightly more general case, so does the solution of the model.

The cost function from (2.6) is

$$J = E \left\{ \frac{1}{2} \int_{0}^{t} f \left(x^{T} Q x + u^{T} R u \right) dt \right\}$$
 (2.6)

It is assumed that the mean-squared value of the displayed variable plus that of u is minimized. Thus,

$$Q = C^{T}C (3.38)$$

Since u is of order one and with

$$R = r \tag{3.39}$$

the cost function reduces to

$$J = E \left\{ \frac{1}{2} \int_{0}^{t} f \left[(Cx)^{T} (Cx) + ru^{2} \right] dt \right\}$$
 (3.40)

3.3 MODEL VALIDATION

The general problem is: given models of the plant, the neuromuscular lag, and the time delay; what noise and cost function are required to match experimental data? This might be called the "inverse optimal filter and control problem." More specifically for the case considered here, the problem is: given the simple models for the neuromuscular lag and time delay as defined by (3.13) and (3.14) with $T_N = 0.3$ and $\tau = 0.1$, and given the forcing function defined by (3.23) and (3.27); what values of n, r, and m_{22} are required to match the model results to the experimental data for the plants defined by (3.10), (3.11), and (3.12)? Bode plots showing selected matches for these three plants are given in Figures 3.3, 3.4, 3.5, and 3.6.

The model plots correspond to the complete man-plant combination with a unity feedback open-loop transfer function $G(j\omega)$. The solid and dashed lines are gain and phase respectively where,

Gain in db =
$$20 \log_{10} |G(j\omega)|$$
 (3.41)

and

Phase in degrees =
$$\chi G(j\omega)$$
 (3.42)

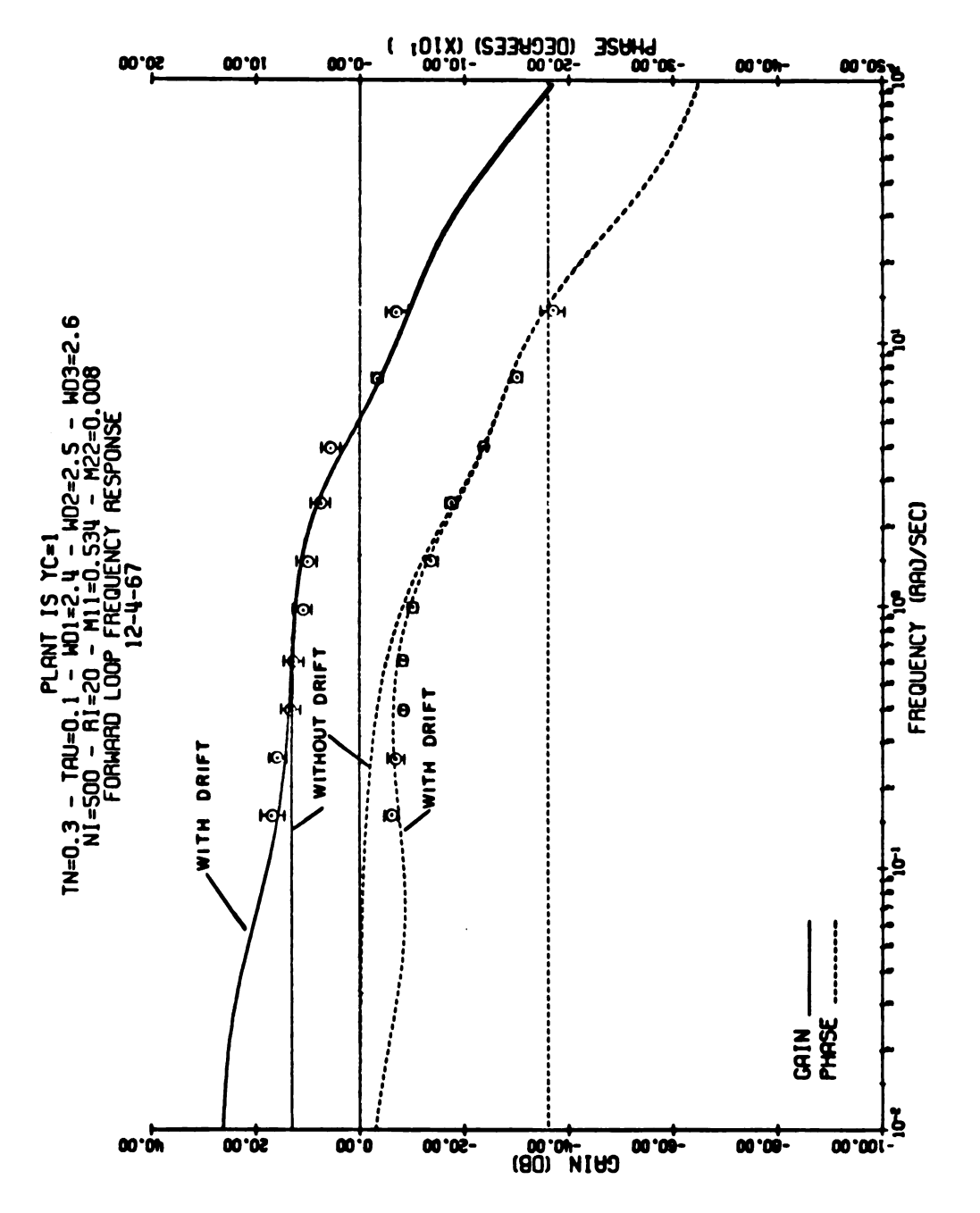
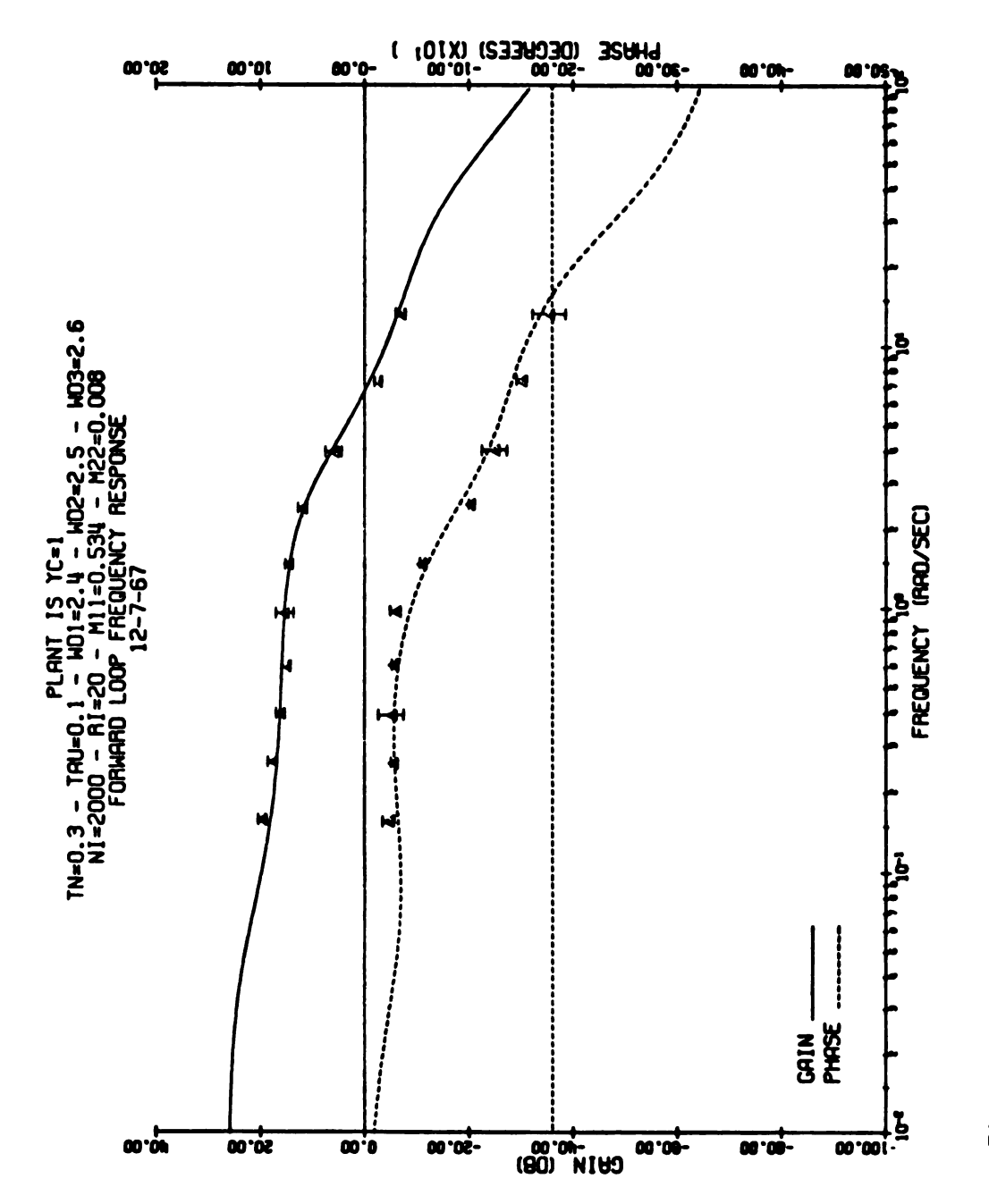


Figure 3.3. Match for the constant gain plant.



Match for the constant gain plant with a highly trained pilot. Figure 3.4.

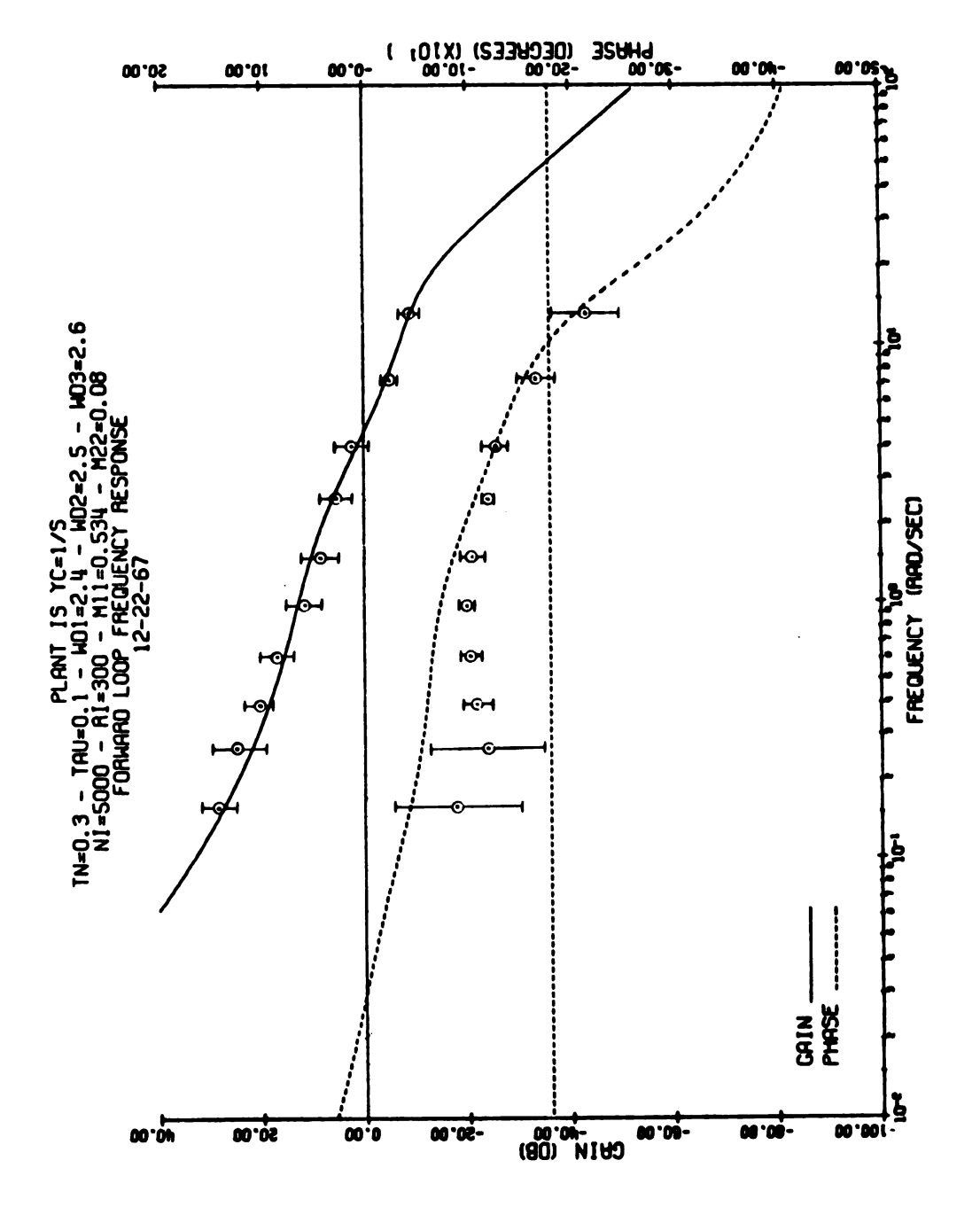


Figure 3.5. Match for the integrator plant.

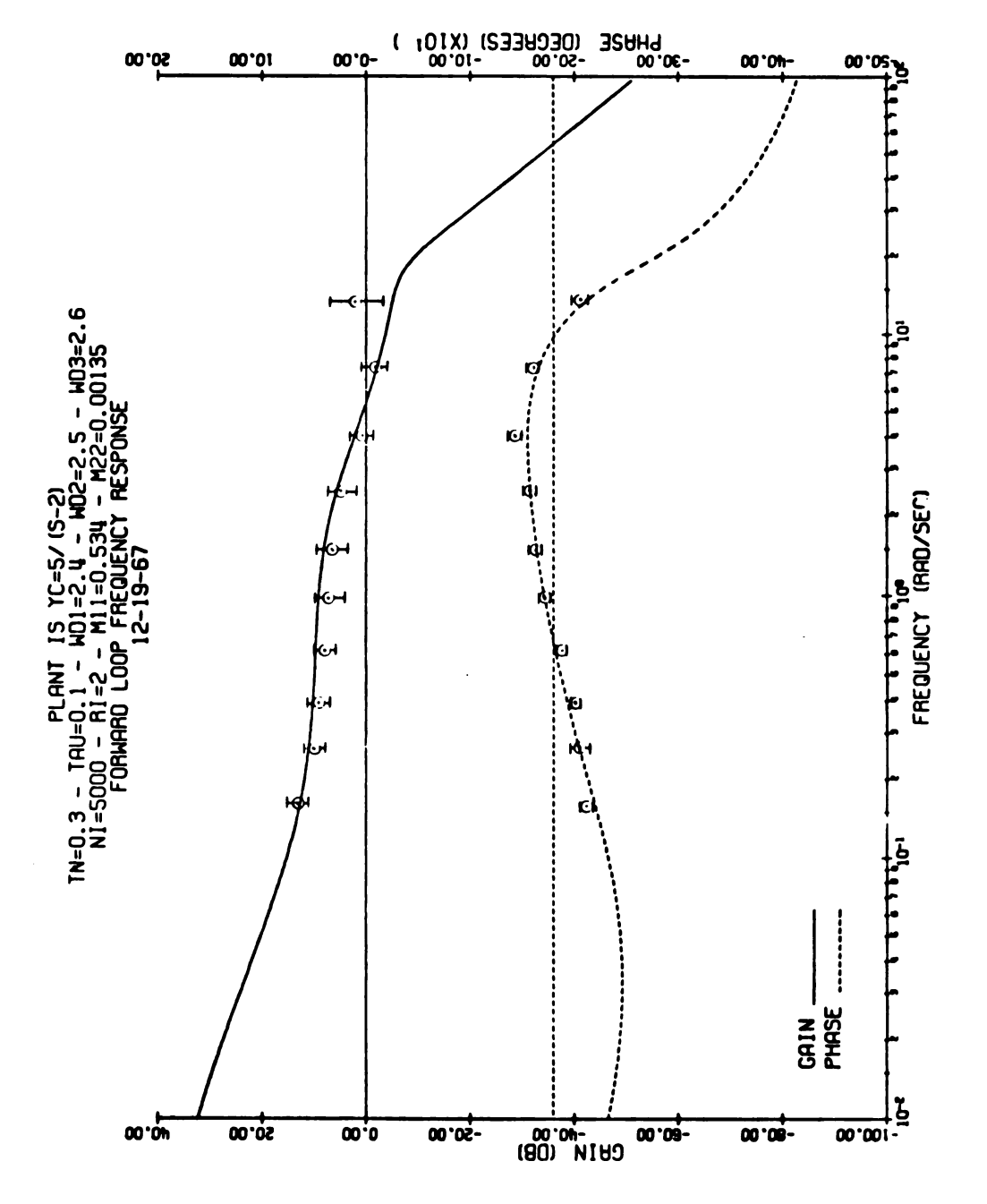


Figure 3.6. Match for the unstable plant.

Superimposed on the model results are the experimental data at the ten forcing function frequencies. The ranges shown are $\pm 1\sigma$ ranges around the mean where the mean is indicated by the symbol. The data given by the circles (\odot) are from [5] while those given by the triangles (Δ) in Figure 3.4 are from [41].

The matching was achieved heuristically varying n, r, and m_{22} . Formal optimization procedures were not used to select these parameters primarily because it was desired to obtain a "feel" for the effect of each parameter, but also because of potential convergence problems and digital computer running time.

Figure 3.3 shows the model results with and without the drift provided by w_2 . (The model without drift is the example problem solved in detail in Appendix B.) Comparison shows that drift provides a low frequency gain increase and additional low frequency phase shift, and consequently provides a better match with the data.

Figure 3.4 shows how pilot training might be accounted for by the model. The data from [41] are for one of the nine pilots used in [5], but after much more training. Detailed comparison of Figures 3.3 and 3.4 shows that the gain is higher and the phase shift is less in Figure 3.4. This is accounted for in the model by simply reducing the measurement noise. (It might be said that his perception ability was improved.) The noise term needed to match the data in [5] is NI = 500 while that needed to match the data in [41] is NI = 2000. As indicated by the parameter variations in the next section, the gain increases can also be accounted for by

decreasing the cost $\, r \,$ associated with the control action. The change in phase shift at mid-frequencies, however, is in the opposite direction and therefore $\, r \,$ is not the appropriate parameter to change. The remaining parameter of the three available to account for the difference is $\, m_{22} \,$, but as indicated above and in the next section, $\, m_{22} \,$ primarily affects the low frequency characteristics.

Figures 3.5 and 3.6 show the matches for the plants $Y_c = 1/s$ and $Y_c = 5/(s-2)$. The gain matches for both are very good. The phase match for the plant $Y_c = 1/s$ is good, but not as good as desired.

It was found that the model results are quite sensitive to the selected values of the parameters n, r, and m_{22} . In addition, the results are very sensitive to P when the solution for P is stopped before it has converged. Figure 3.7 shows the effect on the results for the plant $Y_C = 5/(s-2)$ starting at an arbitrary P. The solution for P is stopped at 1, 8, and 16 seconds. At 16 seconds the solution has converged to a point where the convergence requirement in Appendix B is met. Note that there are drastic differences at low frequencies but very little change occurs near the cross-over frequency and above. Since the low frequency gain is high, the convergence of P has very little effect on the closed loop response characteristics.

It is interesting to note that in the solution of the P matrix for each of the plants considered, the particular elements of P associated with the state of the plant that is being controlled do not approach zero for the unstable plant but they do for

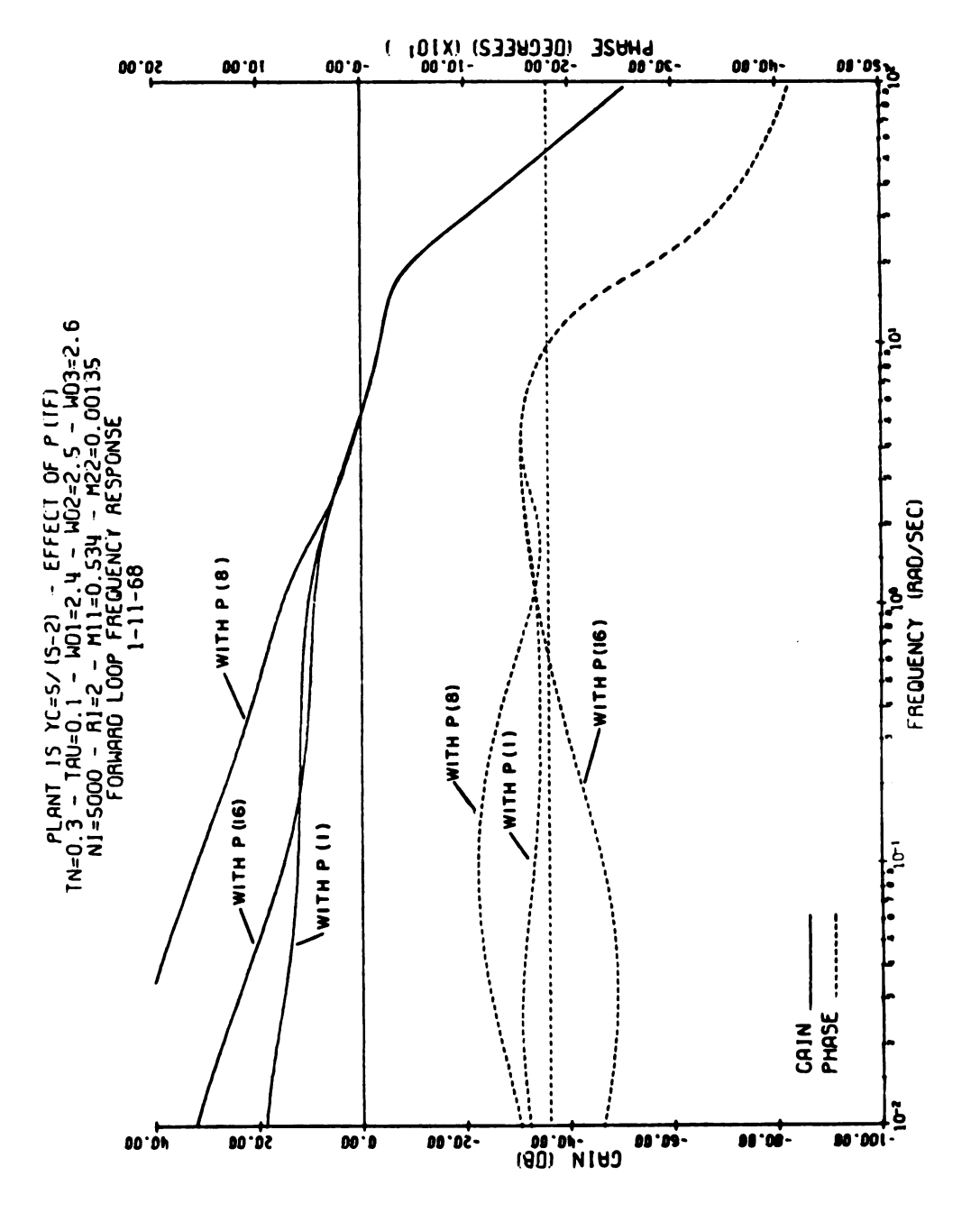


Figure 3.7. Model results as P converges.

other plants. In other words, for the unstable plant, non-zero steady-state variances and cross-variances of the plant variables are present. This means that comparatively poor estimates of the state of the unstable plant are made while essentially exact estimates are made for the other plants. This intuitively agrees with what the human operator actually does since the unstable plant is difficult to control, where according to [5], there are "momentary losses of control." Consequently, a human operator may well have relatively large variances on the estimates of the state of the plant.

The values chosen for n, r, and m_{22} to match the data in [5] for the three plants are summarized in Table 3.2. There seems to be little correspondence between the parameters required for the

			<u> </u>
PLANT	n	r	m ₂₂

Table 3.2. Parameters for model validation.

PLANT	n	r	m ₂₂
1	1/500	1/20	0.008
1/s	1/5000	1/300	0.08
5/(s-2)	1/5000	1/2	0.00135

models. However, consideration of the total noise at the input to the man gives some agreement as explained below.

The normalized noise power spectrum injected at y is given by (3.37) and is plotted for the three plants in Figure 3.8. Some of the remnant data in [5] and [7] are given as power spectra injected in the same way, and are also shown in Figure 3.8. Both

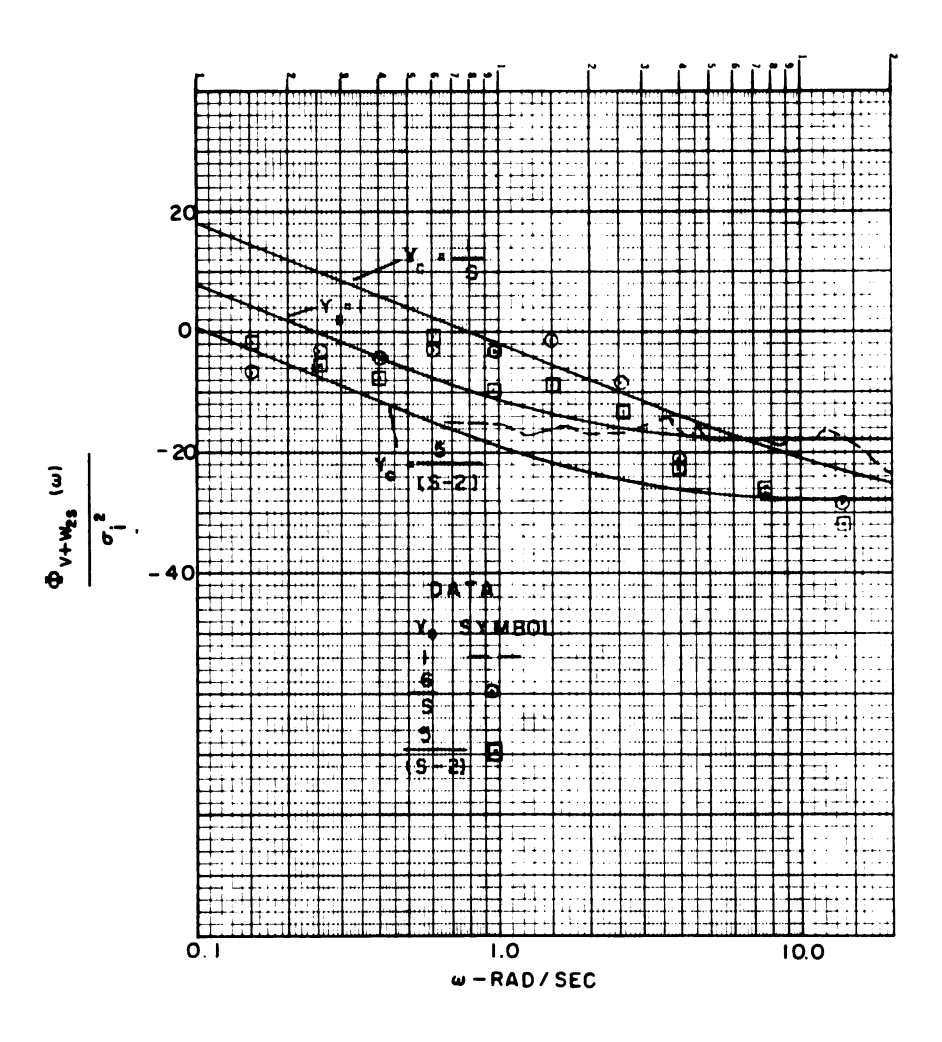


Figure 3.8. A comparison of the remnant with model noise.

the model results as given by (3.37), and the data from [5] and [7] are normalized by the variance of the forcing function. The dashed line is the remnant data for the plant $Y_c = 1$ as adapted in [7] from [40]. The data indicated by the key of the figure are from selected runs for the plants $Y_c = 1/s$ and $Y_c = 5/(s-2)$ as reported in [5]. The data for the plant $Y_c = 1$ are taken from the average of several runs while those for the other two plants are from single runs.

As shown in Figure 3.8, there is general agreement between the experimentally measured remnant and the noise used in the model. However, only the noise and remnant for the plant $Y_c = 1$ agree closely. According to [5], the plant $Y_c = 1$ is the only one where noise is the majority of the remnant, where the significant part of the remnant for the other plants is nonstationarity. Thus, it might be concluded that since the noise for the plant $Y_c = 1$ matches the remnant data best, a noise input that yields the desired Bode plot is not closely related to the remnant when nonstationarity is important. Consequently, the noise needed to obtain a steady-state P which will give the desired Bode plot is not the noise which will be equivalent to the remnant. On the other hand, the forcing function used in the model is not identical to that used to generate the data (Figure 3.2), and may have a significant effect on the noise required to generate the model transfer function. Also, the remnant is on the order of 5 percent of the total power and it may not be accurate. Nevertheless, it appears as though the noise and remnant are not equivalent. More experimental data are required, however,

with forcing functions that can be exactly included in the model to sufficiently support this conclusion.

Though it is theoretically possible to use the exact expression for the ten sine-waves as the model forcing function, such a representation requires twenty state variables and is not feasible with the present computer program. (The maximum number of state variables allowed is seven.) Also, if the exact expressions were used, it is possible that the P matrix would not converge, even in the four minute run time considered in [5]. (The sum of sine-waves would "appear random" in the model although the estimates of each would be improving with time.) To obtain a time stationary transfer function, it would be necessary, as with experimental studies, to use a ratio of cross-spectral densities (see Appendix D). Under these conditions, the noise used to generate a Bode plot to match experimental data along with the nonstationarity that would be present might be closer to the remnant. Further experimental and model studies are required.

The addition of drift provides the low frequency phase shift that McRuer et al. in [5] attribute to the neuromuscular system (see Section 1.5). Also, the lightly damped second-order characteristic at high frequency, attributed to the neuromuscular system in [5], is present in the models for all the plants considered here. (see Figures 3.3 through 3.6). The model results along with the data from [5] for the human operator alone (without the plant) for the plant $Y_c = 5/(s-2)$ are shown in Figure 3.9. The model exhibits the same characteristics attributed to the

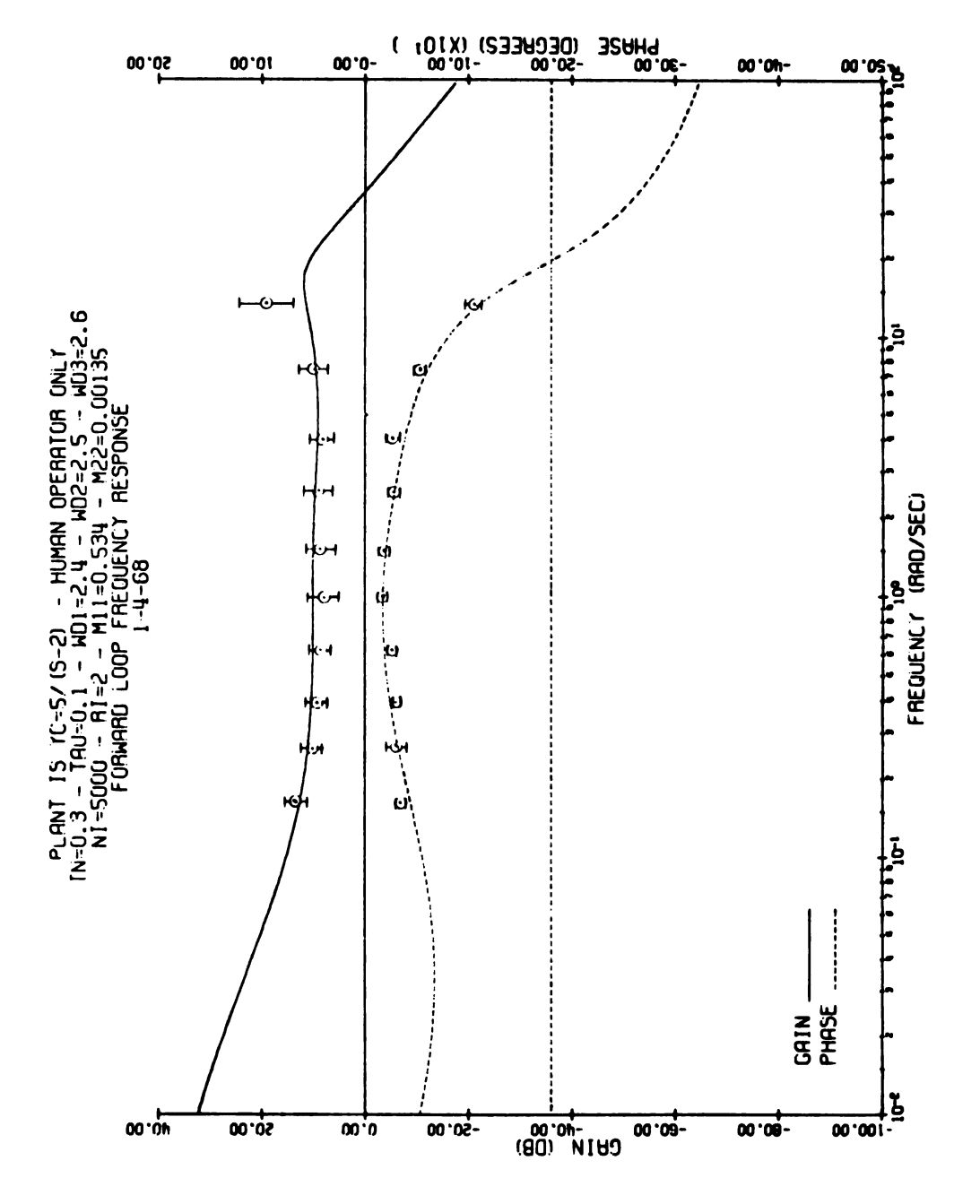


Figure 3.9. Unstable plant match -- human operator only.

neuromuscular system in [5] as given in (1.1). However, since the neuromuscular system is assumed to be representable here by a first-order lag, it can be concluded that the gain and phase characteristics come from the controller and filter, and not from the neuromuscular system. Since the very high frequency gain does not match well, a second-order neuromuscular characteristic may give better results, but it should be more heavily damped than advocated in [5]. On the other hand, the forcing function used in the model has the greatest deviation from the experimental function at high frequencies (Figure 3.2), and may give rise to the discrepancy.

3.4 SENSITIVITY STUDIES

The effects of changes in the parameters of the system are now studied to determine the sensitivity of the results to these changes. Some of the results are compared with experimental data. Unless otherwise indicated, the plant is $Y_{\rm c}=1$ without drift. Caution should be used in extrapolating these results to other plants since the effects are not necessarily the same.

Figures 3.10 and 3.11 show the effect of the neuromuscular time constant $\,T_{N}^{}\,$ and the time delay $\,\tau$. Note that the complete gain curves move vertically with changes in both $\,T_{N}^{}\,$ and $\,\tau$, but the phase shift is altered only at high frequencies.

Let it now be assumed that the precision neuromuscular characteristic given in [5] is better than the first-order lag (contrary to some of the statements in Section 3.3) and will improve the match. This characteristic as expressed by (1.1) is

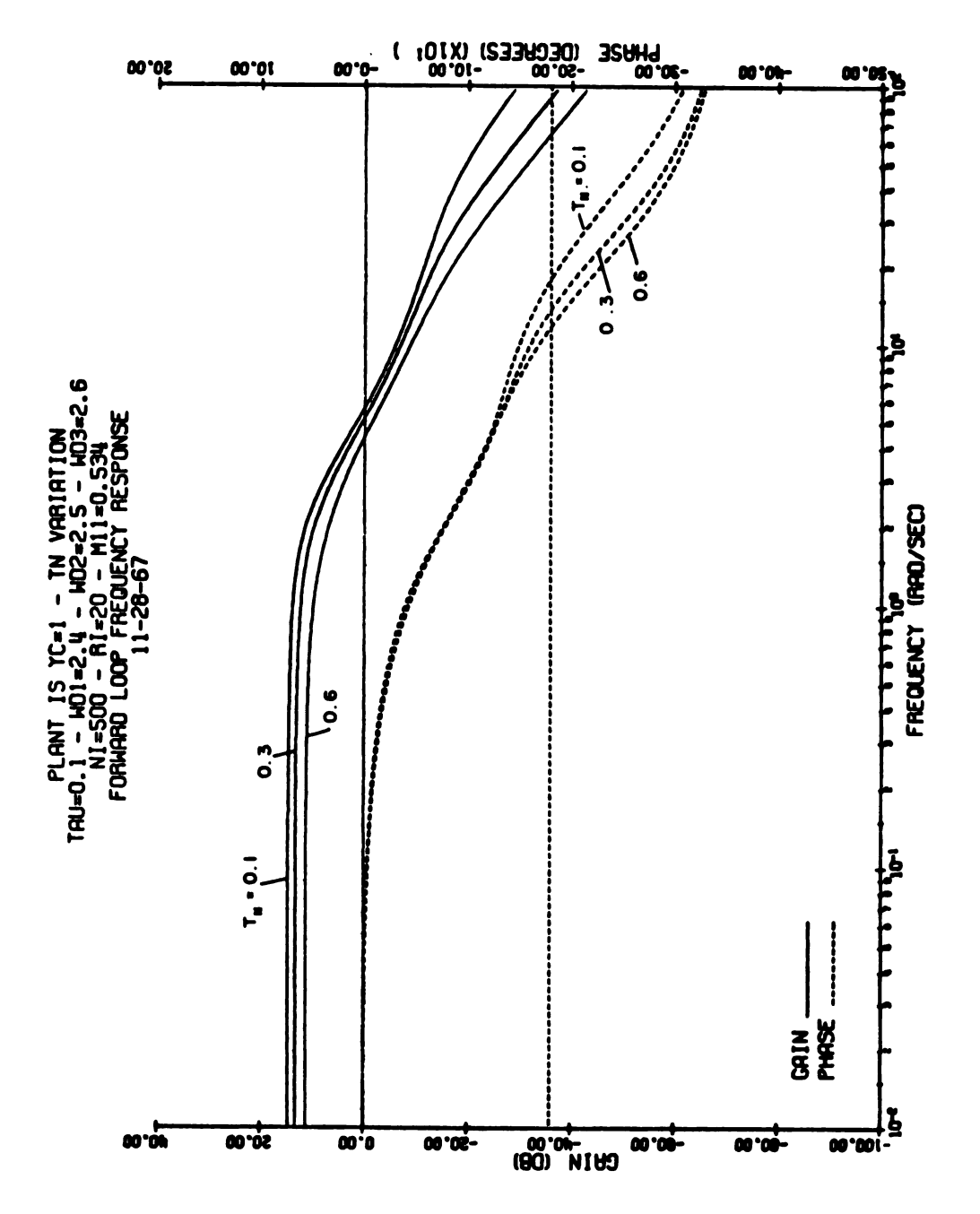


Figure 3.10. Effect of various $T_{
m N}.$

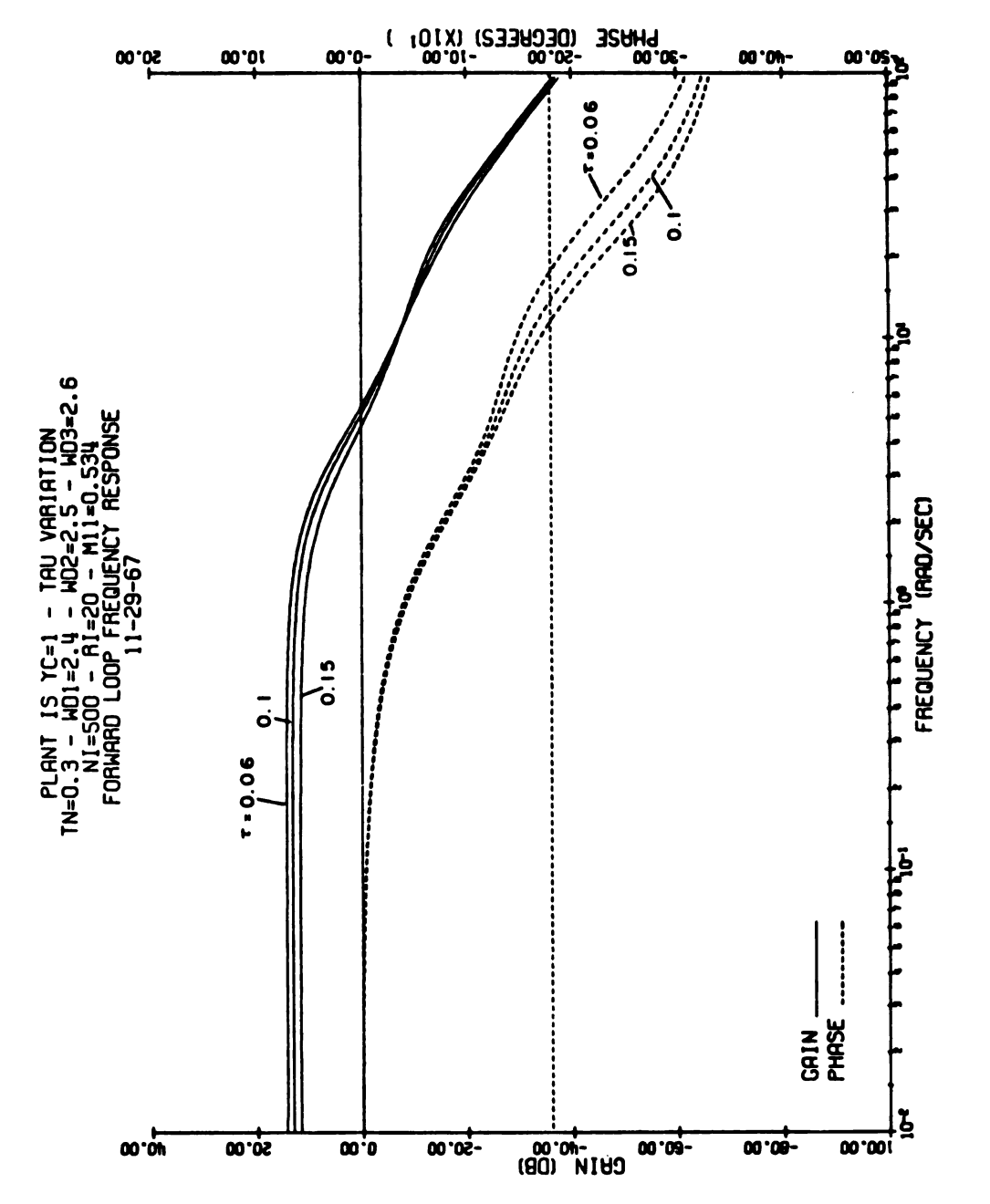


Figure 3.11. Effect of the time delay.

$$Y_{N} = \left(\frac{\frac{s}{0.3} + 1}{\frac{s}{0.05} + 1}\right) \left(\frac{1}{(0.1 \text{ s+1}) \left[\frac{s^{2}}{(16.5)^{2}} + \frac{0.24}{16.5} \text{ s} + 1\right]}\right)$$
(3.43)

The model results with this neuromuscular characteristic are shown in Figure 3.12 along with the results using the simple first-order characteristic. The forcing function in both cases is gaussian white noise shaped by a second-order filter with corner frequencies at 2.4 and 2.6 rad/sec rather than the third-order filter used in all previous studies. This was done because the computer program is limited to a state vector consisting of seven elements. To make the cross-over frequencies the same, a value of $RI_p = 1000$ was used with the precision model while a value of $RI_s = 100$ was used with the simple model. It is evident by consideration of the fit in Figure 3.3 that, in general, the model with the first-order lag neuromuscular system gives the best results.

Figure 3.13 shows the effect of a more accurate approximation of the time delay. The first-order approximation of the time delay used in all studies thus far is

$$e^{-\tau S} = \frac{-s + 2/\tau}{s + 2/\tau}$$
 (3.44)

A more accurate second-order approximation is

$$e^{-\tau S} = \frac{(-s + 4/\tau)^2}{(s + 4/\tau)^2}$$
 (3.45)

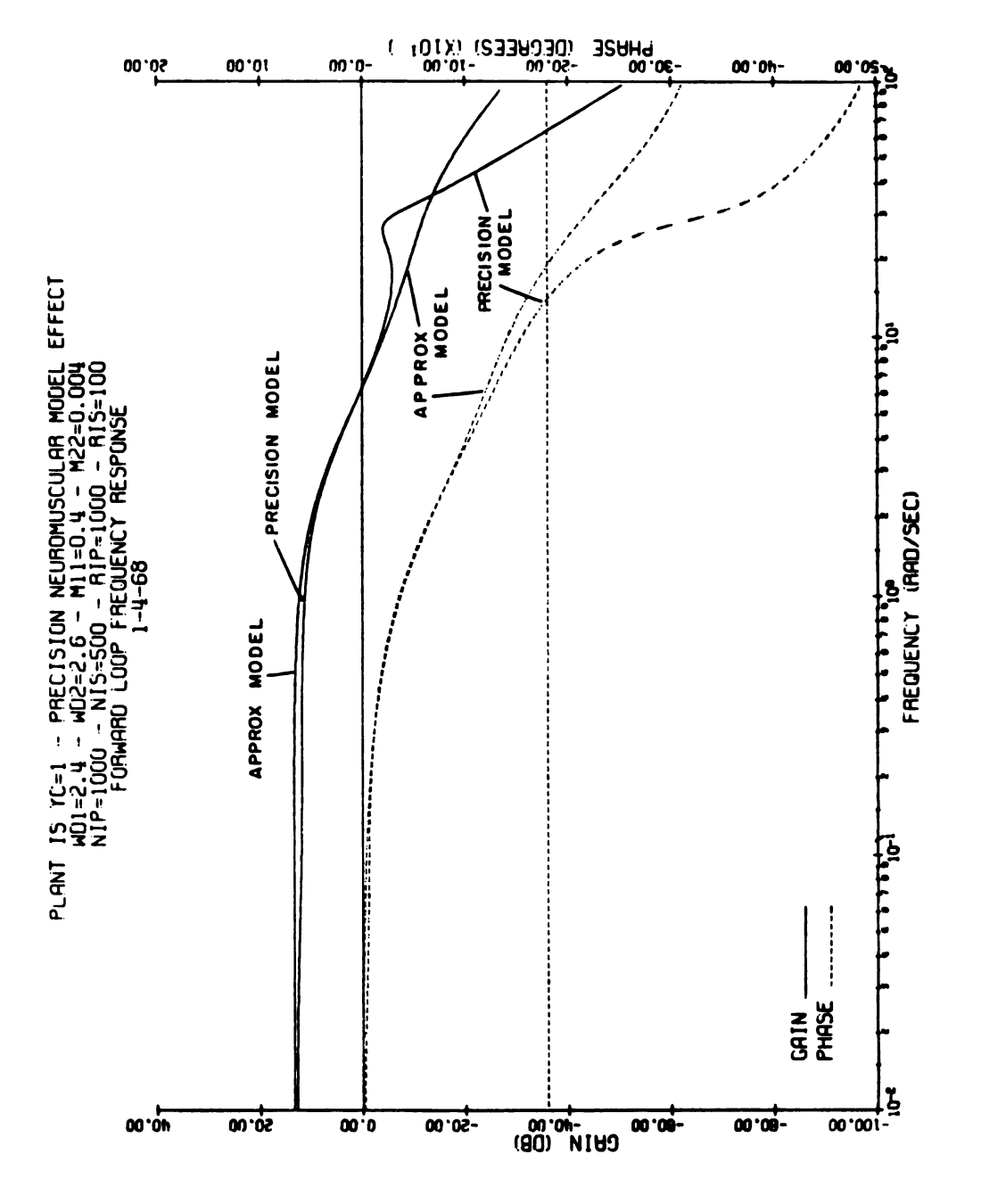


Figure 3.12. Effect of a precision neuromuscular lag.

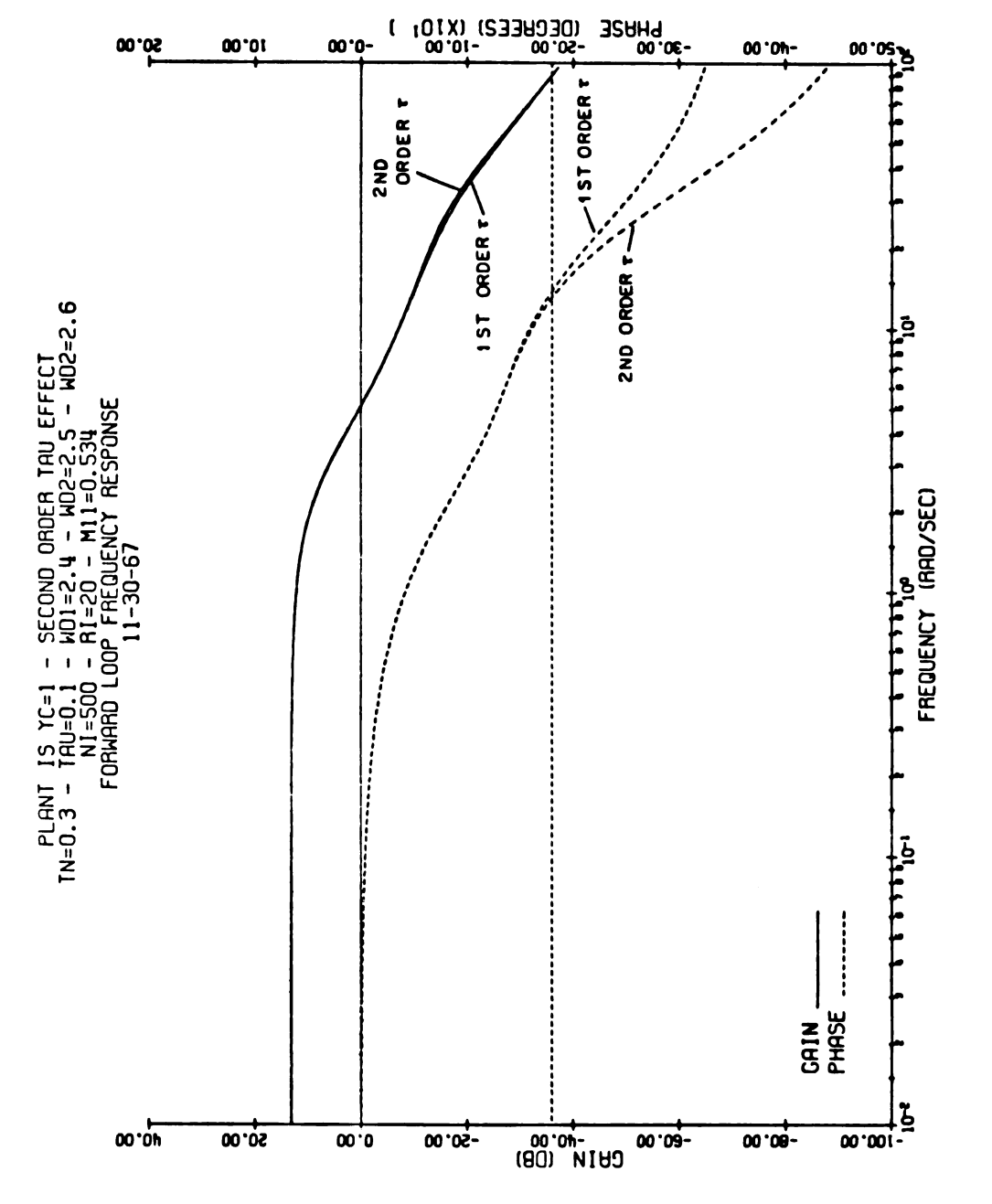


Figure 3.13. Effect of a second-order time delay.

Comparison of Figure 3.13 with the data given in Figure 3.3 shows that the high frequency gain and phase characteristics are improved somewhat by the more accurate approximation of the time delay.

Figure 3.14 shows the effect of changing the measurement noise n. The smaller the noise, the higher the overall gain. Also, the smaller the noise, the smaller the phase shift. Controlled experiments given by Bearne and Kahn [44] on the addition of noise to the display variable confirm this result.

Figure 3.15 shows the effect of changes in the cost function associated with the control. Since the cost function can be written as

$$J = E \left\{ \int_{0}^{t} \left(x^{T} \frac{Q}{r} x + u^{2} \right) dt \right\}$$
 (3.46)

(see Appendix C), this plot essentially shows the relative effects of changes in the weightings associated with x and u. Referring to Figure 3.15, the results are unaffected as $\frac{1}{r}$ becomes very large, i.e., the effect of the cost on u becomes negligible.

Figure 3.16 shows the effect of changes in the forcing function variance. As given by (3.26), the variance is

$$\sigma_i^2 = 0.468 \, m_{11}$$
 (3.28)

and, with variances of 0.1, 0.25, and 0.5, the corresponding values for m_{11} are 0.214, 0.534, and 1.068. Since a change in the

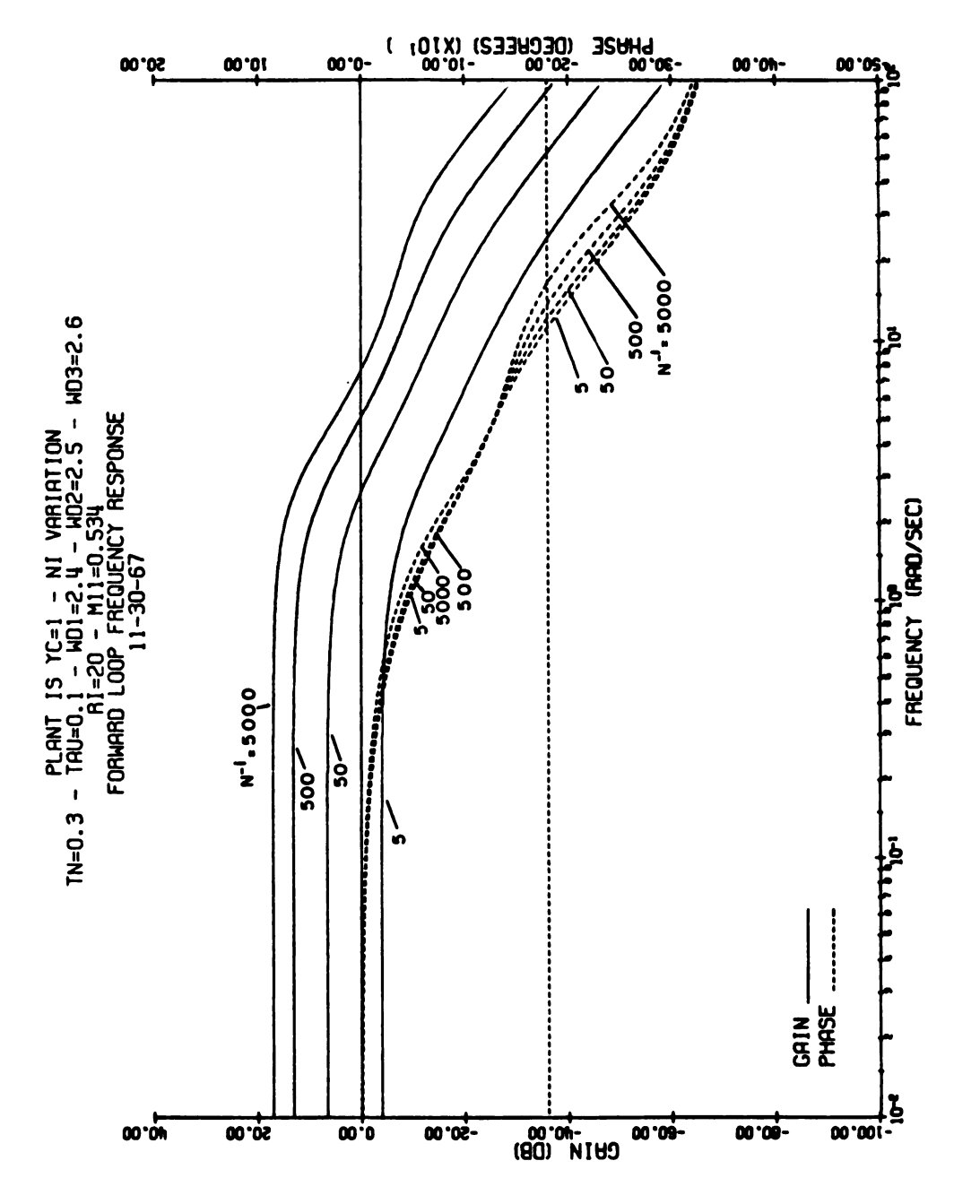


Figure 3.14. Effect of the measurement noise.

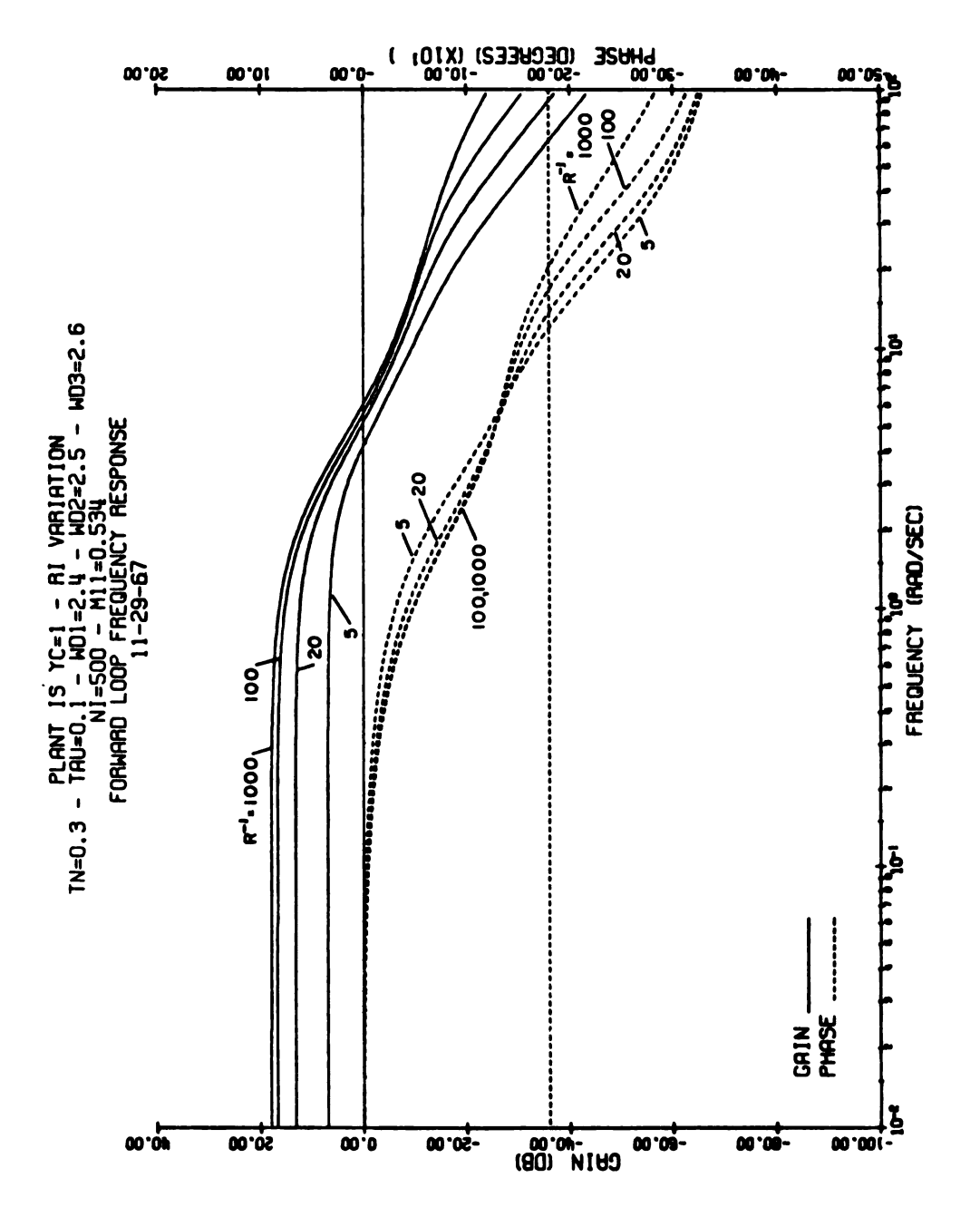


Figure 3.15. Effect of the cost associated with u.

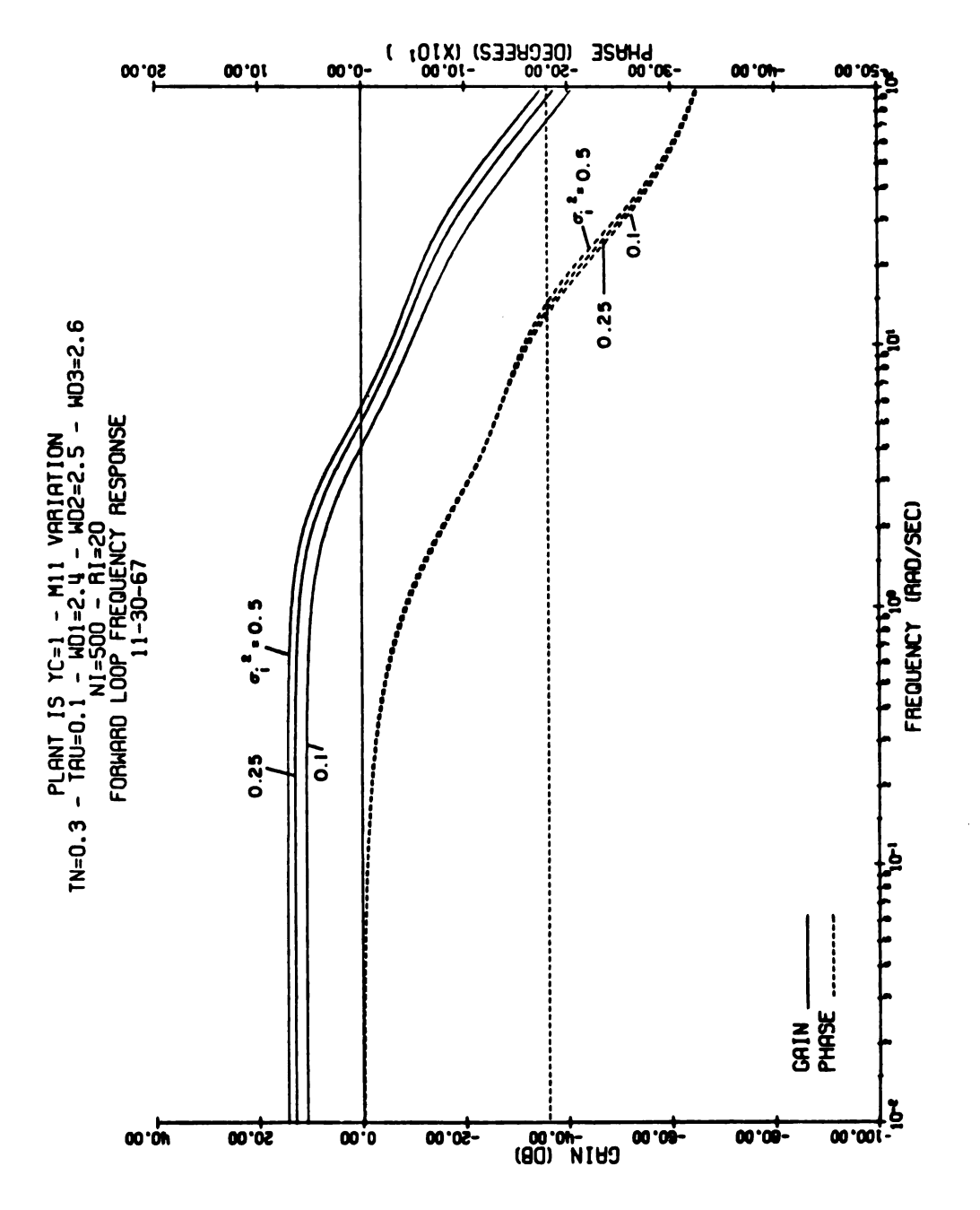


Figure 3.16. Effect of the forcing function variance.

amplitude of the inputs changes the results, so that superposition does not hold, a nonlinear characteristic of the model is evident.

Figure 3.17 shows the effect of drift for the plant $Y_c = 1$. A higher drift gives a higher gain at low frequencies and increased phase shift at mid-frequencies.

Figure 3.18 shows the effect of the forcing function bandwidth on the plant $Y_c = 1/s$ holding the variances of the forcing functions constant at

$$\sigma_i^2 = 0.534$$
 (3.47)

The data points shown are the mean values of the experimental data reported by McRuer et al. in [5] using the three forcing functions $F_{1..5}$, $F_{2..5}$, and F_4 shown in Table 3.1. The \pm 1σ ranges for the data with the $F_{2..5}$ input are given in Figure 3.5. The \pm 1σ ranges for the data with the $F_{1..5}$ and F_4 forcing functions are essentially the same although some of the low frequency ranges are somewhat larger. The gain curves fit quite well but there seems to be greater effect on the model than on the data. The fits of the phase shift curves are good but not as close. Nevertheless, the general trend of the changes in gain and phase shift are present.

Figure 3.18 also shows that there is a marked difference in low frequency phase shift for the three forcing functions. In fact, at ω = 0.01 the phase shift with F₄ is almost -180 degrees, while for F_{1.5} and F_{2.5} it is greater than zero. It was found that the low frequency phase shift is very sensitive to the

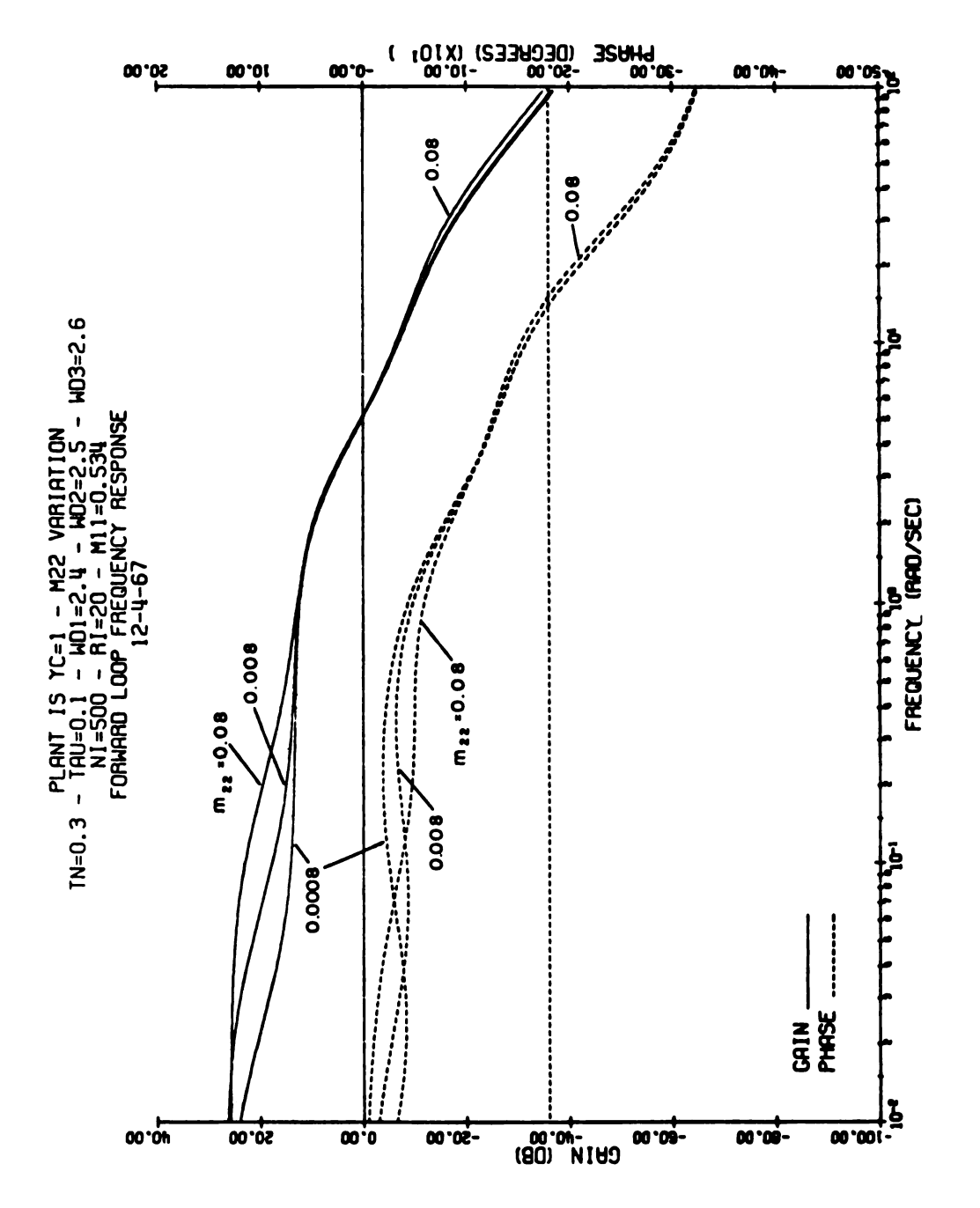


Figure 3.17. Effect of the drift.

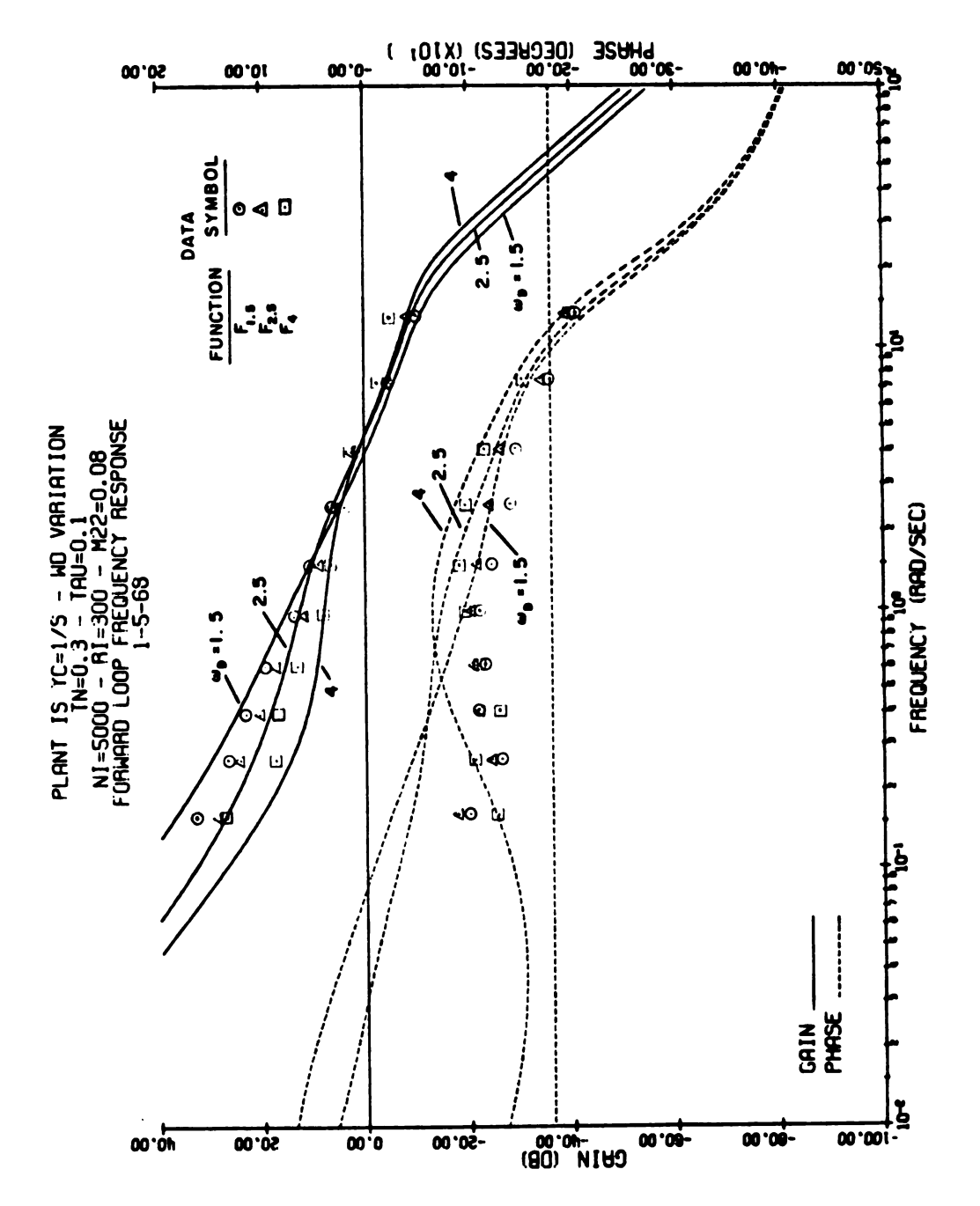


Figure 3.18. Effect of the forcing function corner frequency.

parameters n, r, and m_{22} . This sensitivity may account for the much greater low frequency variability present in the data for some of the plants in [5] which has been attributed to "indifference" on the part of the operator.

Figure 3.19 compares the responses using first, second, and third order bandlimited white noise forcing functions with constant variance. The bandlimiting functions considered are

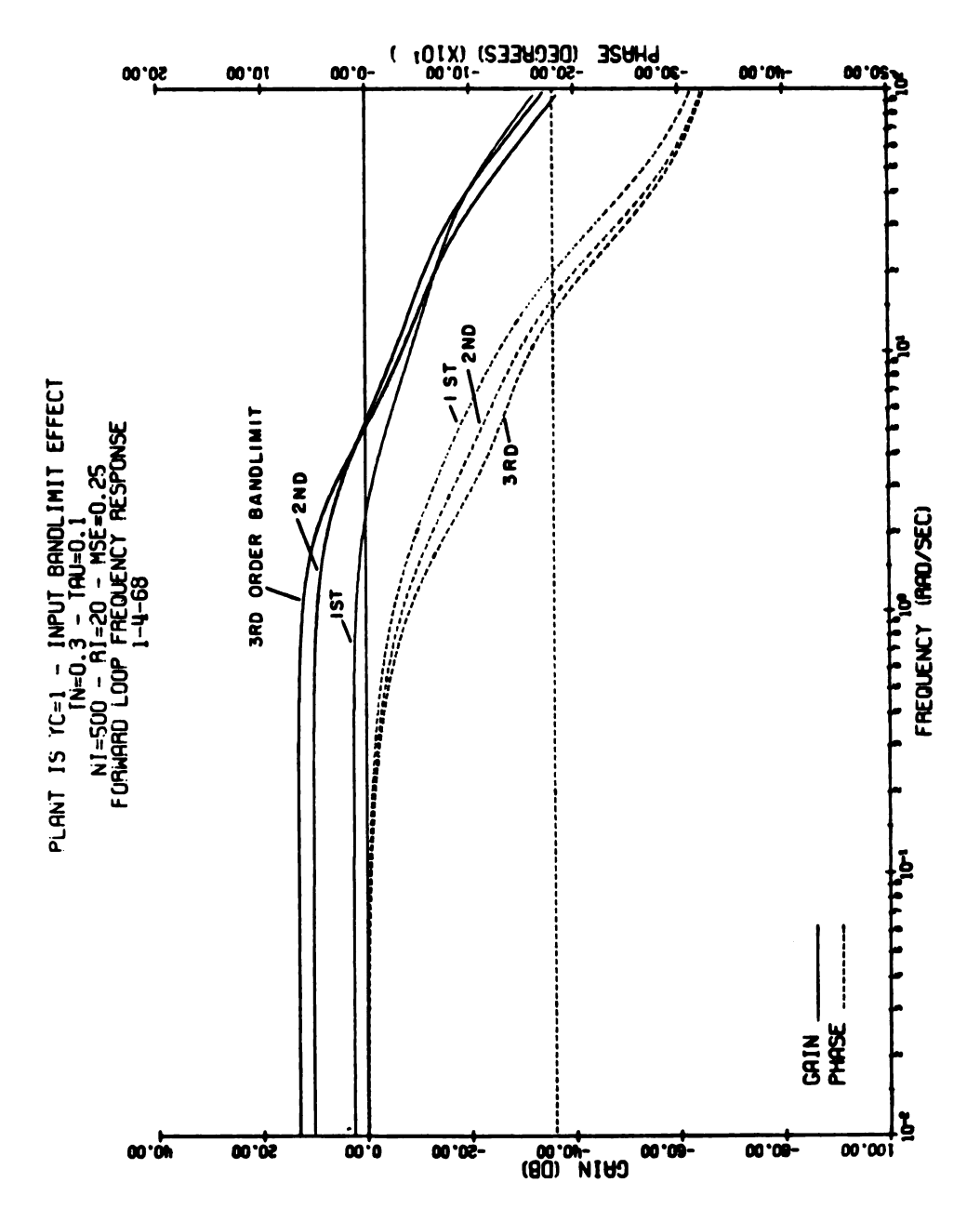
$$G_{F_1}(s) = \frac{1}{\left(\frac{s}{2.5} + 1\right)}$$
 (3.48)

$$G_{F_2}(s) = \frac{1}{\left(\frac{s}{2.4} + 1\right)\left(\frac{s}{2.6} + 1\right)}$$
 (3.49)

$$G_{F_3}(s) = \frac{1}{\left(\frac{s}{2.4} + 1\right)\left(\frac{s}{2.5} + 1\right)\left(\frac{s}{2.6} + 1\right)}$$
 (3.50)

It is shown in [4], for $Y_c = 1$, that the rectangular forcing function (Figure 3.2) produces essentially the same operator response as the third-order characteristic. Note that changes in the form of the bandlimiting has a significant effect on the gain and phase shift. The characteristics indicated in Figure 3.19 are consistent with the experimental results given in [4] and [5].

Figure 3.20 shows the effect of changes in the form of the cost function of x. The nominal cost function used in all



Effect of the order of the forcing function bandlimit. Figure 3.19.

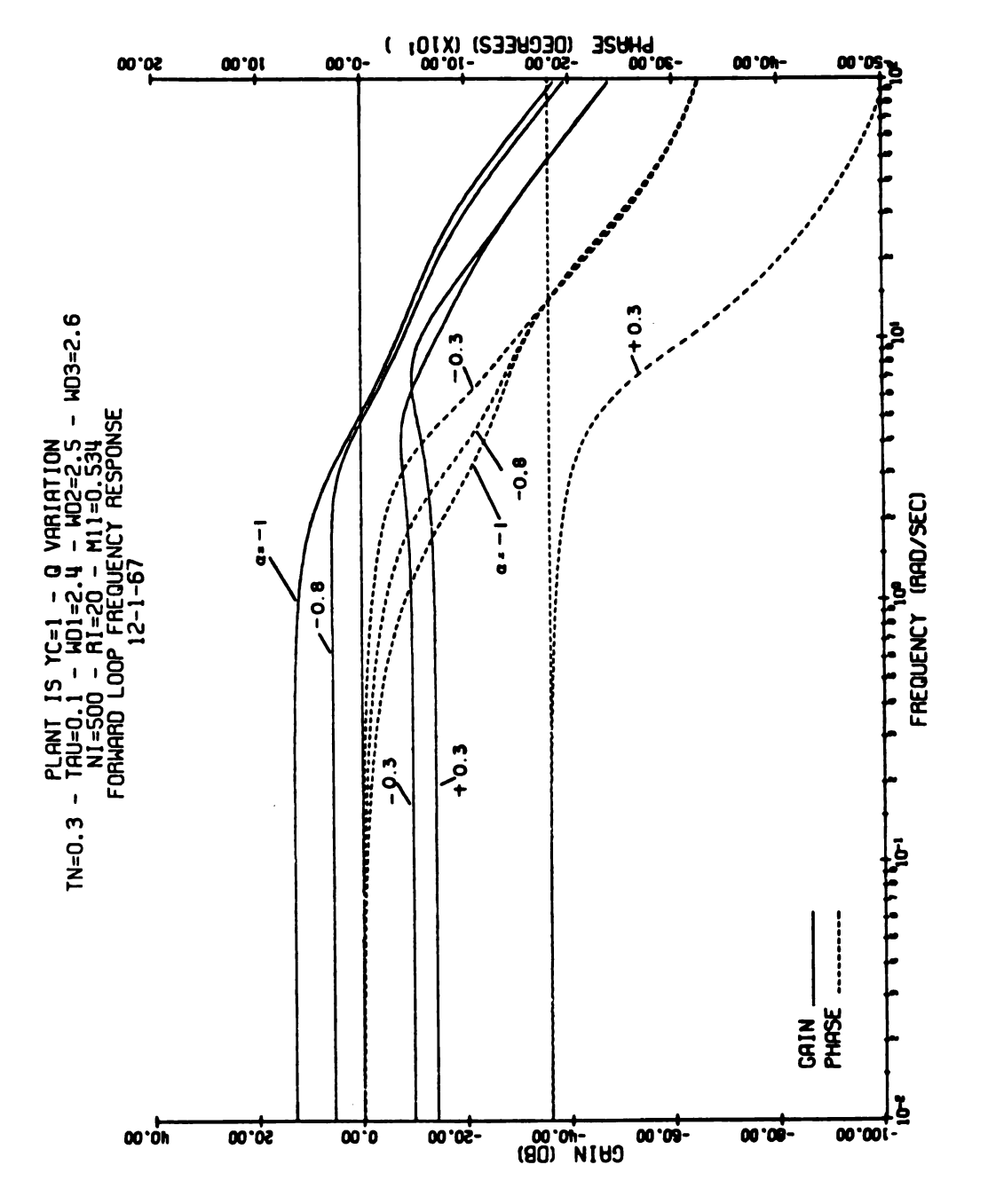


Figure 3.20. Effect of the off diagonal elements of Q.

analyses so far is

$$\mathbf{x}^{\mathsf{T}} \mathbf{Q}_{-1} \mathbf{x} = \mathbf{x}^{\mathsf{T}} \mathbf{C}^{\mathsf{T}} \mathbf{C} \mathbf{x} \tag{3.51}$$

$$= (x_1 - x_3)^2 (3.53)$$

where for the plant $Y_c = 1$ (Appendix B), x_1 is the man's output and x_3 is the forcing function. This cost function is altered to the form

$$= x_1^2 + 2a x_1 x_3 + x_3^2$$
 (3.55)

where a = -0.8, -0.3, +0.3. The results shown in Figure 3.20 indicate that vast change in the response occurs with changes in a. It is interesting to note for the case when a = 0 that the best thing the operator can do is nothing. This can be explained by

considering the complete cost function where

$$J = E \left\{ \frac{1}{2} \int_{0}^{t} f \left(x^{T}Qx + ru^{2} \right) dt \right\}$$
 (3.56)

$$= E \left\{ \frac{1}{2} \int_{0}^{t_{f}} \left(x_{1}^{2} + x_{3}^{2} + ru^{2} \right) dt \right\}$$
 (3.57)

Since nothing can be done about the forcing function x_3 , the best value for both x_1 and u is zero for all t. Since

$$x_1(0) \equiv u(0) \equiv 0$$
 (3.58)

this amounts to no control action by the human operator -- a transfer function of zero.

It is stated in [5] that the plant gain has very little effect on the man-plant transfer function. If the gain of the plant in the model is changed, there is a significant change in the resultant Bode plot. However, if the cost function associated with u is changed by an amount proportional to the square of the change in plant gain, the model solution remains the same. This is true since the augmented plant (Figure 3.1) is linear and the plant gain can always be moved back to the input u. Therefore, the plant gain will appear as a coefficient in the matrix B in the state model of

the augmented plant [see (2.1)]. If $BR^{-1}B^{T}$ remains unchanged, the solutions for K in (2.12) and for \hat{x} in (2.7) remain unchanged. In addition, from (2.11)

$$Bu = -BR^{-1}B^{T}K\hat{x} \tag{3.59}$$

indicating that the solution for x in (2.1) would also be unchanged. Therefore, if $BR^{-1}B^T$ is held constant with changes in plant gain, the model results will be unchanged. This implies that man changes his cost function R with plant gain. This also implies that the values for R required to match the data are directly related to the plant gains used to obtain the data.

4. SINE-WAVE TRACKING

One of the important features of the model of the human operator presented here is that it includes precognition. That is, it accounts for man's ability to predict the characteristics of a forcing function, for example, and to take advantage of this knowledge, so that a better or higher level of control is accomplished. This characteristic of man is demonstrated by using a sine-wave forcing function in a compensatory task as shown in Figure 4.1. Once the operator has tracked the sine-wave for a short period of time, he will have essentially zero time delay. Furthermore, he can close his eyes, eliminating the error signal, and still continue to track.

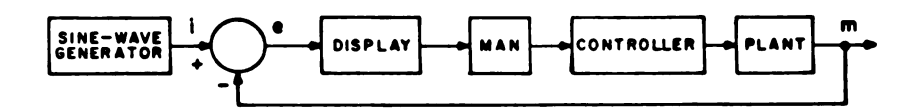


Figure 4.1. Sine-wave tracking block diagram.

In this chapter, the results of a sine-wave tracking experiment are given and related to the results of the model.

These results are also related to the experimental work reported by Pew et al. in [8]. In addition, tracking with the "eyes closed" is considered both experimentally and with the model.

4.1 EXPERIMENTS

Experiments were performed with the aid of an analog computer using the system shown in Figure 4.1. The sine-wave forcing function had a frequency of 7.159 rad/sec and a half-amplitude of 1.414 volts. A five-inch CRT (cathode ray tube) display was used (Figure 4.2) with the gain set at 2 cm/volt. The controller was a hand operated force sensing device (Figure 4.3), operated around its pitch axis, with an output of 0.003 volts/gram at a 3 inch moment arm. The displacement of the stick was approximately 0.005 mm/gram. A two minute run length was used.

A single subject was trained until his mean-squared error and integrated-absolute error reached a relatively consistent level from run to run. Typical recordings after training are shown in Figures 4.4 and 4.5. The measured mean-squared error of the run shown in Figure 4.4, normalized by the measured mean-squared error if the operator did nothing, is .083/1. The measured normalized integrated-absolute error is 2.32/8.78 = 0.265. The results of a corresponding experiment reported in [8] yielded a normalized integrated-absolute error of approximately 0.32. Thus, the results are reasonably close.

The top traces in both Figures 4.4 and 4.5 are the forcing function sine-wave i(t). The middle traces are the output m(t), and the lower traces are the difference or error e(t). Figure 4.4 shows a complete run while Figure 4.5 gives just the first part of a run with a greatly expanded time scale. Note that, in general, i(t) and m(t) are in phase, indicating that precognition is present. At



Figure 4.2. CRT display used for sine-wave tracking.

77



Figure 4.3. Controller used for sine-wave tracking.

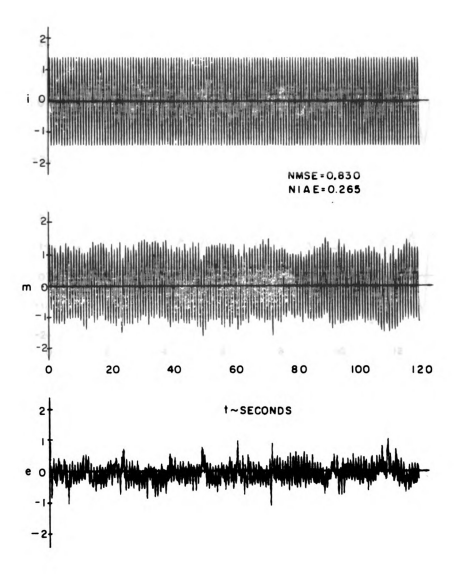


Figure 4.4. Complete sine-wave tracking run.

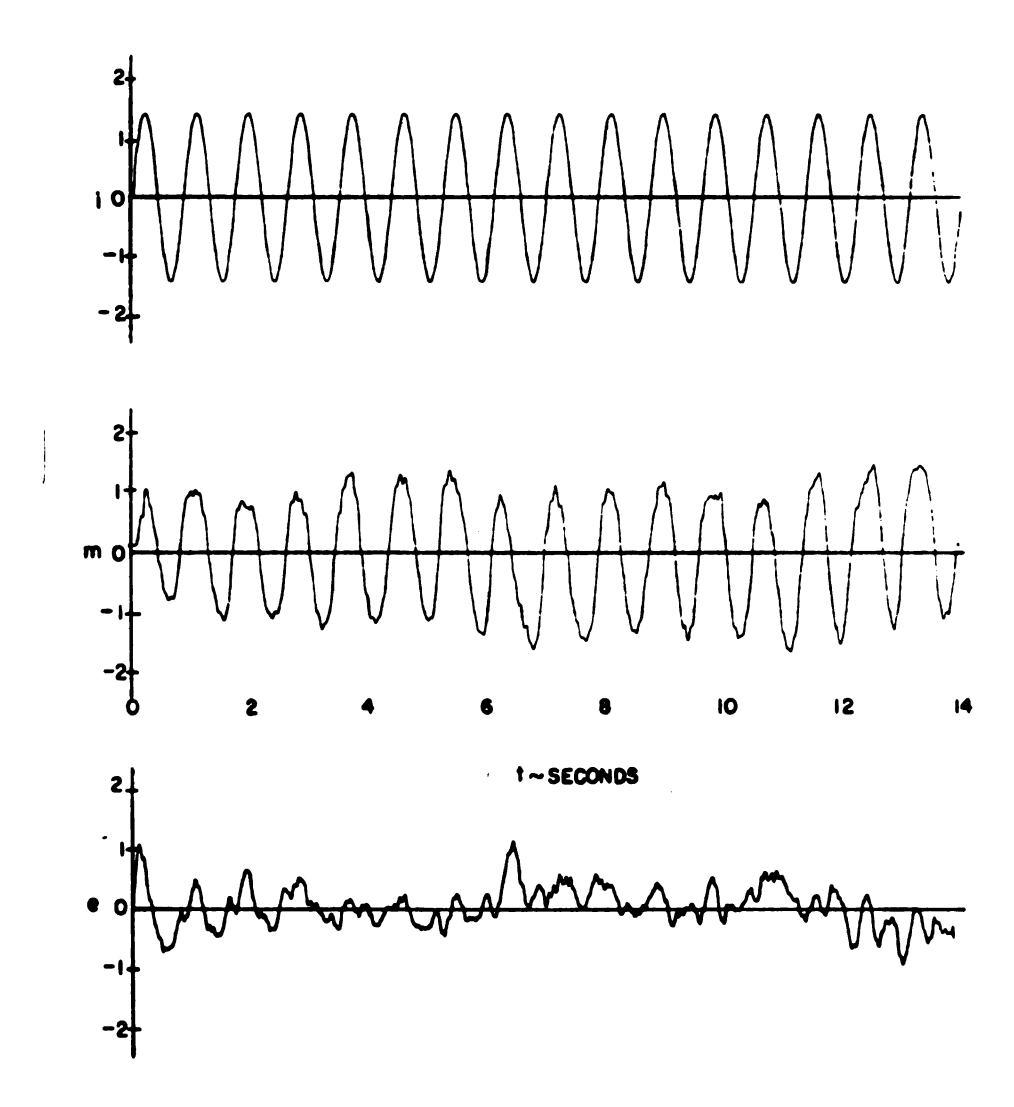


Figure 4.5. Partial sine-wave tracking run.

time zero, however, there is a delay of approximately 0.15 seconds before the subject starts to track, indicating no prediction initially. Also note that m(t) and e(t) contain frequencies (both higher and lower) other than the forcing function frequency. This illustrates the presence of noise. Figure 4.4 shows that the output m(t) is almost always of smaller amplitude than i(t), implying that the open loop gain is not very high. The first part of e(t) appears to consist primarily of the forcing function frequency. The amplitude appears to start out large and essentially damp out after about 4 seconds.

Figure 4.6 shows the results when, after tracking for six seconds, the operator closes his eyes. Thus, for t > 6, the operator performs as an open loop system without an error signal. The results show, however, that the operator continues to track the sine-wave, but with increased error. In a few runs, m(t) and i(t) were as much as 180 degrees out of phase after the eyes were closed. The operator apparently operates from a "built-in" source of information "learned" during pervious operations.

4.2 TRACKING MODEL

4.2.1 State Model of the Augmented Plant

The augmented plant employed in this study of sine-wave tracking is shown in Figure 4.7. This block diagram can be expanded as shown in Figure 4.8.

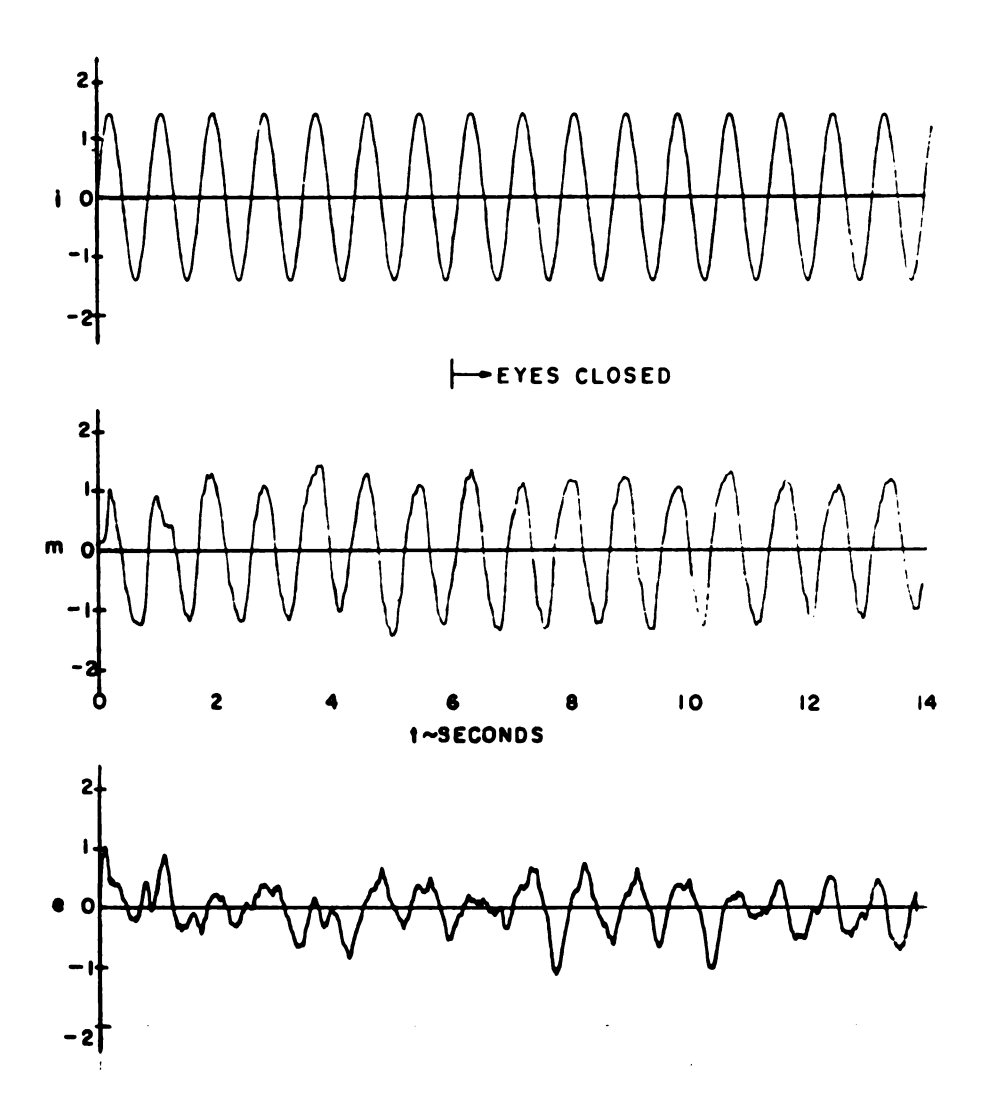


Figure 4.6. Sine-wave tracking with the eyes closed after 6 seconds.

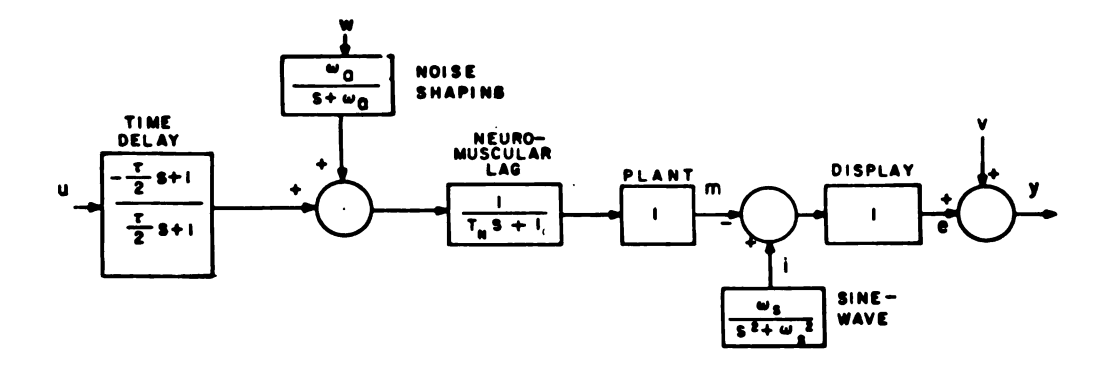


Figure 4.7. Augmented plant for sine-wave tracking.

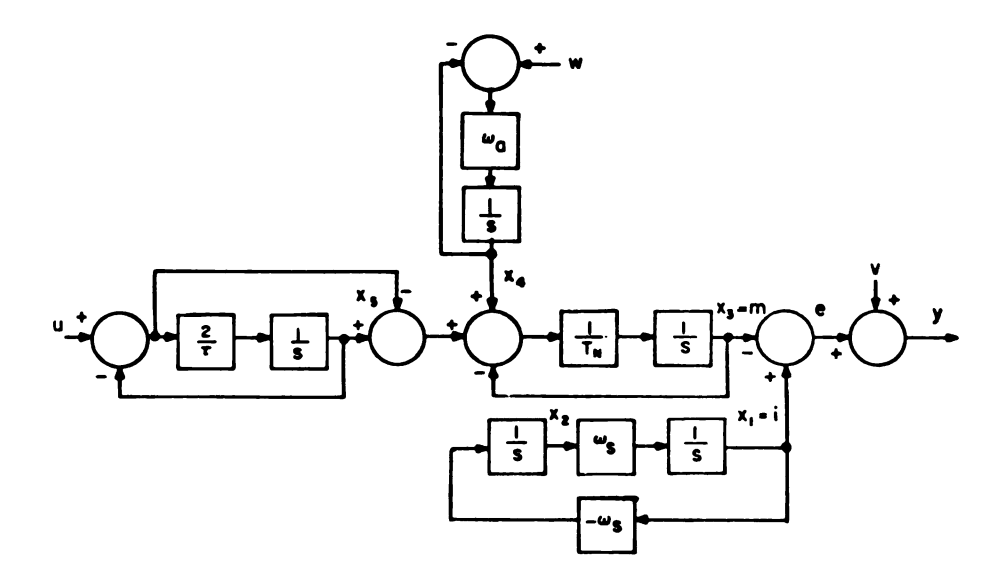


Figure 4.8. Block diagram for sine-wave tracking.

From Figure 4.8 the state model process equations are

$$\frac{d}{dt} \begin{bmatrix} \mathbf{x} & 1 \\ \mathbf{x} & 2 \\ \mathbf{x} & 3 \\ \mathbf{x} & 4 \\ \mathbf{x} & 5 \end{bmatrix} = \begin{bmatrix} 0 & \omega_{S} & 0 & 0 & 0 & 0 \\ -\omega_{S} & 0 & 0 & 0 & 0 & 0 \\ 0 & 0 & -1/T_{N} & 1/T_{N} & 2/T_{N} \\ 0 & 0 & 0 & -\omega_{a} & 0 \\ 0 & 0 & 0 & 0 & -2/\tau \end{bmatrix} \begin{bmatrix} \mathbf{x}_{1} \\ \mathbf{x}_{2} \\ \mathbf{x}_{3} \\ \mathbf{x}_{4} \\ \mathbf{x}_{5} \end{bmatrix} + \begin{bmatrix} 0 \\ 0 \\ 0 \\ -1/T_{N} \\ 0 \\ 2/\tau \end{bmatrix} \mathbf{w} + \begin{bmatrix} 0 \\ 0 \\ 0 \\ \omega_{a} \\ 0 \end{bmatrix} \mathbf{w} \quad (4.1)$$

and the measurement is

$$y = (1 \ 0 \ -1 \ 0 \ 0) \begin{bmatrix} x_1 \\ x_2 \\ x_3 \\ x_4 \\ x_5 \end{bmatrix} + v \tag{4.2}$$

4.2.2 Model Parameters

As in Chapter 3, the neuromuscular lag time constant and the time delay are, respectively

$$T_{N} = 0.3$$
 (4.3)

$$\tau = 0.1 \tag{4.4}$$

The sine-wave forcing function has a frequency

$$\omega_{s} = 7.159$$
 (4.5)

and half amplitude

$$a = 1.414$$
 (4.6)

A gaussian white noise source w shaped by a first-order lag

$$G_{s}(s) = \frac{\omega_{a}}{s + \omega_{a}} \tag{4.7}$$

is applied at the input to the neuromuscular system. In addition, a gaussian white noise input v uncorrelated with w is added to the measurement y. Since v and w are white noise, their covariances are

$$E \{v(t + \tau)v(t)\} = n\delta(\tau)$$
 (4.8)

$$E \{w(t + \tau)w(t)\} = m\delta(\tau)$$
 (4.9)

As in previous models, the cost function matrices are

$$R = r \tag{4.11}$$

where Q has been chosen so that e^2 is minimized.

The parameters n, m, ω_a , and r in (4.7), (4.8), (4.9), and (4.11) are selected so that the model gives results consistent, insofar as possible, with the experimental results. As described in more detail below, the values selected for these parameters are

$$n = 1/300 (4.12)$$

$$m = 0.25$$
 (4.13)

$$\omega_{a} = 4 \tag{4.14}$$

$$r = 1/50$$
 (4.15)

4.2.3 Covariance Matrix

The covariance of $(x-\hat{x})$ as given by (2.9) is

$$\dot{P} = AP + PA^{T} - PC^{T}N^{-1}CP + DMD^{T}$$
 (2.9)

where from (2.10) the initial condition with $\hat{x}_0 = 0$ is

$$P(0) = E \left\{ x_0 x_0^T \right\}$$
 (2.10)

Upon substitution of the appropriate matrices from (4.1), (4.2), (4.8), and (4.9) into (2.9), the covariance of $(x-\hat{x})$ becomes

	L		_			<i>c</i>	
	$^{2\omega}_{\rm s}p_{12}$	-w _s (p ₁₁ -p ₂₂)	w _S P23+ T	$^{6}_{8}p_{23} + \frac{1}{1}(p_{14} - p_{13} + 2p_{15})$	ω _S P24-ω ₂ P14	6 2 2 2 2 2 2 2 2 2	
	-w _s (p ₁₁ -p ₂₂)	-2w _s p12	- ° p13+	$-\omega_{s}p_{13}+\frac{1}{T}(p_{24}-p_{23}+2p_{25})$	-45P14-4aP24	$-\omega_{S} p_{15} - \frac{2}{\tau} p_{25}$	
н • <u>с</u> .	$\begin{bmatrix} u_{s}p_{23} + \frac{1}{T_{N}}(p_{14}-p_{13}+2p_{15}) \end{bmatrix}$	(5) $-\omega_{S}P_{13} + \frac{1}{N}(P_{24} - P_{23} + 2P_{25})$	$p_{23}^{+}2p_{25}) = \frac{2}{T_N}(p_{34}^{-}p_{33}^{+}2p_{35})$		$-\omega_{a}p_{3u} + \frac{1}{N}(p_{uu} - p_{3u} + 2p_{u_{5}})$	$-\frac{2}{\tau} p_{35} + \frac{1}{\tau_N} (p_{45} - p_{35} + 2p_{\xi\xi})$	
	μ _S ρ2μ-ω _a ρ1μ	-wsp14-wap24	- p3++	$-\omega_{a}p_{34} + \frac{1}{I_{N}}(p_{44} - p_{34} + 2p_{45})$	-E 20 0 4 4	- 2 p45-wap45	
	$\omega_{\rm S} p_{25} - \frac{2}{\tau} p_{15}$	$-\omega_{\rm S} p_{15} - \frac{2}{\tau} p_{25}$	- 2 p35+ :		- 1 p45-wap45	- 4 P55	
	J						
	(p ₁₁ -p ₁₃) ²	(p13-p13) (p12-p23)	(p11-p13) (p13-p33)	(p11-p13) (b14-b34)	(P11-P13) (P15-P35)		
	(p ₁₂ -p ₂₃)(p ₁₁ -p ₁₃)	(p ₁₂ -p ₂₃) ²	(p ₁₂ -p ₂₃) (p ₁₃ -p ₃₃)	(p12-p23) (p14-p34)	(p ₁₂ -p ₂₃)(p ₁₅ -p ₃₅)		
- E	(p13-p33) (p11-p13)	(p ₁₃ -p ₃₃) (p ₁₂ -p ₂₃)	(p ₁₃ -p ₃₃) ²	(p13-p33) (b14-p34)	(p ₁₃ -p ₃₃) (p ₁₅ -p ₃₅)		
	(p14-p34)(p11-p13)	(P14-P34) (P12-P23)	(p14-p34) (p13-p33)	(p ₁₄ -p ₃₄) ²	(p14-p34) (p15-p35)		
	(P15-P35) (P11-P13)	(P15-P35) (P12-P23)	(p15-p35) (p13-p33)	(p15-p35) (p14-p34)	(p ₁₅ -p ₃₅) ²		
		ء د د	ر د د				
		, 0					
		0 0	0			(4.16)	
		0	e a a			,	
		•	<u> </u>				

In the time solutions for P that follow, it is assumed that, after training, the operator has non-zero initial estimates of the covariance of the forcing function only. By (3.3) and (4.6), the initial variances of x_1 and x_2 are 1. Since x_1 and x_2 are orthogonal, the cross-variances are zero. Hence

In view of the assumption that

$$p_{15}(0) = p_{25}(0) = p_{35}(0) = p_{45}(0) = p_{55}(0) = 0$$
 (4.18)

it follows from (4.16) that the time solutions for these elements of P are identically zero for t > 0. Also, since P is symmetric, the unknowns in P for $t \ge 0$ reduce to the 10 elements: p_{11} , p_{12} , p_{13} , p_{14} , p_{22} , p_{23} , p_{24} , p_{33} , p_{34} , and p_{44} .

4.2.4 Optimal Control Law

The optimal control law as given by (3.8) is

$$\hat{C} = -R^{-1}B^{T}K \tag{3.8}$$

Since R^{-1} and B^{T} are known, the control law is known once (2.12) and (2.13) are solved for K. Both K and \hat{C} can be found using the computer program described in Appendix B. For the parameters defined above, this program yields

$$\hat{C}^{T} = \begin{bmatrix} \hat{c}_{11} \\ \hat{c}_{12} \\ \hat{c}_{13} \\ \hat{c}_{14} \\ \hat{c}_{15} \end{bmatrix} = \begin{bmatrix} 3.735 \\ 5.567 \\ -4.388 \\ -1.952 \\ -1.753 \end{bmatrix}$$

$$(4.19)$$

4.2.5 Filter Model

From (2.7), (2.8), and (2.11), the state model for the filter is

$$\hat{x} = A\hat{x} + PC^{T}N^{-1}(y-C\hat{x}) + Bu$$
 (4.20)

where it is assumed that

$$\hat{\mathbf{x}}_{0} = 0 \tag{4.21}$$

With this assumption, it is implied that the operator's initial estimate of the augmented plant state vector is zero.

By substitution and simplification (4.20) becomes

This model is the same as the state model for the augmented plant, except for the last term. As shown, the last term involves the measurement y, the estimate of y which is $(\hat{x}_1 - \hat{x}_3)$, the noise term n, and elements of the covariance of $(x - \hat{x})$.

4.3 MODEL VALIDATION

Time solutions for the complete sine-wave tracking model as described above, were realized on an analog computer. Although there are minor accuracy problems with the analog computer in this application, the results shown in Figures 4.9 through 4.16 provide a good "feel" for the solutions.

Figure 4.9 shows the forcing function i(t), the operator's output m(t), and the error e(t), when no noise is applied.

Since there is no noise, these are the mean values of the response.

The amplitude of m(t) is smaller than i(t) and indicates, as for a real human operator (Figure 4.2), an open loop gain that is not very high. The m(t) trace exhibits an initial time delay of approximately 0.1 seconds. After the first cycle, however, there is very little time delay.

Figure 4.10 shows the mean state vector superimposed on the mean estimated state vector. After a half cycle, the two are

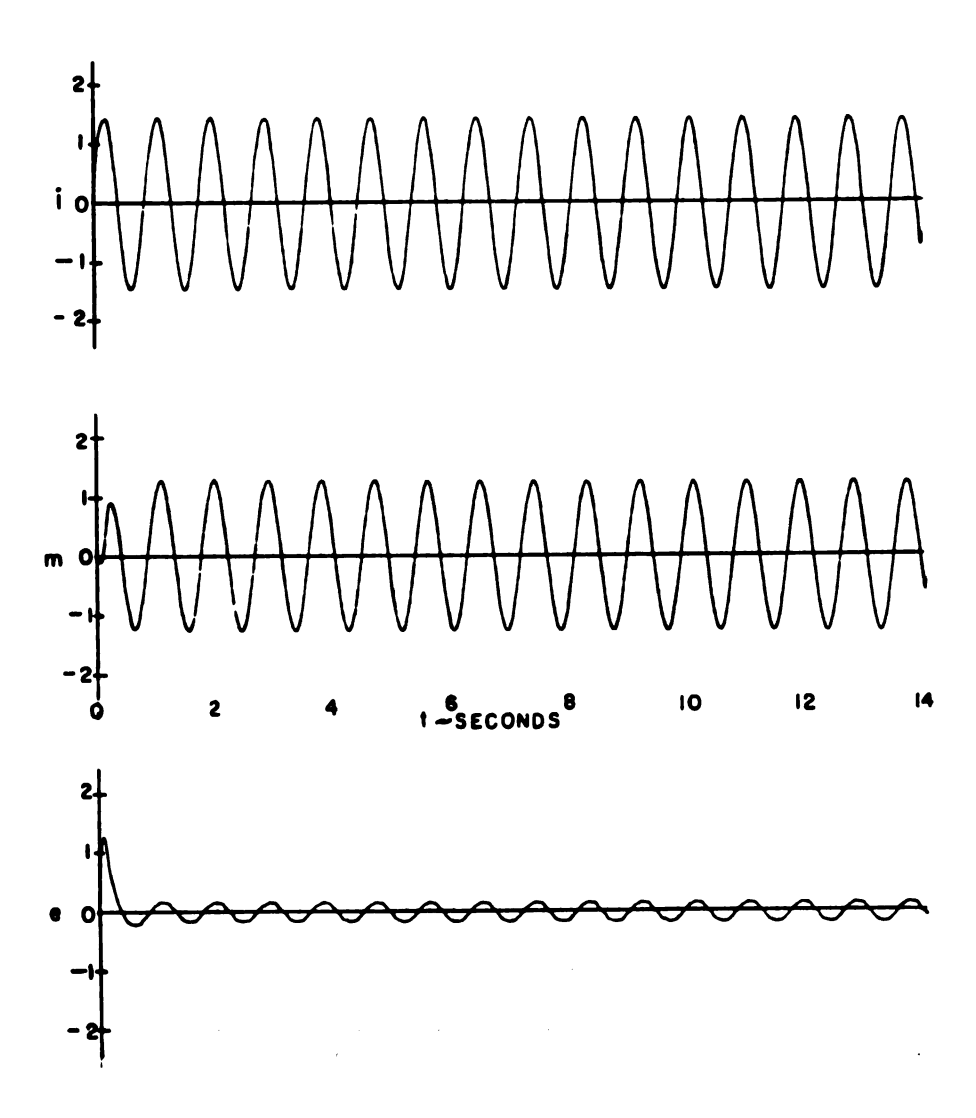


Figure 4.9. Mean sine-wave tracking model response.

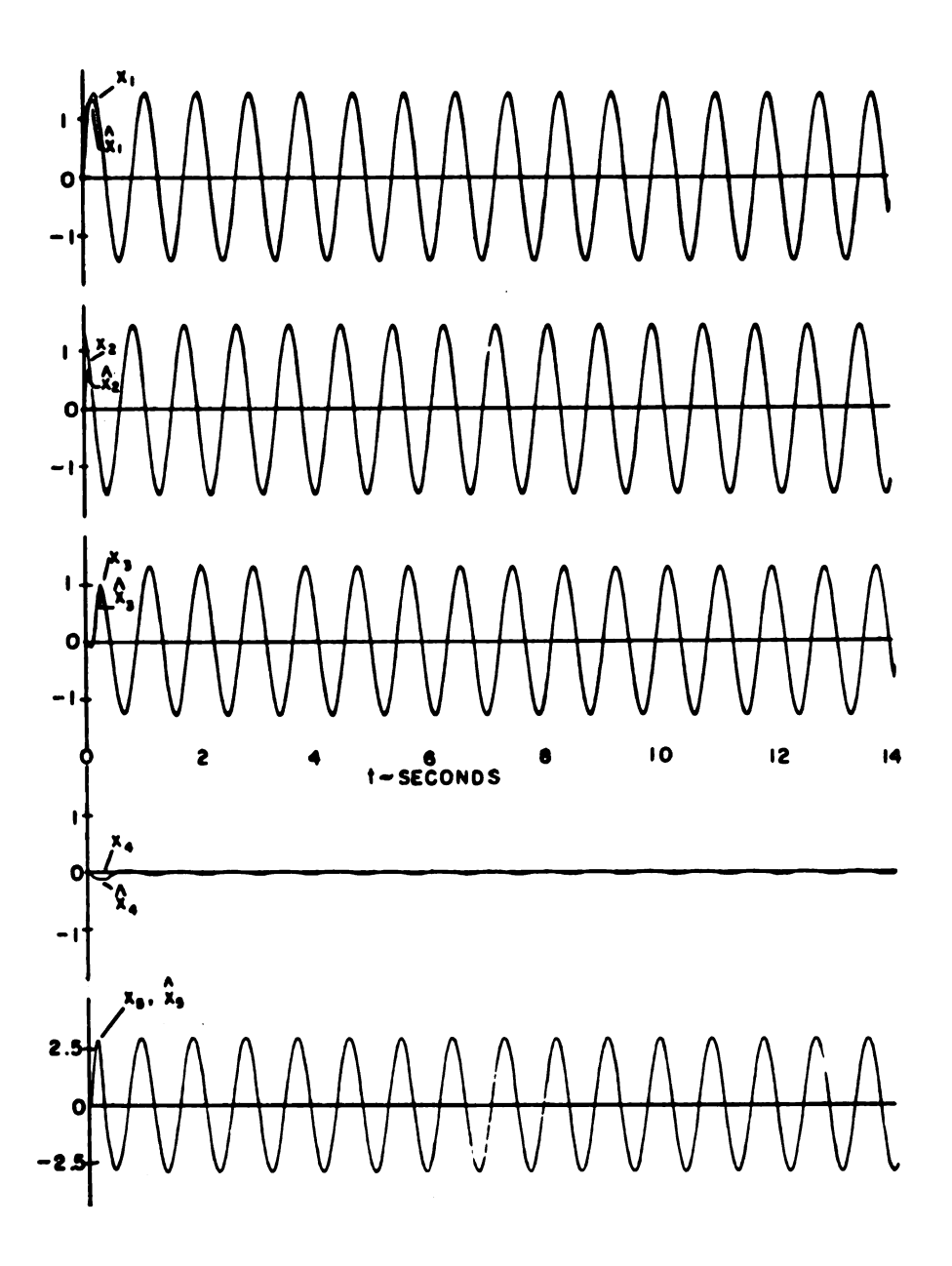


Figure 4.10. Mean x and \hat{x} .

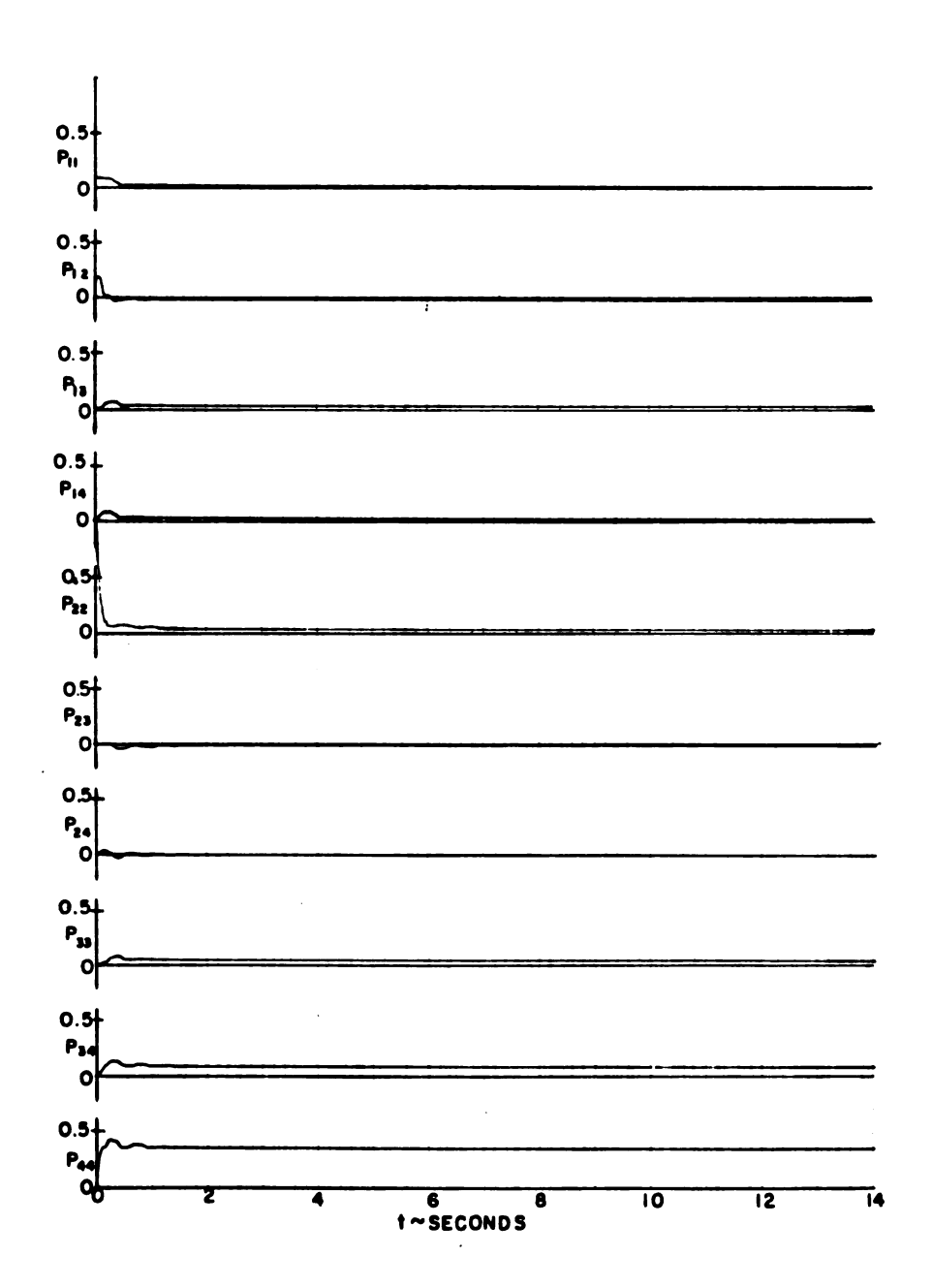


Figure 4.11. Solution for P.

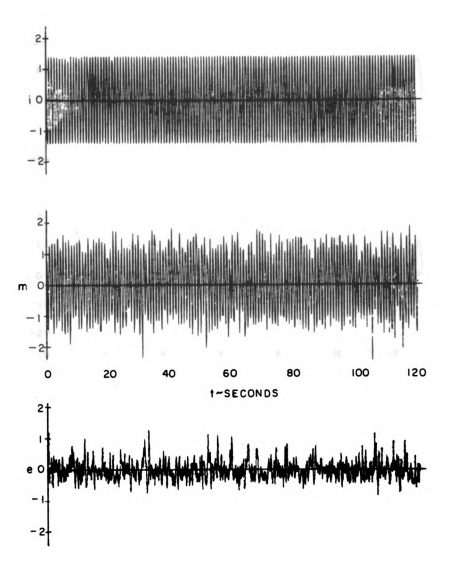


Figure 4.12. Complete sine-wave tracking model run.

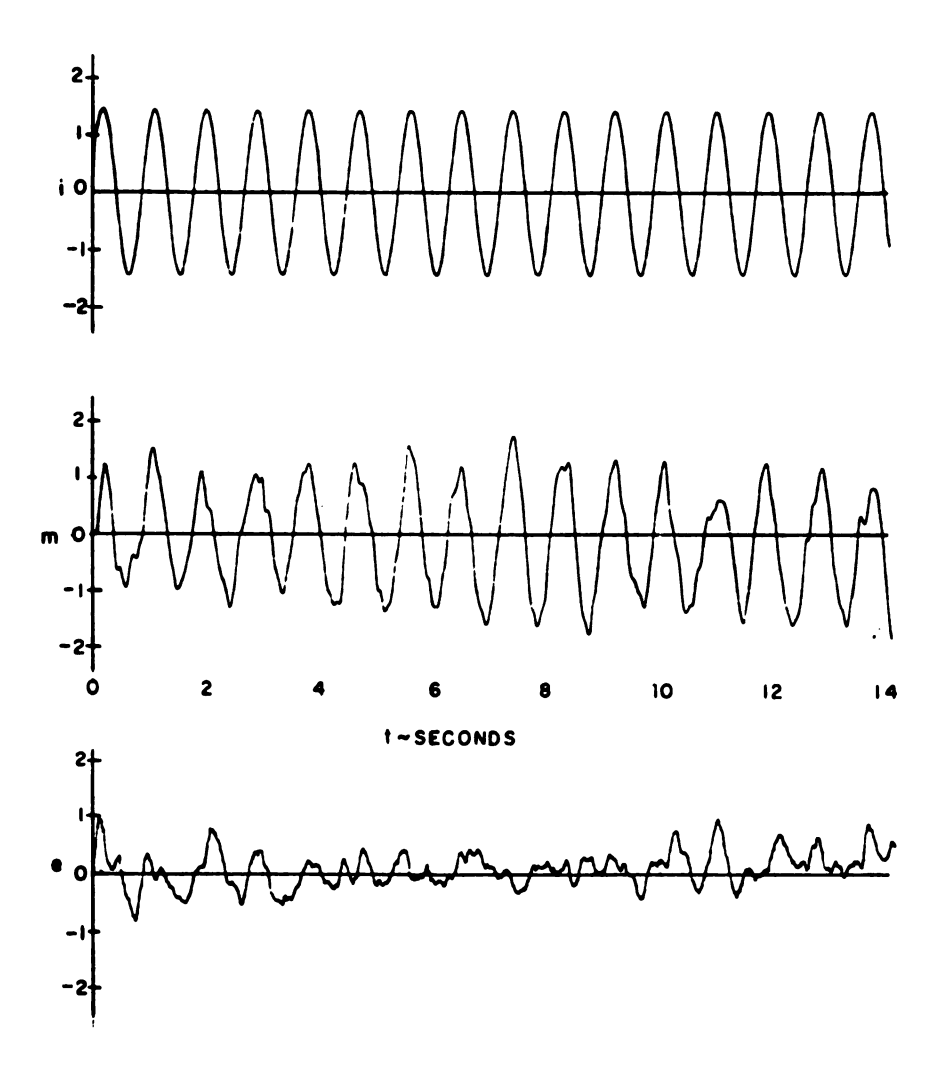


Figure 4.13. Partial sine-wave tracking model run.

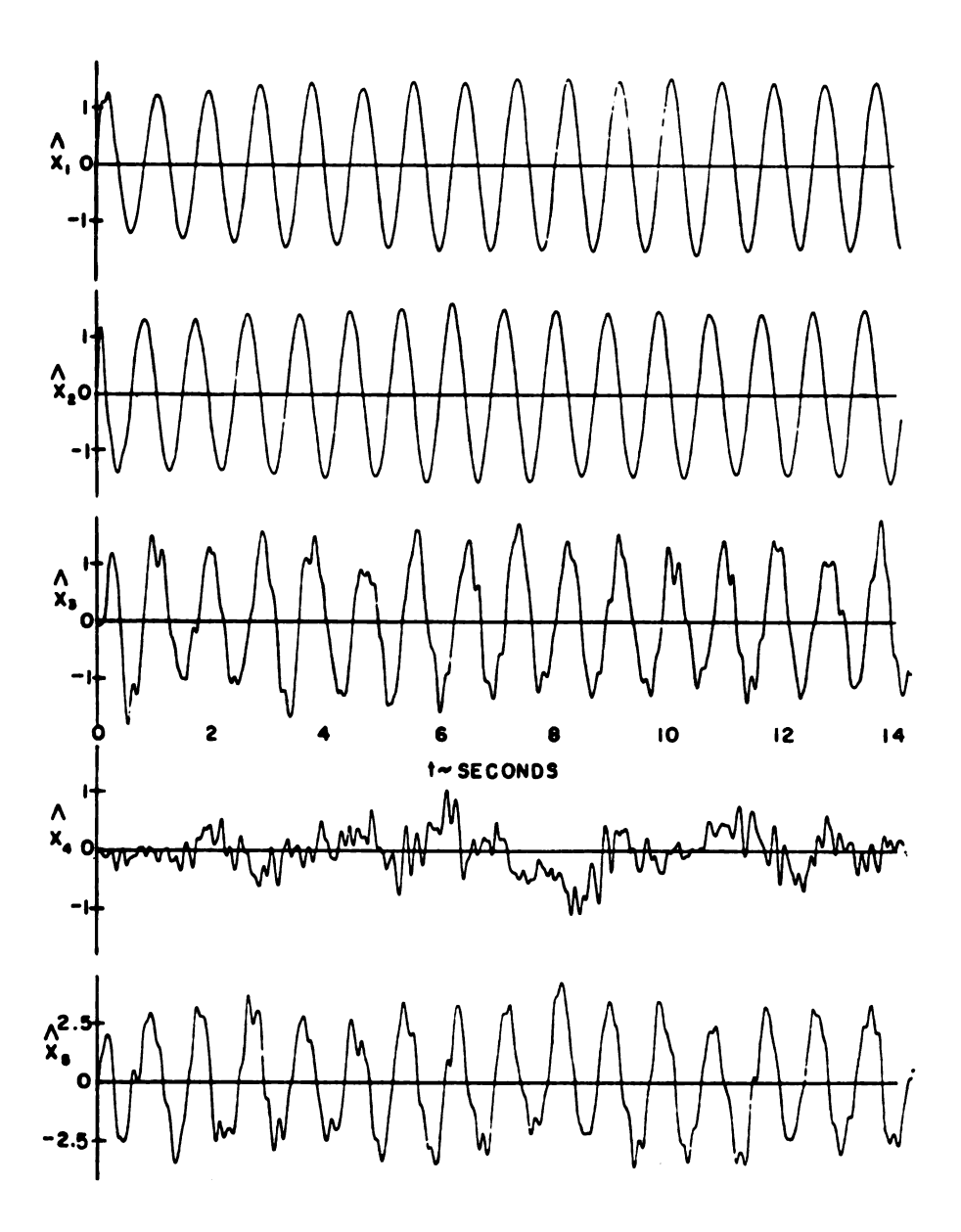


Figure 4.14. Solution for \hat{x} -- with noise.

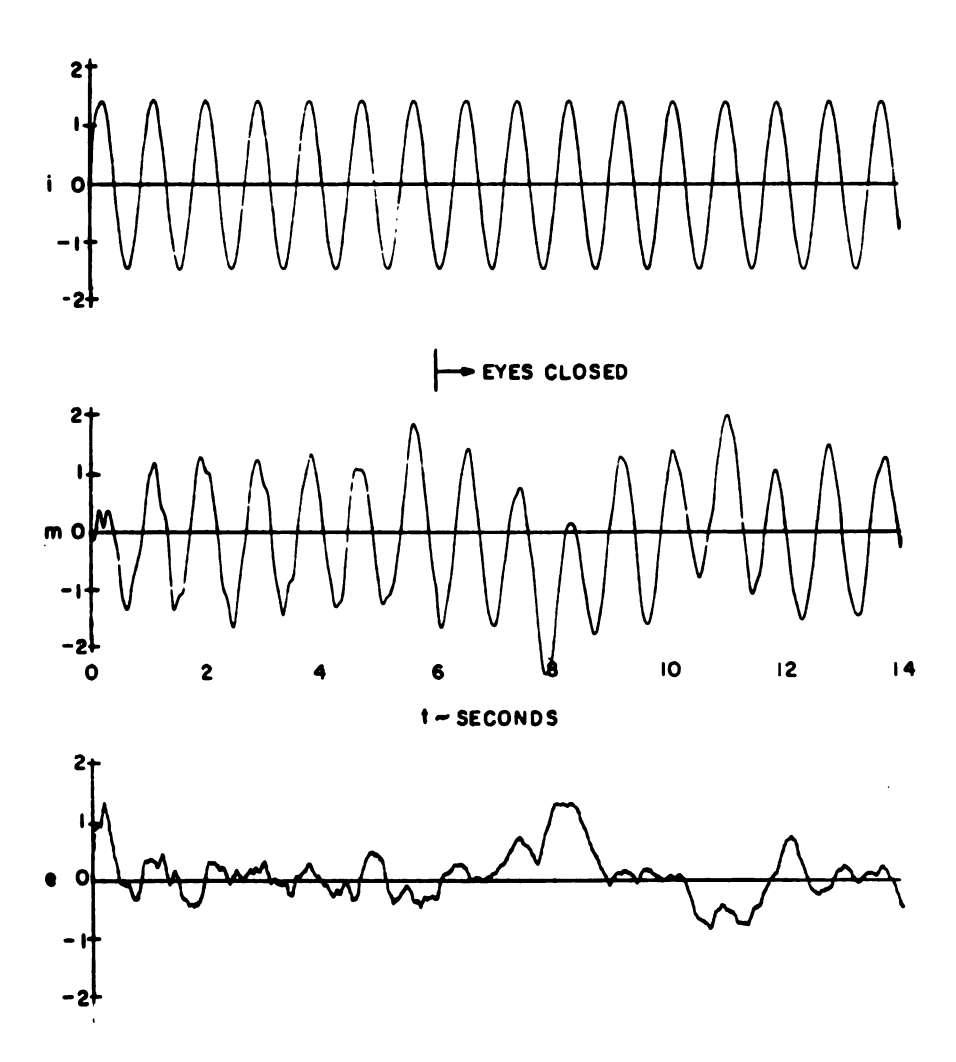


Figure 4.15. Model tracking with eyes closed after 6 seconds.

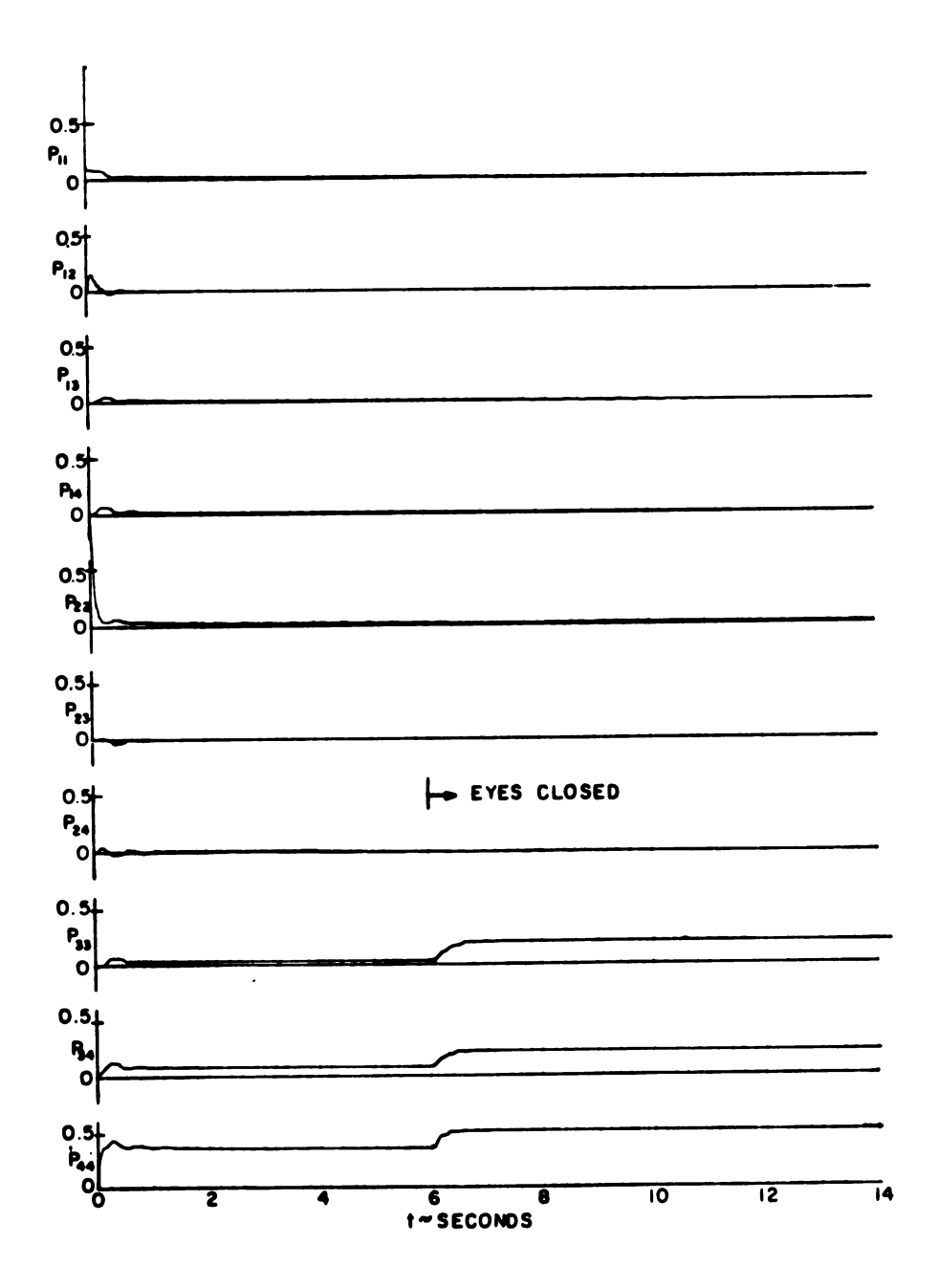


Figure 4.16. Solution for P with the eyes closed after 6 seconds.

essentially the same. The mean estimate of the noise given by x_4 is zero (except for computer error) after the same period of time. The values for x_5 and \hat{x}_5 are the same starting from time zero since the variance of $(x_5-\hat{x}_5)$ is identically zero for all t.

Figure 4.11 shows the solutions for the elements of P. As indicated, the solutions reach nearly steady-state conditions in less than two seconds. Using the digital computer solution described in Appendix B, however, the P matrix solution at 2 seconds is

$$P = \begin{bmatrix} 1.292E-02 & 9.467E-04 & 9.846E-03 & 1.572E-02 & 0.0 \\ 9.467E-04 & 9.983E-03 & -3.684E-03 & 2.079E-03 & 0.0 \\ 9.846E-03 & -3.684E-03 & 3.871E-02 & 7.934E-02 & 0.0 \\ 1.572E-02 & 2.079E-03 & 7.934E-02 & 3.470E-01 & 0.0 \\ 0.0 & 0.0 & 0.0 & 0.0 & 0.0 \end{bmatrix} (4.23)$$

and at 10 seconds it is

$$P = \begin{bmatrix} 2.669E-03 & -1.198E-04 & 2.175E-03 & 3.219E-03 & 0.0 \\ -1.198E-04 & 2.632E-03 & -1.265E-03 & 1.012E-04 & 0.0 \\ 2.175E-03 & -1.265E-03 & 3.154E-02 & 7.029E-02 & 0.0 \\ 3.219E-03 & 1.012E-04 & 7.029E-02 & 3.317E-01 & 0.0 \\ 0.0 & 0.0 & 0.0 & 0.0 & 0.0 \end{bmatrix} (4.24)$$

(The convergence criterion defined in Appendix B is met at t=10 seconds.) Considerable reductions in the elements of P occur that are not evident in Figure 4.11. These changes could have a large effect on the solution for x, and because of the large dynamic range dictated, it is the primary reason for accuracy problems with the analog computer.

Figure 4.12 shows a two-minute run corresponding to the two-minute run of the real human operator shown in Figure 4.4. The measured mean-squared error divided by the measured mean-squared error, if no control were applied, is 0.094/1. This agrees reasonably well with the value of 0.083/1 obtained for the real human operator. In addition, the normalized measured integrated-absolute error is 0.265/0.936 = 0.283. This also agrees quite well with the value of 0.265 obtained for the run shown in Figure 4.4 and with the value of 0.32 obtained by Pew et al. in [8].

Figure 4.13 is a partial run of the analog solution showing the first 14 seconds when the noise terms are included. Visual comparison with Figure 4.5 indicates that "generally" the same frequencies and characteristics are present. Note that, as in Figure 4.5, the forcing function appears to be predominant in e(t) for the first 4 seconds. The initial time delay, as in the case when no noise is applied, is approximately 0.1 second.

Figure 4.14 shows the solutions for the estimates of the state vector when noise is included. The solutions for \hat{x}_1 and \hat{x}_2 are quite close to the desired sine-waves while the solutions for \hat{x}_3 , \hat{x}_4 , and \hat{x}_5 are "noisy." The solutions for \hat{x}_1 and \hat{x}_2 take about four seconds to reach the forcing function amplitude. Note that this is longer than the corresponding time of one second for the mean values in Figure 4.10.

Figure 4.15 shows the solution when the "eyes" of the model are closed at six seconds by setting C = 0 in the solution for both P and \hat{x} . Note that after the "eyes" are closed the model

Continues to track, although the error has obviously increased. Figure 4.16 shows the solution for the covariance of $(x-\hat{x})$ for the same length of time. Note that p_{33} , p_{34} , and p_{44} increase rapidly to higher levels. A digital computer solution for P (Figure 4.17) shows that the other elements of P do not increase. This is contrary to what the human operator would do after a long period of time since after some unknown period of time he "loses" his estimates of the system parameters. This could be accounted for by including a parameter estimator block, in addition to the filter and controller. Nevertheless, for the time period of 14 seconds considered here, the results of Figure 4.15 for the model are close to those in Figure 4.6 for the real human operator.

Figure 4.18 is a Bode plot of the steady-state man-plant transfer function while tracking the sine-wave as obtained from the model. Note the high gain rise and sharp spike in the phase angle in the neighborhood of the forcing function frequency. Inspection of the printout for the plot shows that the forcing function frequency is located between the high and low gain spikes where at the sine-wave frequency

$$G_{10}(j7.159) = 18.88 \text{ db } 10.36 \text{ degrees}$$
 (4.25)

Since the phase shift at the forcing function frequency is nearly zero, there is essentially no time delay. This result agrees with the general characteristics in Figure 4.5 and with the statements of Pew et al. in [8], that no time delay is observed when a sine-wave is tracked.

P	T =	0.0	SECUNDS			
,	1.00 0.0 0.0	0E+0C	0.0 1.0CCE+00 0.0	0.0 0.0 0.0	0.0 0.0 0.0	0.0 0.0 0.0
	0.0		0.0	0.0	0.0 0.0	0.0
P	T =	1.012	SECONDS			
	3.82 1.06	7E-02 4E-03 7E-02 8E-02	3.824E-03 2.576E-02 -8.4C4E-03 7.024E-03 0.0	1.067E-02 -8.404E-03 4.145E-02 7.989E-02 0.0	1.916E-02 7.024E-03 7.989E-02 3.516E-01 0.0	0.0 0.0 0.0 0.0
P	T = -	2.012	SECONDS			
•	9.46	2E-02 7E-04	9.467E-04 9.983E-03	9.846E-C3 -3.684E-C3	1.572E-02 2.079E-03	0.0
		6E-03 2E-02	-3.684E-03 2.079E-03 0.0	3.871E-02 7.934E-02 0.0	7.934E-02 3.470E-01 0.0	0.0 0.0 0.0
P	T =	3.012	SECONDS			
	-1.06 7.16	3E-03 3E-03 7E-03 9E-02	-1.063E-03 7.831E-03 -4.325E-03 -5.536E-04 0.0	7.167E-03 -4.325E-G3 3.687E-G2 7.604E-02	1.009E-02 -5.536E-04 7.604E-02 3.399E-01 0.0	0.0 0.0 0.0 0.0
P	T =	4.012	SECONDS			
r	-2.08 4.54	6E-03 0E-04 0E-03 1E-03	-2.080E-04 6.966E-03 -3.261E-03 3.999E-04 0.0	4.540E-03 -3.261E-03 3.430E-02 7.296E-02 0.0	6.751E-03 3.999E-04 7.296E-02 3.360E-01 0.0	0.0 0.0 0.0 0.0

Figure 4.17. Digital computer printout of P with the eyes closed after 6 seconds.

```
T =
      5.022 SECUNDS
 5.076E-03
             3.715E-04
                         3.870E-C3
                                     6.177E-03
                                                 0.0
                                                 0.0
                       -1.971E-C3
 3.715E-U4
             5.099E-03
                                     9.264E-04
 3.870E-03
           -1.971E-03
                                     7.227E-02
                         3.320E-02
                                                  0.0
                                                  0.0
 6.177E-03
             9.264E-04
                         7.227E-02
                                     3.353E-01
 0.0
             0.0
                         0.0
                                     0.0
                                                  0.0
C=O AT T= 6.002 SECUNDS
T = 6.022 SECUNDS
                                     5.1CCE-03
 4.556E-03
            -9.926E-05
                        3.477E-03
                                                  0.0
-9.926E-05
            4.066E-03 -2.199E-03
                                   -4.115E-04
                                                  0.0
 3.477E-03
            -2.199E-03
                         3.857E-02
                                     8.371E-02
                                                  0.0
 5.100E-03 -4.115E-04
                         8.371E-02
                                     3.590E-01
                                                  0.0
 0.0
             0.0
                         0.0
                                     0.0
                                                 0.0
T =
      7. G47 SECONDS
 4.100E-03 -1.595E-04
                         1.69CE-04
                                     3.577E-05
                                                  0.0
                                                  0.0
            4.522E-03 -5.126E-04 -7.688E-05
-1.595E-04
                                     2.269E-01
                                                  0.0
           -5.126E-04
                         2.252E-C1
 1.690E-04
 3.577t-C5
          -7.688E-05
                         2.269E-01
                                     5.0CCE-01
                                                  0.0
 0.0
             0.0
                         0.0
                                     0.0
                                                  0.0
T =
      8.071 SECONDS
             2.629E-04 -1.594E-C5 -8.157E-C7
                                                  0.0
 4.282E-03
                                    -1.144E-06
                                                  0.0
 2.629E-04
             4.339E-03
                        -1.879E-05
                         2.271E-01
                                     2.271E-01
                                                  0.0
-1.594E-05
           -1.879E-05
-8.157E-07
           -1.144E-06
                         2.271E-01
                                     5.000E-01
                                                  0.0
 0.0
             0.0
                         0.0
                                     0.0
                                                  0.0
T =
      8.616 SECONDS
                                     1.559E-07
                                                  0.0
                         4.331E-06
 4.571E-03
             4.196E-05
                                                  0.0
                                     3.023E-08
             4.049E-03
                         4.954E-C7
 4.196E-05
                                                  0.0
 4.331E-06
             4.954E-07
                         2.271E-01
                                     2.271E-01
                                     5.000E-01
                                                  0.0
 1.559E-07
             3.023E-08
                         2.271E-01
             0.0
                                                  0.0
                                     0.0
 0.0
                         0.0
```

ABOVE MATRIX IS SS SOLUTION FOR P. TC WITHIN 0.01%

Figure 4.17. (Con't).

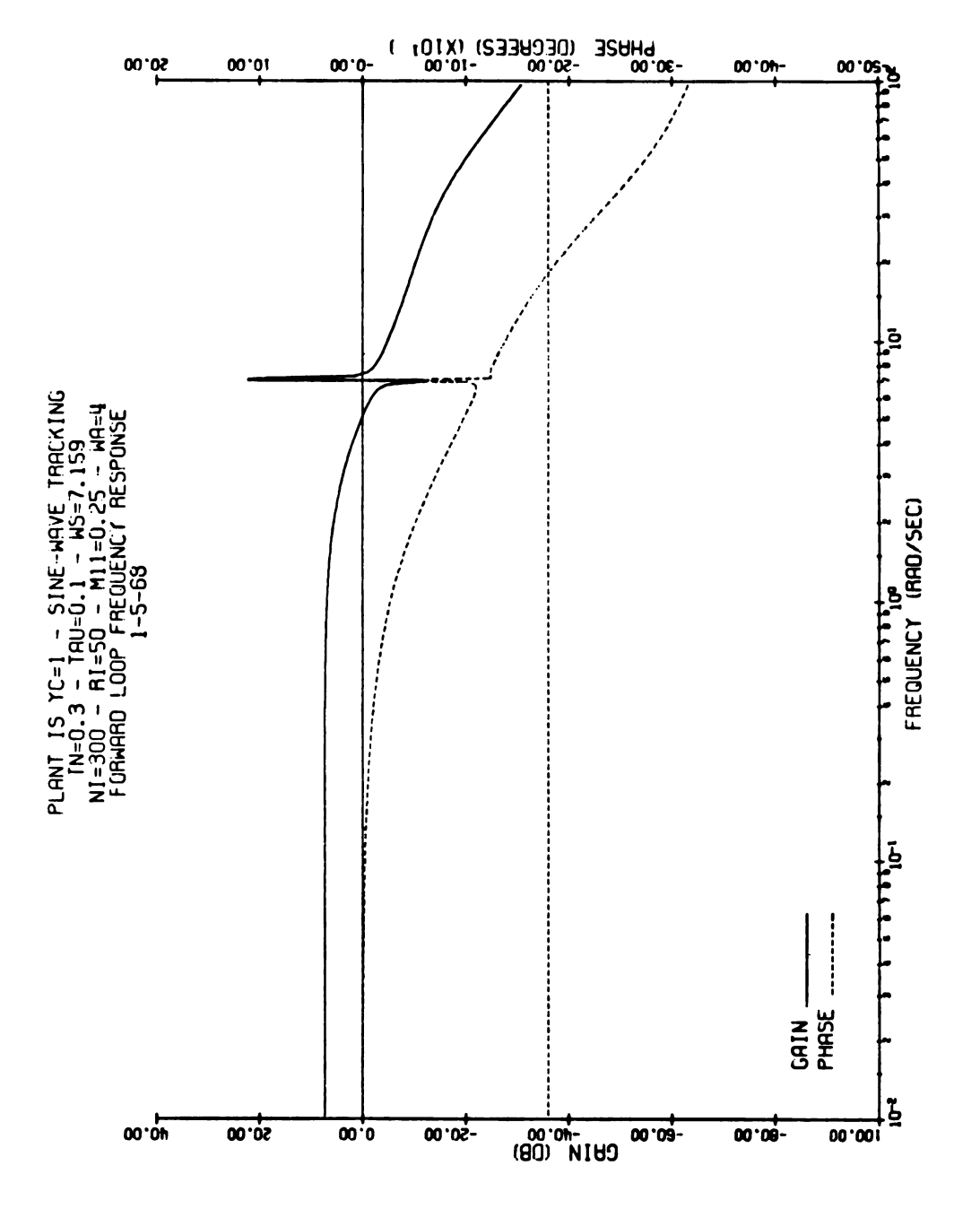


Figure 4.18. Frequency response with P(10).

Consider now the effects of inaccuracies in P on the response of the model. The results given above correspond to P(t_f) as determined by the convergence requirement given by (B.7). The solution for P ended at a time of 10 seconds. The results when the solution for P is terminated at 1 second are shown in Figure 4.19. The results when P is terminated at 35 seconds are shown in Figure 4.20. (This latter result is obtained by changing the convergence requirement on P from 0.01% to 0.0001%.) Comparison of these figures indicates that, as the solution for P converges, the gain and phase characteristics become better-and-better "tuned" to the forcing function frequency.

The gains and phase angles at the forcing function frequency at 1 second and 35 seconds are, respectively

$$G_1$$
 (j7.159) = 18.97 db $\chi 0.06$ degrees (4.26)

$$G_{35}(j7.159) = 18.46 \text{ db } \cancel{20}.74 \text{ degrees}$$
 (4.27)

Comparison of (4.25), (4.26), and (4.27) along with Figures 4.18, 4.19, and 4.20 shows that the gain and phase angle at the forcing function frequency remain essentially the same as P converges.

Consider now the power spectrum of the error signal e. If $G(j_{\omega})$ represents the complete man-plant transfer function, the closed-loop block diagram of the sine-wave tracking model can be drawn as shown in Figure 4.21. The power spectrum of e is

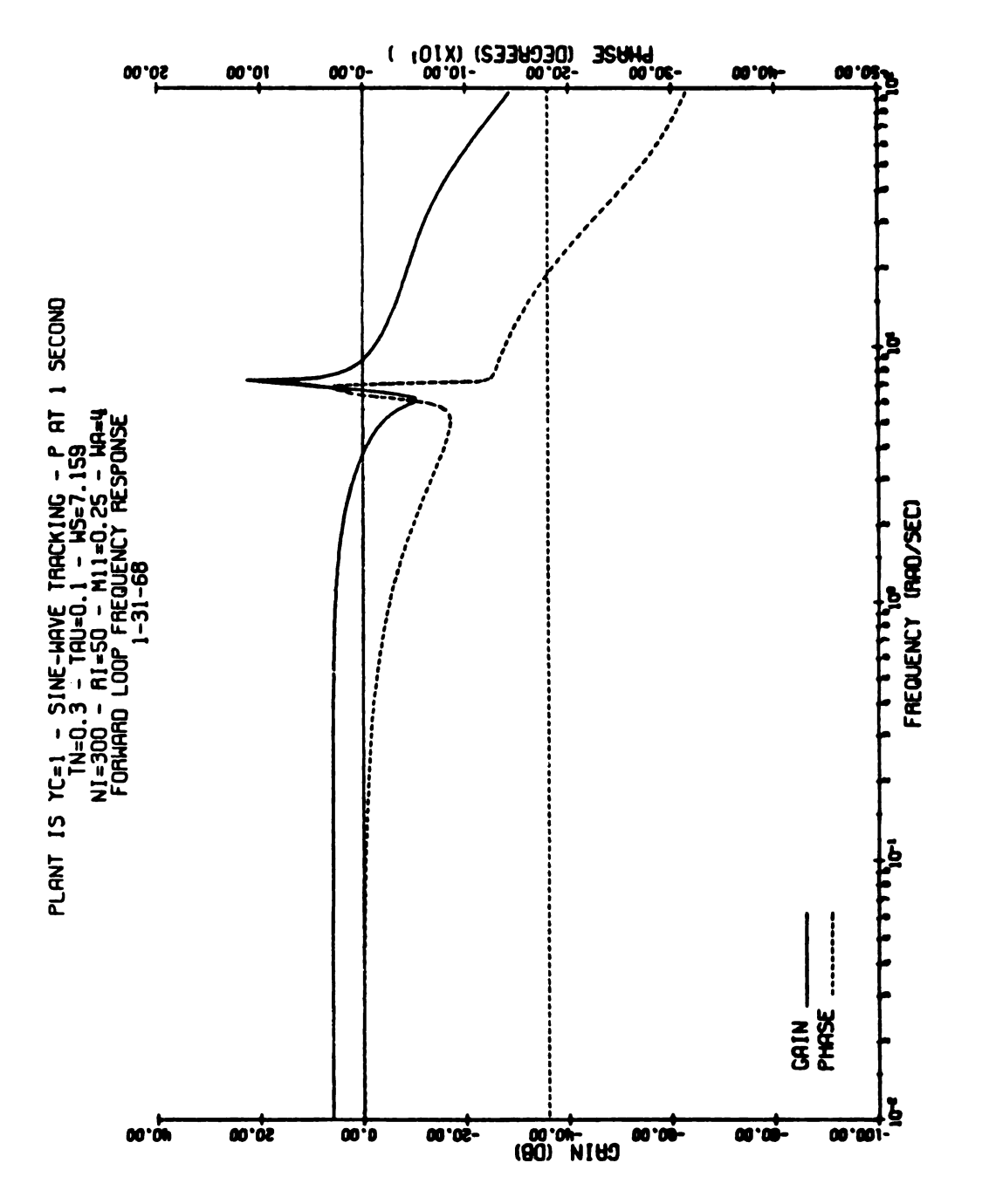


Figure 4.19. Frequency response with P(1).

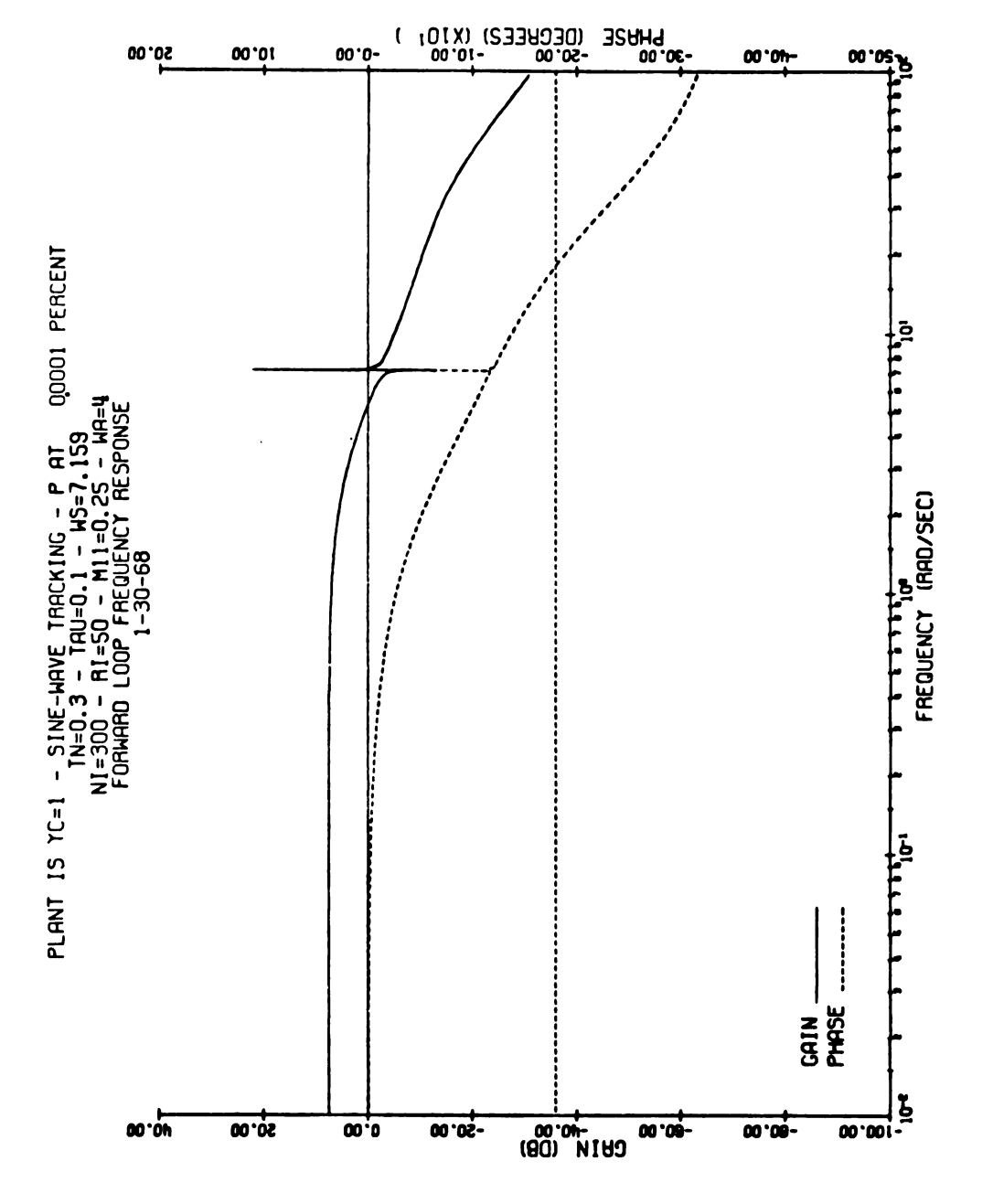


Figure 4.20. Frequency response with P(35).

$$\Phi_{ee}(\omega) = \left| \frac{G(j\omega)}{1+G(j\omega)} \right|^2 \Phi_{vv}(\omega) + \left| \frac{\omega_a}{(j\omega+\omega_a)(T_N j\omega+1)(1+G(j\omega))} \right|^2 \Phi_{ww}(\omega)$$

$$+ \left| \frac{1}{1 + G(j\omega)} \right|^2 \Phi_{ii}(\omega) \tag{4.28}$$

and the variance is

$$\sigma_{\rm e}^2 = \frac{1}{2\pi} \int_0^{\infty} \Phi_{\rm ee}(\omega) d\omega \qquad (4.29)$$

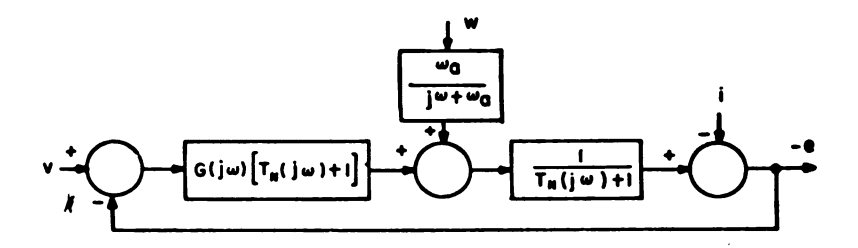


Figure 4.21. Sine-wave tracking model block diagram.

The power spectrums of i, v, and w from (4.5), (4.6), (3.21), (3.22), (4.12), and (4.13) are

$$\Phi_{i,i}(\omega) = \pi (1.414)^2 \delta(\omega - 7.159) \tag{4.30}$$

$$\Phi_{VV}(\omega) = \frac{2}{300} \tag{4.31}$$

$$\Phi_{WW}(\omega) = 0.5 \tag{4.32}$$

The transfer function for the man-plant combination for the 0.01% accuracy requirement on P (as plotted in Figure 4.18) is

$$S(j\omega) = \frac{-80.39[j\omega+7.410] [(j\omega)^2 - .000092(j\omega) - 400] [(j\omega)^2 + 0.0603(j\omega) + 49.92131]}{[0.3(j\omega)+1] [j\omega+20] [j\omega+4.292] [(j\omega)^2 + 52.43(j\omega) + 1160.7] [(j\omega)^2 + 0.01144823(j\omega) + 51.33896]}$$

Using the values of $\,\omega_{a}\,$ and $\,T_{N}\,$ defined by (4.3) and (4.14), the variance of $\,e\,$ by numerical integration is

$$\sigma_{\mathbf{e}}^2 = 0.07238 + 0.0104 \tag{4.34}$$

$$= 0.8278$$
 (4.35)

The power spectrum from (4.28), normalized by this variance, is plotted in Figure 4.22 along with data points adapted from [8]. (The data in [8] are in terms of $\dot{\mathbf{e}}$, and were adapted by first multiplying $\Phi_{\mathbf{e}\mathbf{e}}^{\bullet\bullet}(\omega)$ by $1/\omega^2$, and then normalizing by the area under $\Phi_{\mathbf{e}\mathbf{e}}^{\bullet\bullet}(\omega)/\omega^2$ obtained by graphical approximation.) There is good general agreement, although a sharper high frequency break in the model results would improve the match.

In general, it can be said that in view of

- 1) visual comparison of the human operator time responses with the time solutions of the model
- 2) the closeness of the error power spectrum of the model with the experimental data in [8]
- 3) the fact that the model time delay at the forcing function frequency is essentially zero
- 4) the model tracks with its "eyes closed"

the model comes very close to what the human operator does.

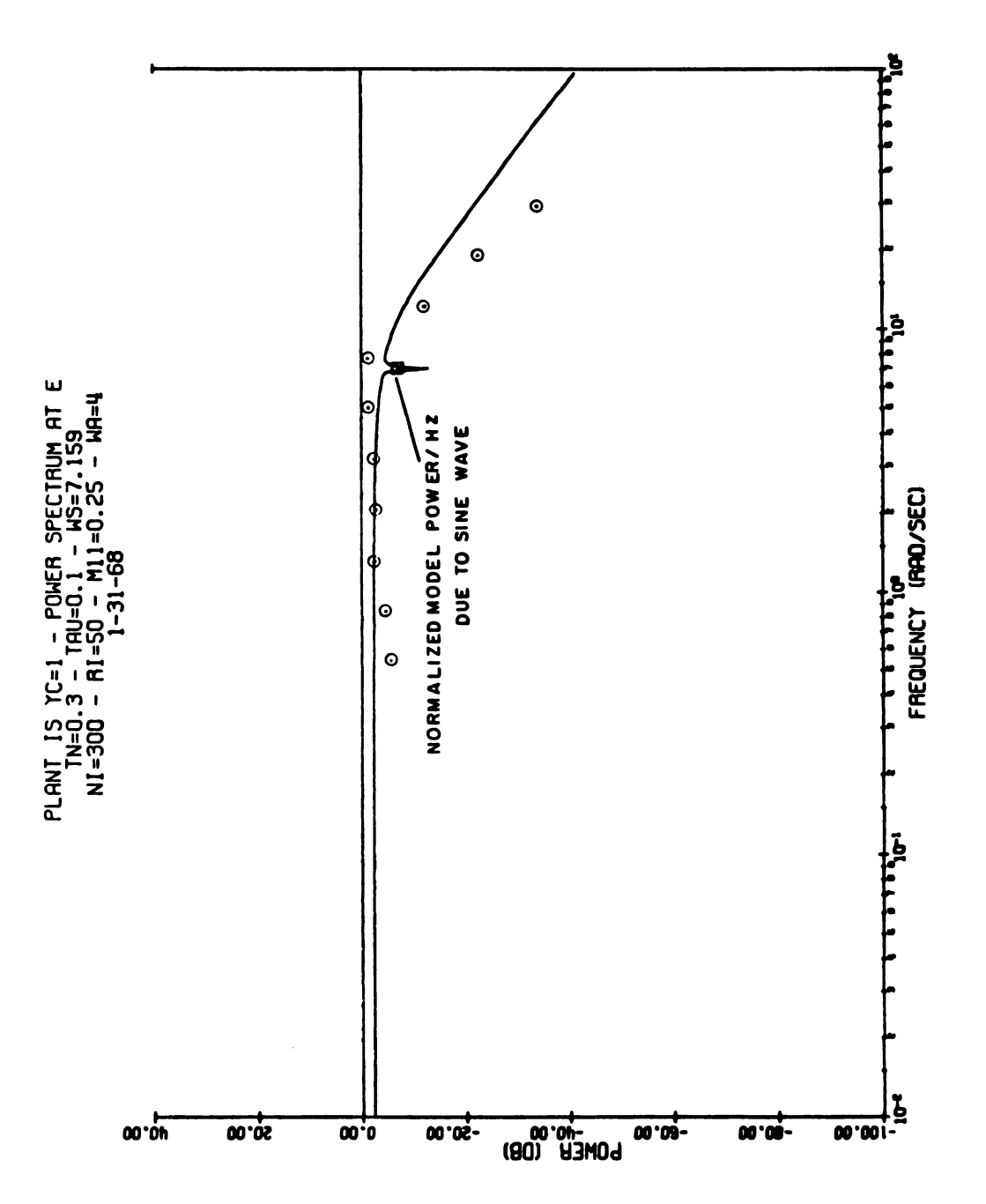


Figure 4.22. Power spectral density match.

5. DISPLAY EFFECT

The effects of changes in the form of display on the transfer function of the human operator are considered in this Chapter.

Both experimental results and model results are considered. The combination of parameters required to match the model results with the experimental results provide insight into possible ways of evaluating displays.

5.1 DESCRIPTION OF EXPERIMENTS

Experiments were performed using the Applied Dynamics AD-256 analog computer and associated equipment shown in Figure 5.1. A simple "pitch axis" compensatory task as shown in Figure 5.2 was used wherein the difference between the forcing function and the plant output is displayed to the operator.



Figure 5.2. Display study block diagram.

Two vastly different displays are considered. The first is the 5-inch CRT (cathode ray tube) display shown in Figure 5.3, and the second is the DVM (digital voltmeter) display shown in Figure 5.4. Since with the DVM, the operator must read the sign of the displayed

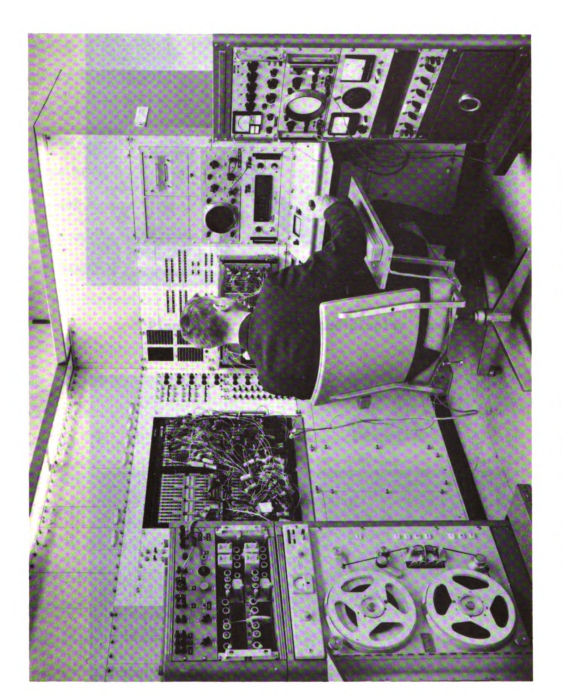


Figure 5.1. Display study experimental equipment.



Figure 5.3. CRT for the display study.



Figure 5.4. DVM for the display study.

voltage as well as read its numerical value, it is much more difficult to use.

with the CRT display, a vertical display motion was used with a gain of 2 cm/volt. A large dot with a diameter of approximately 3 mm was used as the moving index. The zero position was indicated but no numerical scale was provided. The background grid of the CRT, however, was visible. The operator was expected to judge the error (including sign) by the relative distance between the dot and the zero position. A "fly to" sign convention was utilized where, in effect, the zero position is flown to the dot. For example, if the dot is above the zero position, a pulling action of the controller is required.

The DVM gain was 10 volts/volt. The display used provides up to 1000 readings/sec with no sign change, and up to 100 readings/sec with a sign change. Consequently, the maximum time delay was 0.01 second. This is small compared with the minimum time delay of 0.1 second used for the human operator and, therefore, has an insignificant influence on the experiment. As shown in Figure 5.4 with a typical reading, the sign and two digits are displayed. In terms of the CRT display, a plus voltage on the DVM corresponds to the dot above the zero position. Accordingly, a plus voltage on the DVM required a pulling action of the controller.

The controller employed in the study is the three-axis "force sensing stick" shown in Figure 5.5. (The same controller is shown in Figure 4.3 without the handle.) It is considered a force sensor because approximately \pm 1 mm of horizontal motion at



Figure 5.5. Controller for the display study.

the center of pressure is the maximum travel required in the experiments. As stated above, the task was a pitch axis task, so only the pitch axis of the stick was used. The gain was 2.49 volts/deg and the force gradient was 1.62 lbs/deg.

The plant was a simple constant gain with a transfer function of

$$Y_{c} = 1 \tag{5.1}$$

The forcing function was the sum of ten sine-waves with frequencies and amplitudes as given in Table 5.1. The frequencies are the same as those used in [5] (See Table 3.1). The amplitude characteristic corresponds to that of a pure second-order lag with a corner frequency at 2.54 rad/sec. The shaping transfer function is

$$G_s(s) = \left(\frac{1}{\frac{s}{2.54} + 1}\right)^2$$
 (5.2)

The variance of the forcing function in terms of inches of display motion was

$$\sigma_i^2 = 1.7 \text{ in}^2/\text{Hz}$$
 (5.3)

The transfer function of the human operator is determined from the cross-spectral density between the forcing function and the error, and that between the forcing function and the controller output. (The assumption is made that the display and controller transfer functions are part of the operator, i.e., the transfer function is between e and c in Figure 5.2.) The operator transfer func-

tion as given in [43] is

$$Y_{p}(\omega_{n}) = \frac{\phi_{ic}(\omega_{n})}{\phi_{ie}(\omega_{n})}$$
 (5.4)

where ω_n is the frequency at which the cross-spectral density is measured. Taking advantage of the fact that the forcing function consists of the sum of sine-waves, the cross-spectrums at each of these frequencies is easily obtained as shown in Appendix D. Given the cross-spectrums, the values for the transfer function at the ten forcing function frequencies were obtained by (5.4). The real and imaginary parts of (5.4) provide the information for the gain and phase plots.

Table 5.1. Display study forcing function.

ω _n - Rad/sec	$\phi_{i}^{2}(\omega_{n})$ -db
	i in inches
$\omega_1 = 0.157$	-2.11
$\omega_2 = 0.262$	-2.17
$\omega_3 = 0.393$	-2.28
$\omega_{4} = 0.602$	-2.56
$\omega_5 = 0.969$	-3.26
$\omega_6 = 1.490$	-4.64
$\omega_7 = 2.540$	-8.10
$\omega_8 = 4.030$	-13.03
ω ₉ = 7.570	-21.00
$\omega_{10} = 13.800$	-31.70

With the analog computer equipment available, it was possible to evaluate the cross-spectrums of $\Phi_{ie}(\omega_n)$ and $\Phi_{ic}(\omega_n)$ at ω_6 , ω_7 , ω_8 , ω_9 , and ω_{10} at the same time the subject was performing. The time histories of e and c were recorded using the FM tape recorder shown in Figure 5.1. After the run, these recordings were used to find the cross-spectrums of $\Phi_{ie}(\omega_n)$ and $\Phi_{ic}(\omega_n)$ at the remaining frequencies ω_1 , ω_2 , ω_3 , ω_4 , and ω_5 . The majority of the computer patching shown in Figure 5.1 is the cross-spectral analyzer.

Figure 5.6 illustrates the accuracy of the cross-spectral analyzer when the human operator, display, and stick were simulated on the computer with

$$Y_{p} = \frac{6.33}{s+1} \tag{5.5}$$

The solid and dashed lines are respectively the theoretical gain and phase from (5.5). The data points are the measured results using the spectral analyzer. At all of the measurement frequencies, the gain is within 2 db and the phase is within 10 degrees. Hence, for the purposes of this study, the analyzer results are quite good.

Three human operators were used. These operators are engineers without formal pilot training. Prior to taking data, they were trained to use the two displays on 120 second practice runs. The choice of which display to use was made on a non-systematic basis. The practice runs were accomplished over a one week period with up to 10 runs a day. The operators were instructed to minimize the displayed error and proficiency was measured during the run by their mean-squared error where

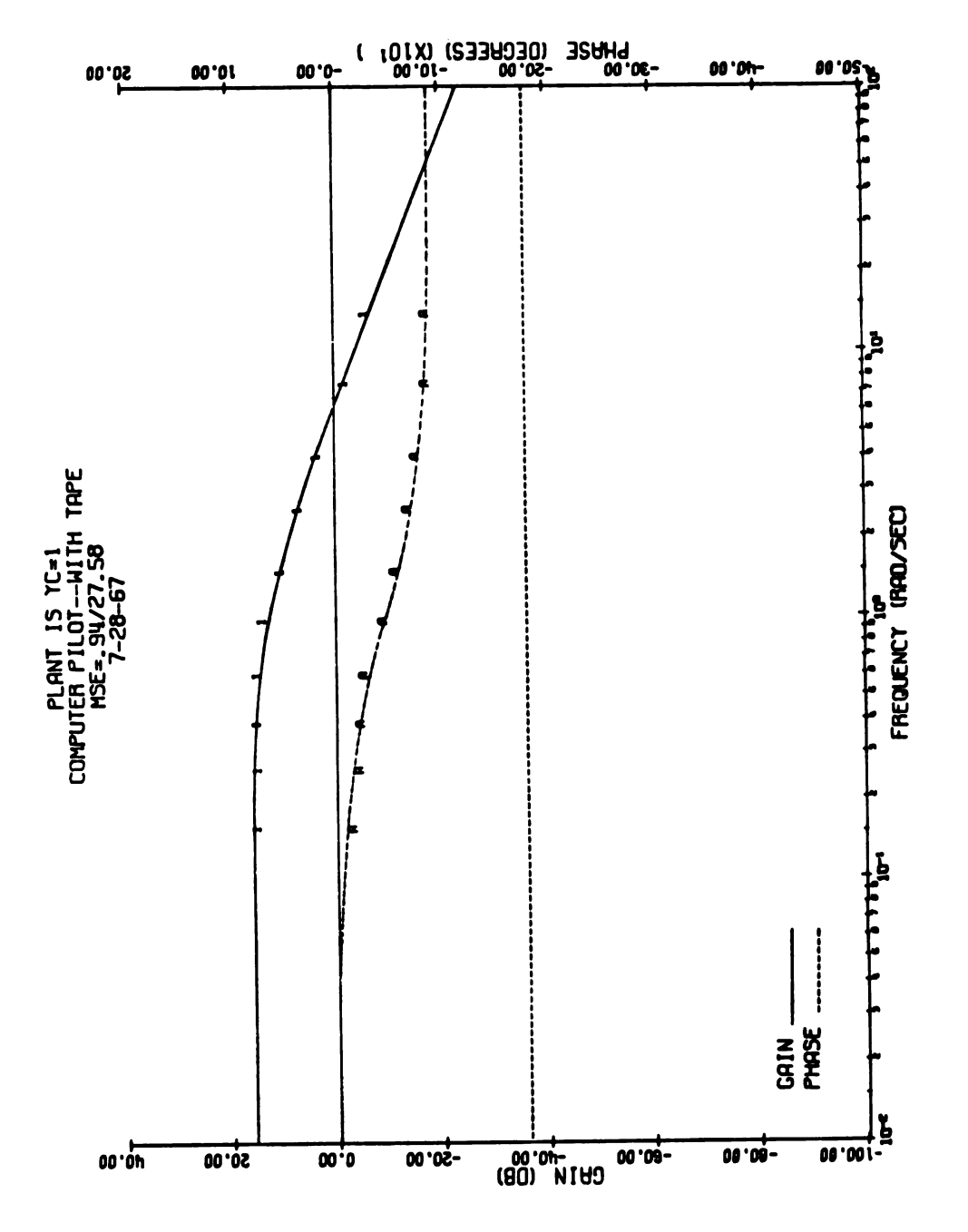


Figure 5.6. Cross-spectral analyzer accuracy.

MSE =
$$\frac{1}{120} \int_{0}^{120} e^2 dt$$
 (5.6)

Once the MSE reached a consistent low level (after 20-30 runs per display), the operator was considered to be trained.

Each recorded experiment extended over a 240 second period.

Up to eight runs were made per eight hour day with two or three in one sitting. The choice of display again was non-systematic. Ten runs for each operator with each display were made.

The gain and phase angle of the transfer function at the ten frequencies for each run and each pilot were computed using (5.4). The mean and unbiased standard deviation (1 σ value) for each gain and phase angle for each operator and both displays were then computed and plotted. In addition, the combined mean and unbiased standard deviation for each gain and phase angle for the three pilots were computed and plotted for both displays.

The time history of a typical CRT run is given in Figure 5.7, and that for a typical DVM run is given in Figure 5.8. The top traces in both are the "random appearing" forcing function. The middle traces are the controller outputs. The bottom traces are the error or differences between the respective top traces. The amplitudes of the error with the DVM display are obviously much larger and generally indicate that the DVM is more difficult to control.

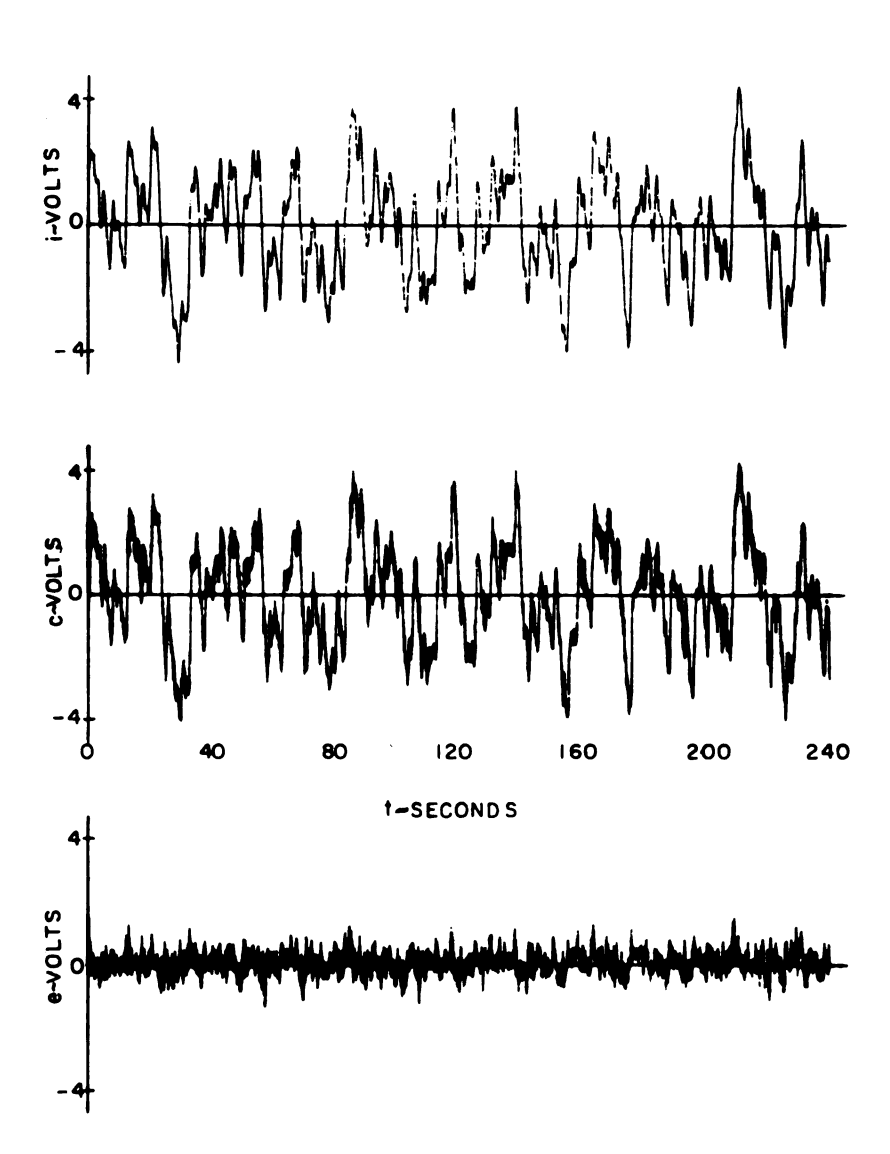


Figure 5.7. Typical CRT run.

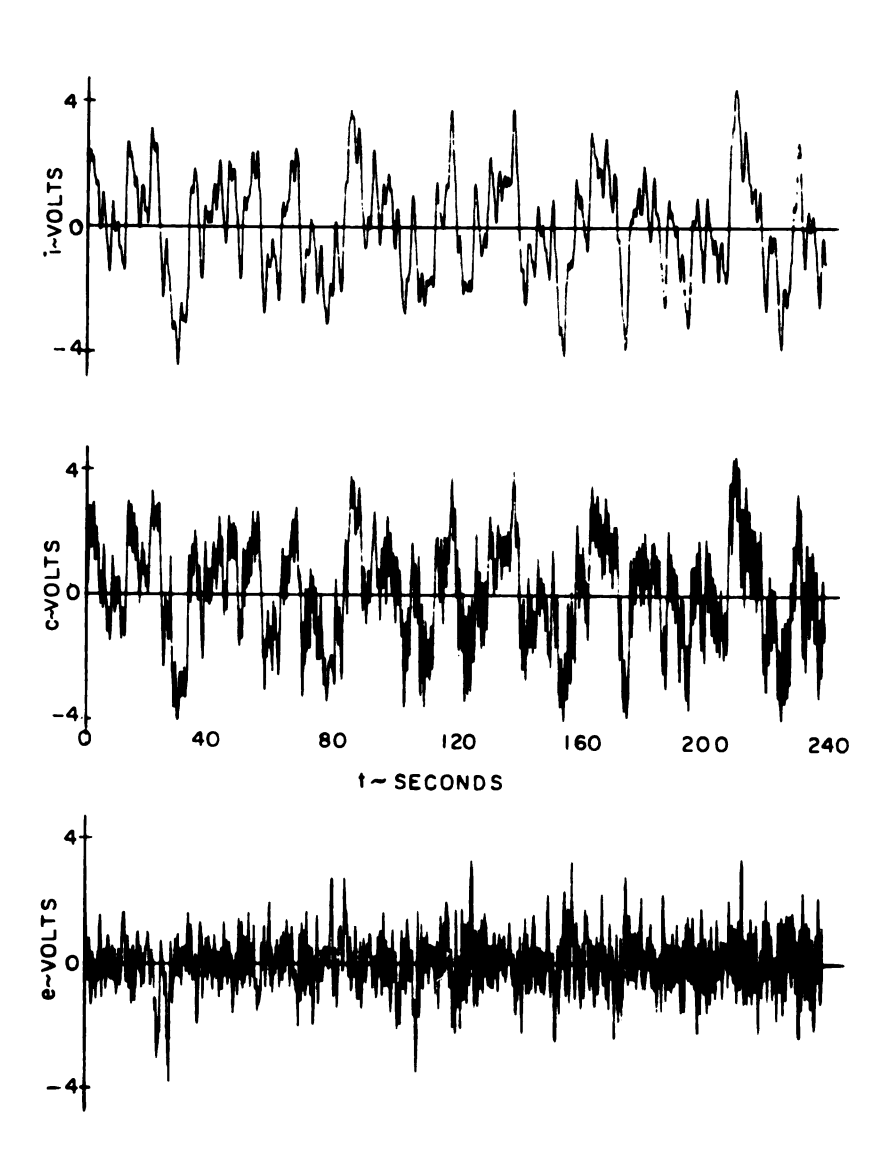


Figure 5.8. Typical DVM run.

5.2 PARAMETER EVALUATION

The results of the experiments are given in Figures 5.9 through 5.16. At each of the ten frequencies, the circle (\bigcirc) indicates the mean value and the bars indicate the \pm 1 σ band around the mean. Figures 5.9, 5.10, and 5.11 are the results for Operators 1, 2, and 3 respectively when using the CRT display, while Figure 5.12 shows the results for the three operators combined using the CRT display. Figures 5.13 through 5.16 are the corresponding results using the DVM display. In general, with the DVM, the gains are lower and the phase angles are more negative.

White noise shaped by

$$G_s(s) = \frac{1}{\left(\frac{s}{2.44} + 1\right)\left(\frac{s}{2.64} + 1\right)}$$
 (5.7)

is used as the model forcing function. For this shaping the variance of the forcing function is

$$\sigma_i^2 = 0.625 \, m_{11}$$
 (5.8)

From (5.3) and (5.8), the white noise input power spectral density required to make the model forcing function variance the same as that used in the experiments is

$$m_{11} = \frac{1.7}{0.625} \tag{5.9}$$

$$= 2.72$$
 (5.10)

With the experimental forcing being the sum of sine-waves with a power spectrum distributed according to a second-order lag (See (5.2)

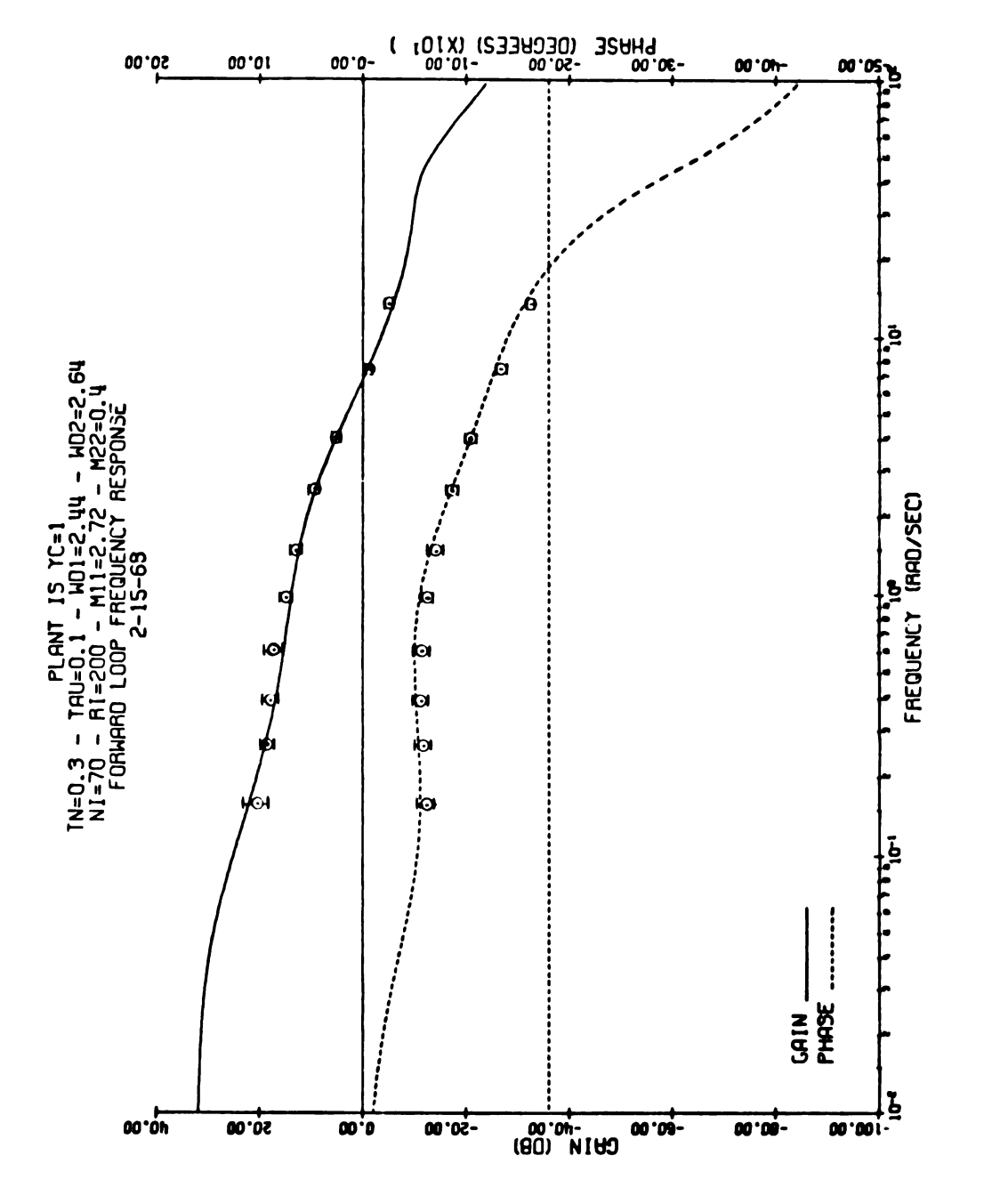


Figure 5.9. CRT match -- operator 1.

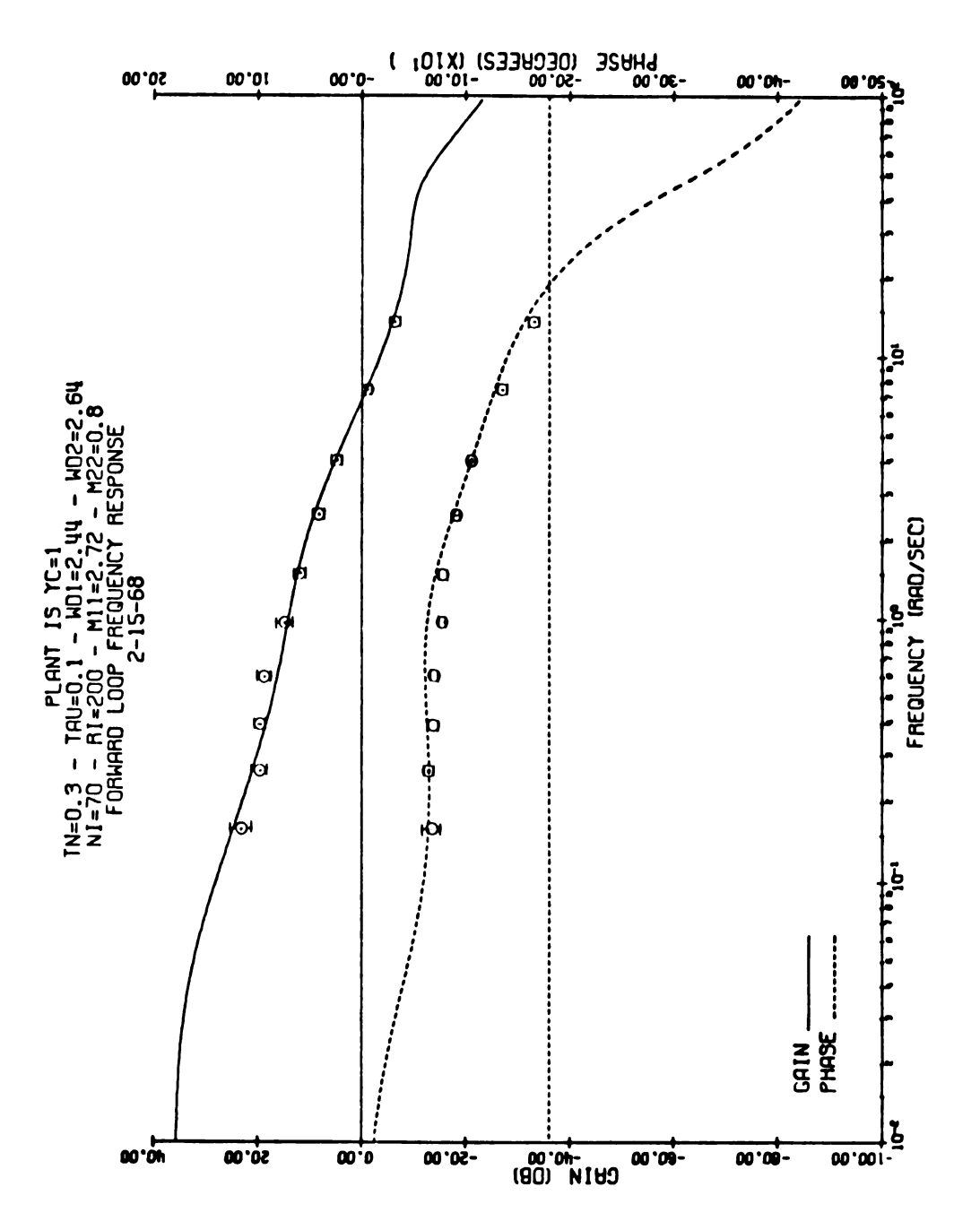


Figure 5.10. CRT match -- operator 2.

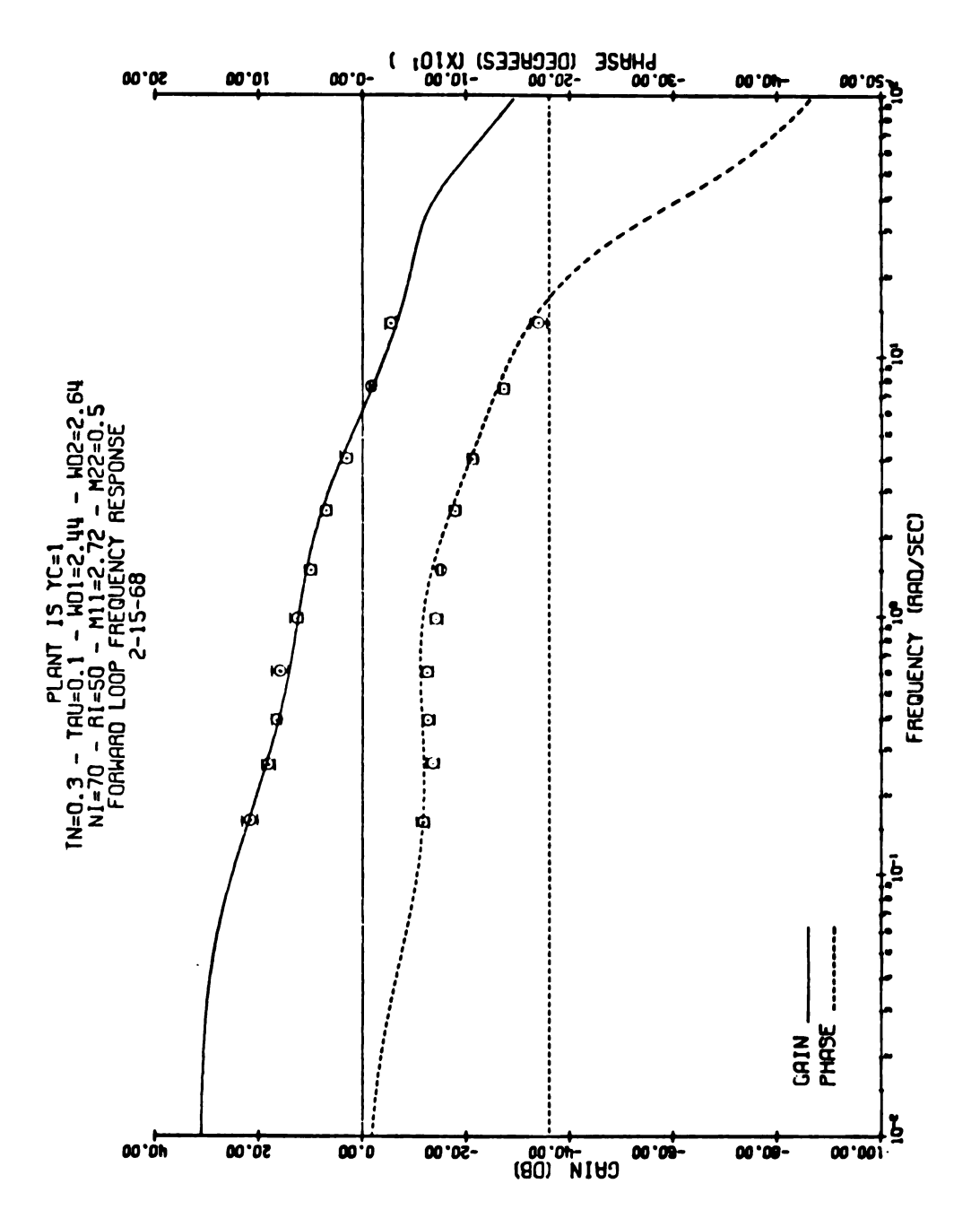


Figure 5.11. CRT match -- operator 3.

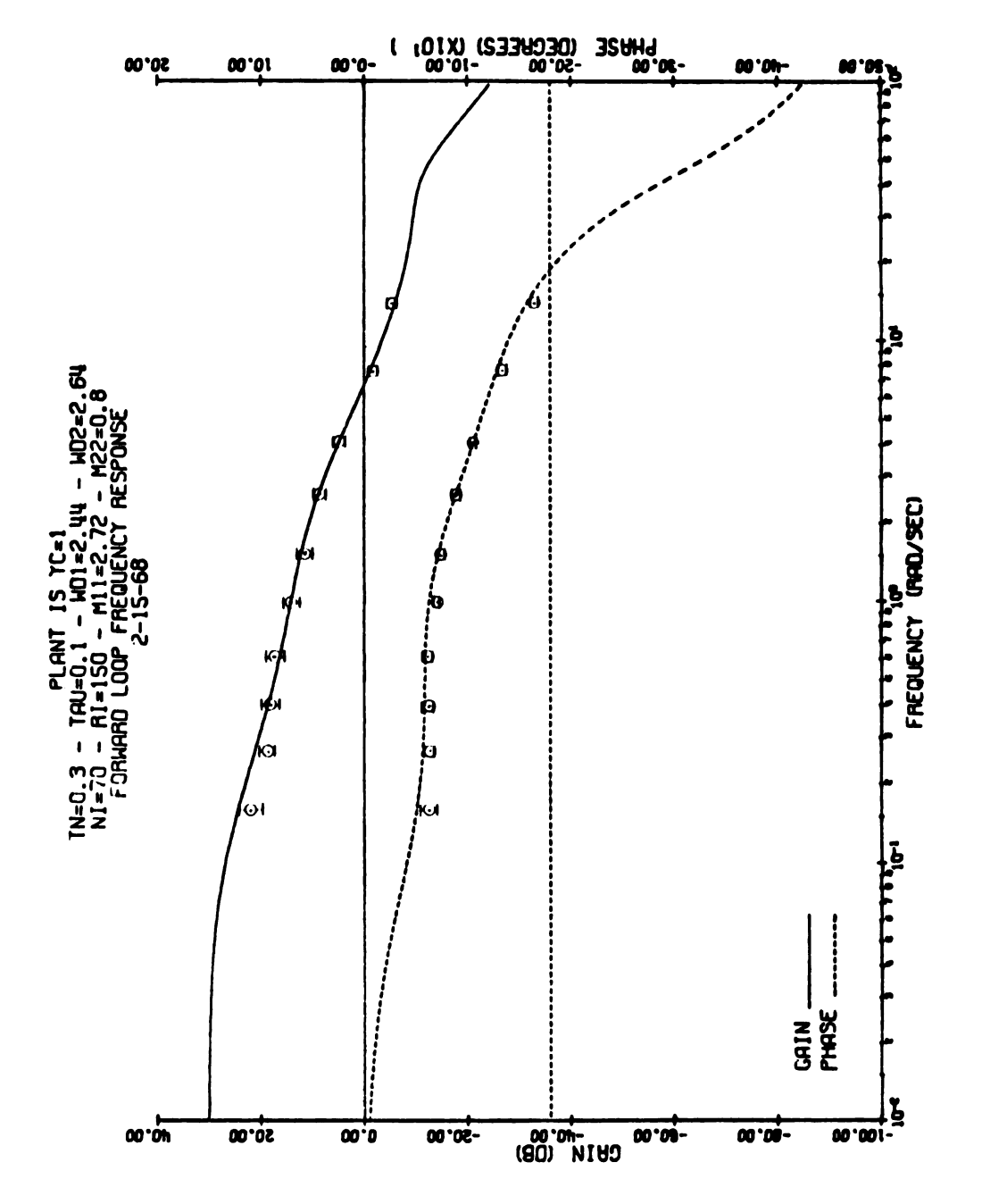


Figure 5.12. CRT match -- operators 1, 2, and 3.

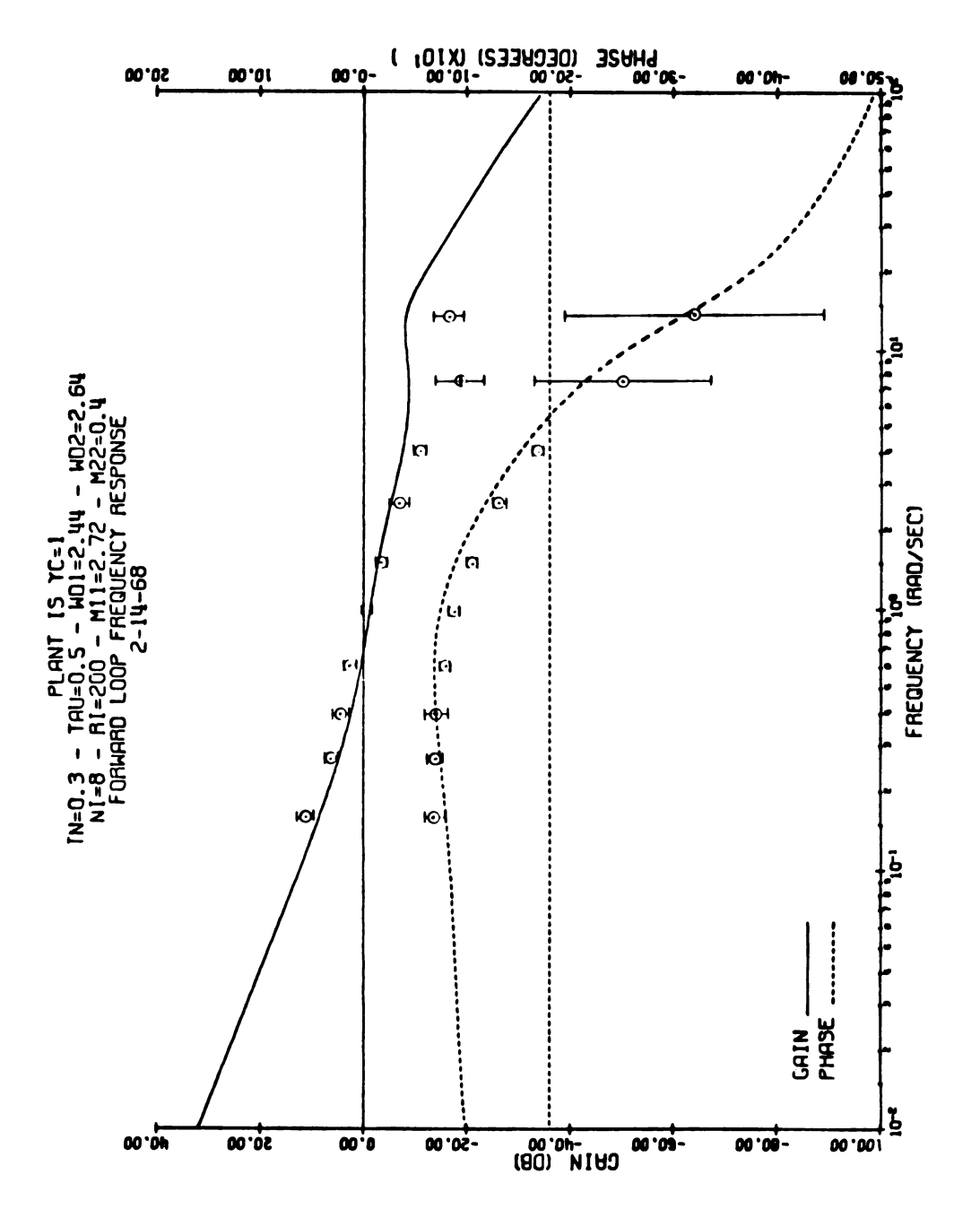


Figure 5.13. DVM match -- operator 1.

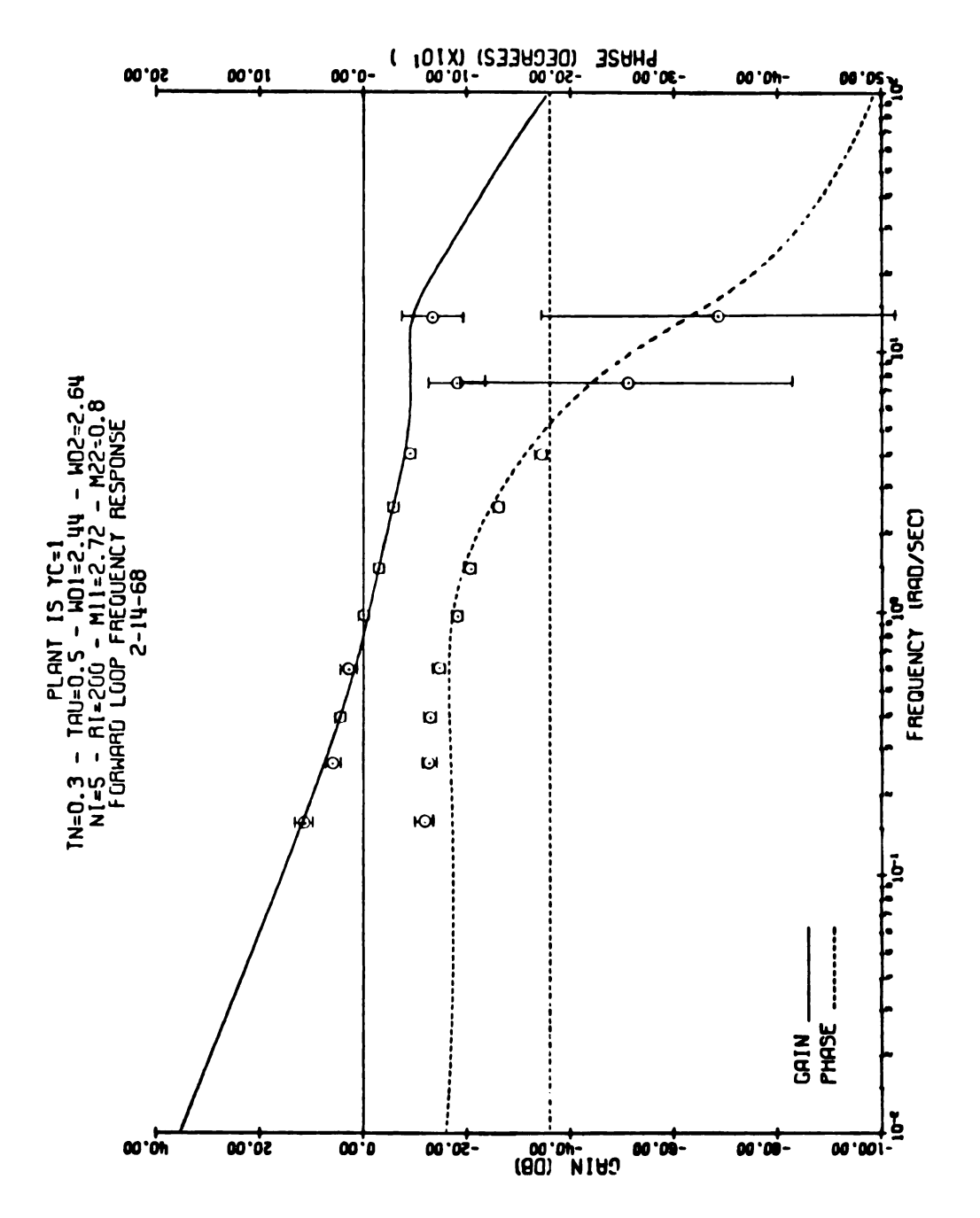


Figure 5.14. DVM match -- operator 2.

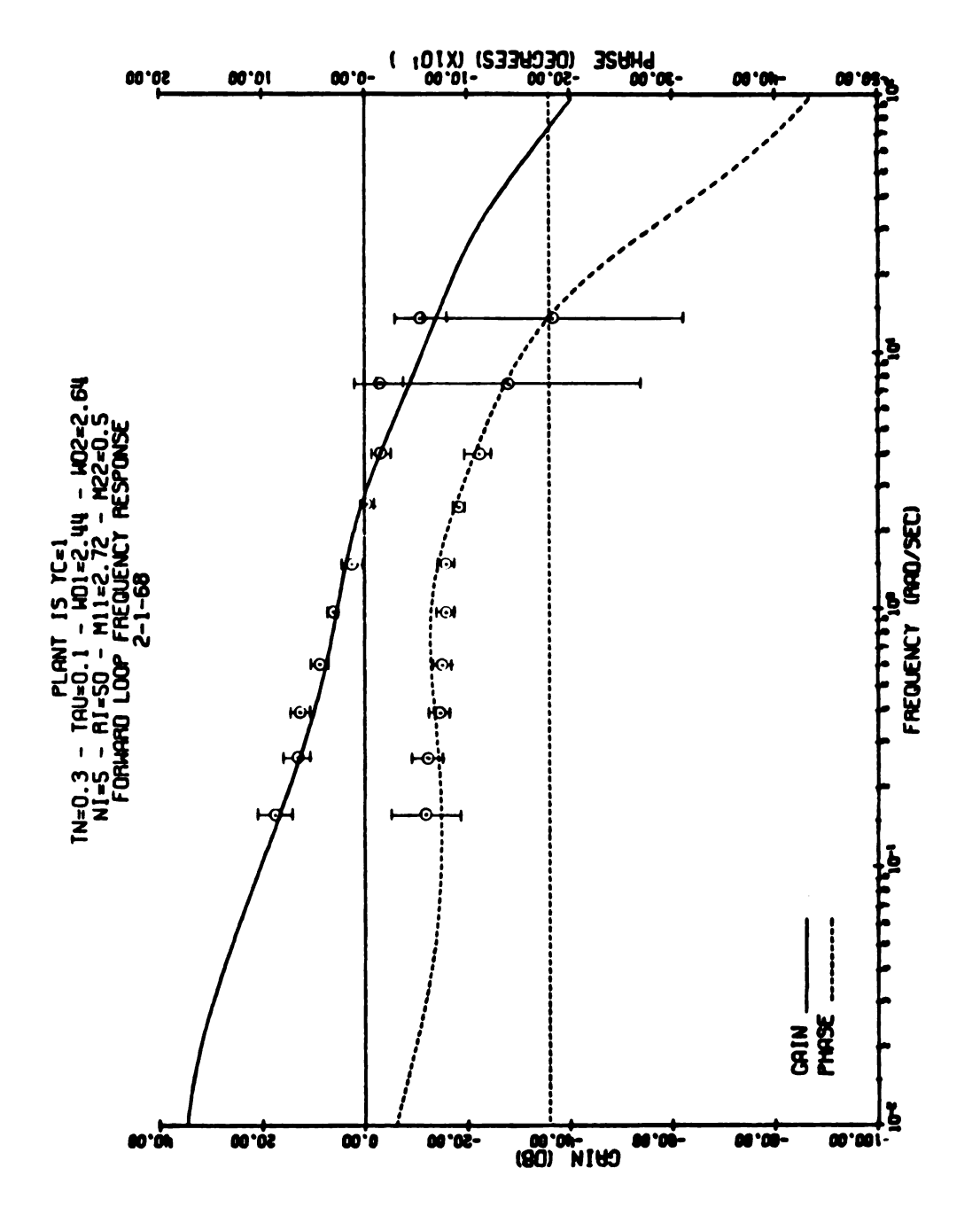


Figure 5.15. DVM match -- operator 3.

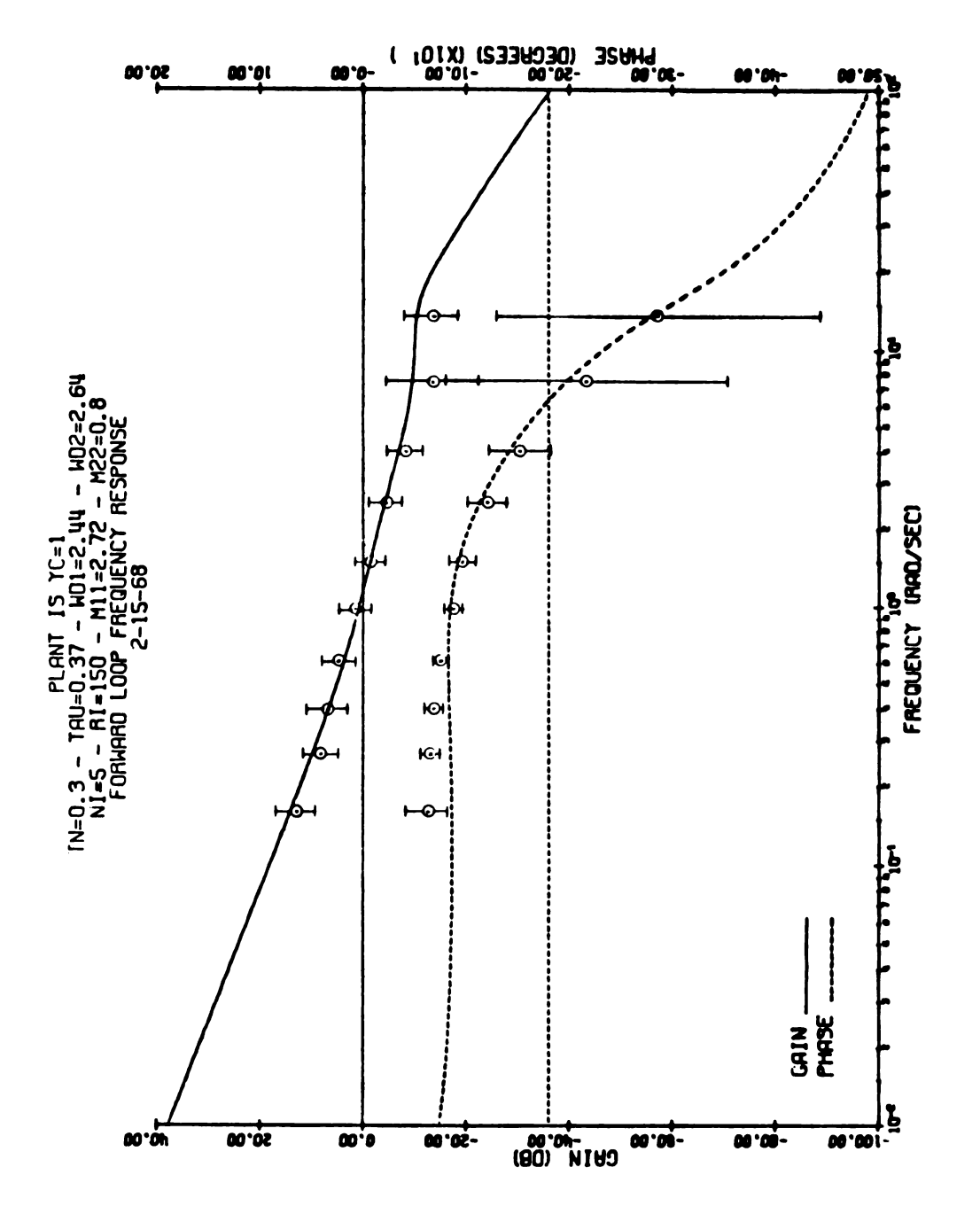


Figure 5.16. DVM match -- operators 1, 2, and 3.

and Table 5.1], the model input approximation is much better than that used in Chapter 3 (see Figure 3.2).

Consider first the match of the model with the CRT data.

Detailed comparison of the experimental data reveals that there are slight differences between the gains and phase angles from operator to operator. The parameters needed to match these data correspondingly are slightly different. The parameters selected to match the operator results individually and combined are summarized in Table 5.2. The match as indicated in Figures 5.9 through 5.12, in each case, is very good.

DADAMETER	OPERATOR NUMBER			
PARAMETER	1	2	3	1,2,63
1/n	70	70	70	70
1/r	200	200	50	150
m ₁₁	0.4	0.8	0.5	0.8
τ	0.1	0.1	0.1	0.1

Table 5.2. Model parameters for CRT match.

In Chapter 3, where a match with the data in [5] is accomplished, the time delay τ is not considered to be a matching parameter. With the DVM display, however, the only parameter that can be changed to improve the match of the high frequency phase angle, in particular, is the time delay. For longer time delays, the corner frequency of the first order Padé approximation is well back in the region of the data and the order of the approximation significantly influences the results. To reduce this error,

a second-order approximation is used (for both CRT and DVM matches).

A comparison with

$$\tau = 0.4 \tag{5.11}$$

is given in Figure 5.17. The high frequency rise is very dependent on the order of the approximation and, as indicated by the DVM data in Figures 5.13 through 5.16, the rise is also present in the data. (A higher order approximation would probably improve the match in Figure 3.9.) Since in some cases severe convergence problems developed in the root extraction routine, even with the corners in the Padé approximation wide apart, a higher than second-order approximation could not be used.

Consider next the match of the model with the DVM data. As with the CRT data there are differences in the results for the three operators. Also, the run-to-run variability of the DVM data for each operator is greater as indicated by the larger ± 1σ bands in the data, especially at high frequencies. The large high frequency variability is probably due to the fact that the forcing function amplitude at these frequencies is very small and consequently almost ignored by the operators. The matches are good but not as good as those with the CRT.

Comparison of the results for Operators 1 and 2 given in Figures 5.13 and 5.14 with the results for Operator 3 in Figure 5.15 indicates that Operator 3 has a considerably different phase angle at high frequencies. This implies a much shorter time delay for Operator 3. Investigation of the "flying" technique of each

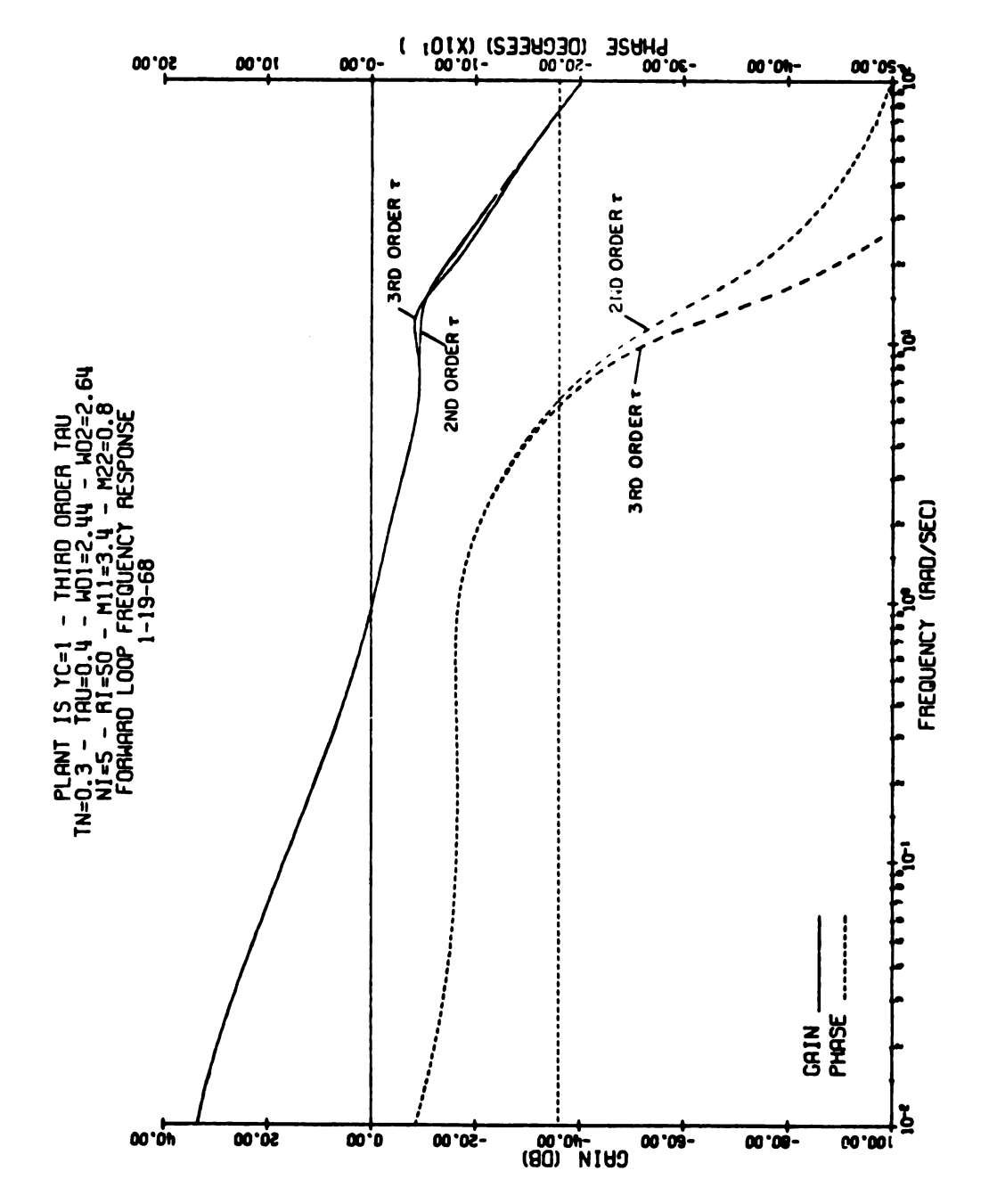


Figure 5.17. Effect of 2nd and 3rd order Pade approximations of the time delay.

operator reveals that Operators 1 and 2 used a "proportional control" while the third used a kind of "dither" control. The first two made corrections based on the sign and size of the displayed voltage while the third built a substantially constant frequency dither into his control. He looked at only the sign of the voltage and attempted to produce + and - signs on the display as rapidly as he could and still have what he considered good control. This technique as compared with the proportional technique produced less high frequency phase shift. Apparently, Operators 1 and 2 needed more time to think about the magnitude of the displayed voltage and consequently produced a longer time delay.

The parameters selected for matching the DVM data are summarized in Table 5.3. Comparison of Tables 5.2 and 5.3 shows

DADAMETER		OPERATO	OR NUMBER	
PARAMETER -	1	2	3	1,2,&3
1/n	8	5	5	5
1/r	200	200	50	150
m ₂₂	0.4	0.8	0.5	0.8
τ	0.5	0.5	0.1	0.37

Table 5.3. Model parameters for DVM match.

that a difference in measurement noise and in the time delay accounts for the difference in the displays. The noise would correspond to reading difficulty while the time delay would correspond to the amount of mental processing needed by the operator.

The results with Operator 3 indicate that a great deal depends

on the operator's technique. Instruction and/or training could minimize this effect.

In conclusion, an ordering of the two displays has been accomplished where greater noise and time delay are associated with the DVM display. Other displays could be classified in the same way and the comparative usefulness of each in a control task evaluated.

6. CONCLUSIONS AND RECOMMENDATIONS

The model, as postulated in Chapter 2, is very general and, on an a priori basis, is capable of handling many of the characteristics of the human operator in a control task. As described in Chapter 2, these characteristics are

- 1) precognition
- 2) noise
- 3) nonlinearity
- 4) nonstationarity
- 5) multiple inputs and outputs
- 6) forcing function characteristics

A great deal of detailed investigation and verification by means of experimental data is needed for each one of these areas. In Chapters 3, 4, and 5 the following topics, covering a cross-section of the above areas, are investigated:

- 1) a time stationary model
- 2) sine-wave tracking
- 3) a display study

In Chapter 3, the validity of the model under time stationary conditions is studied by comparing the model results with those found experimentally. As shown in Figures 3.3, 3.5, and 3.6, the results agree quite well with the experimental data. The results with the plants $Y_c = 1$ and $Y_c = 5/(s-2)$ agree exceptionally

well. The gain match with the plant $Y_c = 1/s$ is very good while the phase angle match at mid-frequencies is not as good as desired. The difference could be attributed to either the fact that the model forcing function is not exactly the same as that used to obtain the experimental data, or possibly due to the approximations used for the neuromuscular lag and/or time delay. Further investigation into the exact form of the neuromuscular lag is required. More experimental work should be done using forcing functions that are more amenable to analysis. Also, the time delay approximation should be improved.

As discussed in Chapter 3, it is assumed that a noise characteristic can be selected that provides, by means of the model, a time stationary transfer function which matches the experimental data. These data are obtained by averaging and the nonstationary characteristics, which are known to be present [5], are eliminated. If the nonstationary characteristics of the model were taken into account, the correspondence of a "time averaged model" may improve the results for all plants, especially for the plant $Y_{\rm C}=1/{\rm s}$ (for both the transfer functions and the remnant). A study should be made in which the nonstationary characteristics are taken into account, possibly in the time domain or with double Fourier transforms.

The sine-wave tracking results, in Chapter 4, show that the model indeed performs very much like the real human operator. A comparison of Figures 4.4 and 4.5 with Figures 4.12 and 4.13 shows the time responses are visually quite similar. Comparison

of the power spectrum of the model with that found experimentally by Pew et al. in [8] (see Figure 4.22), shows that the two are much alike.

The model tracks a sine-wave with essentially zero phase angle as given by (4.25). Also, the model continues to track a sine-wave even after its "eyes" are closed. Both indicate that the model predicts and takes into account precognition. (This cannot be done by any other model presented so far in the open literature.)

The model time response, after the "eyes" are closed, is in general agreement with the human operator time response (see Figures 4.6 and 4.15). After some unknown period of time, however, the model results will not correspond to those of a real human operator. This occurs because the human operator probably "loses" his estimates of the system parameters. (It is assumed that the man knows these parameters in the filter and controller.) A more complete model of the human operator, as indicated in [21], would probably include a "parameter estimator," in addition to the filter and controller and should be investigated.

The display study in Chapter 5 shows that an ordering of the relative values of displays is entirely feasible using the model. It is shown that the change in measurement noise and time delay that are needed to match the model results with the experimental results can be used to quantify the relative values of the displays. (Two vastly different displays are used in the study.) Further study is needed to determine the sensitivity of this technique to display design.

APPENDIX A

MAN-PLANT TRANSFER FUNCTION IN TERMS OF $e^{\hat{A}t}$

The state model for the human operator, excluding the physical characteristics, as given by (3.5) and (3.6) is

$$\hat{\hat{x}} = \hat{A}\hat{x} + \hat{K}y \tag{A.1}$$

$$u = \hat{C}\hat{x} \tag{A.2}$$

where for the purpose at hand u and y are taken as scalars. The general solution for $\hat{x}(t)$ is

$$\hat{\mathbf{x}}(t) = e^{\hat{\mathbf{A}}t}\hat{\mathbf{x}}_{0} + \begin{cases} t \\ e^{\hat{\mathbf{A}}(t-\tau)}\hat{\mathbf{K}}\mathbf{y}(\tau)d\tau \end{cases}$$
 (A.3)

where the initial conditions are

$$\hat{\mathbf{x}}_{0} = \hat{\mathbf{x}}(0) \tag{A.4}$$

To develop a transfer function, the initial conditions are set to zero, whereupon the Laplace transforms of (A.2) and (A.3) yield

$$U(s) = \hat{C}\hat{X}(s) \tag{A.5}$$

$$\hat{X}(s) = \mathcal{I}\left\{e^{\hat{A}t}\right\} \hat{K}Y(s)$$
 (A.6)

Substitution of (A.6) into (A.5) gives the transfer function

$$\frac{U(s)}{Y(s)} = \hat{C} \left\{ e^{\hat{A}t} \right\} \hat{K}$$
 (A.7)

Since it is assumed that there are no repeated elgenvalues, eAt can be written as the sum of first order terms of the form

$$e^{\hat{A}t} = A_1 e^{\lambda_1 t} + A_2 e^{\lambda_2 t} + --- A_n e^{\lambda_n t}$$
(A.8)

where, in general, $(\lambda_1, \lambda_2, ---, \lambda_n)$ are the complex elgenvalues of \hat{A} and $(A_1, A_2, ---, A_n)$ are the complex constitutent idempotents of \hat{A} . Taking the Laplace transform of (A.8) and combining the result with (A.7) gives

$$\frac{U(s)}{Y(s)} = \frac{\hat{C}A_1\hat{K}}{s-\lambda_1} + \frac{\hat{C}A_2\hat{K}}{s-\lambda_2} + --- + \frac{\hat{C}A_n\hat{K}}{s-\lambda_n}$$
(A.9)

Noting that the $\hat{C}A_{i}\hat{K}$ are scalars, (A.9) can be rearranged into

$$\frac{U(s)}{Y(s)} = \frac{C_0(C_1 s^{n-1} + C_2 s^{n-2} + --- + C_n)}{(s - \lambda_1)(s - \lambda_2)(s - \lambda_3) --- (s - \lambda_n)}$$
(A.10)

where the constants $(C_0, C_1, ---, C_n)$ are scalars.

The expression given by (A.10) is the transfer function for the human operator without his physiological characteristics.

The transfer function for the physiological characteristics and the plant are specified with a combined transfer function, in general,

in the form of a ratio of the product of quadratic factors. Thus, the required open loop transfer function for the complete man-plant combination becomes

$$G(s) = \frac{C_{o}(C_{1}s^{n-1}+C_{2}s^{n-2}+\cdots+C_{n})(s^{2}+a_{1}s+b_{1})-\cdots(s^{2}+a_{k}s+b_{k})}{(s-\lambda_{1})(s-\lambda_{2})(s-\lambda_{3})-\cdots(s-\lambda_{n})(s^{2}+c_{1}s+d_{1})-\cdots(s^{2}+c_{m}s+d_{m})}$$
(A.11)

APPENDIX B

SOLUTION FOR THE TIME STATIONARY MODEL

The time stationary model is obtained using a digital computer. The computer yields a time stationary state model and transfer function for the filter and controller, a transfer function for the man-plant combination, and a Bode plot for the man-plant combination. The solution is programmed in Fortran and solved using the IBM System/360, Model 50 digital computer located in the Analytical Engineering Department of the LSI Instrument Division. The Bode plots are made with a Calcomp plotter. Figure B.1 is a flow chart showing the basic blocks of computation that are used.

An example problem is given to illustrate the solution for the time stationary model. The augmented plant is given in Figure B.2 where, as in Chapter 3, simple models of the neuromuscu-

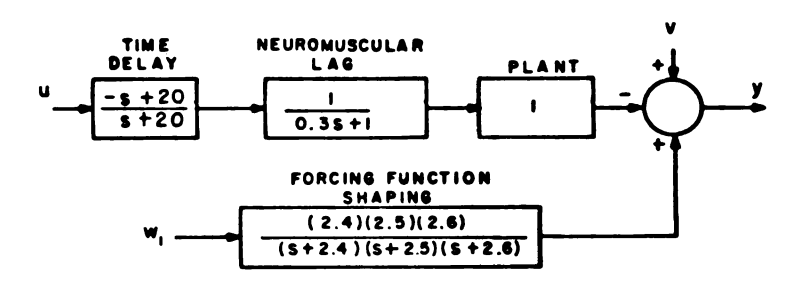


Figure B.2. Example problem augmented plant.

lar lag and time delay are used. As indicated, a first-order lag is used for the neuromuscular lag with a time constant of $T_N = 0.3$.

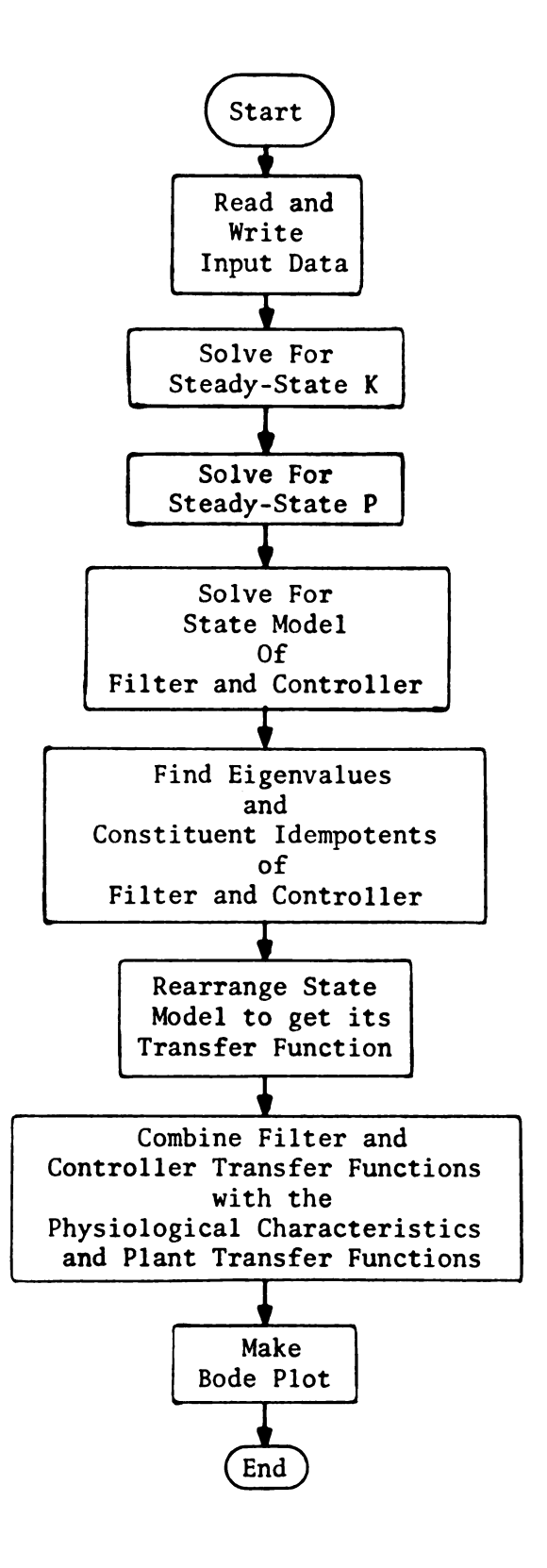


Figure B.1. Basic flow chart for time stationary model solution.

A first order Padé approximation of the time delay (see 35) is used with a delay time of τ = 0.1 seconds. A gaussian white noise input w_1 , colored by a third-order lag with corner frequencies of 2.4, 2.5, and 2.6 rad/sec is used as the forcing function. The plant under control is a simple constant gain plant with Y_c = 1. The measurement noise v is assumed to be white gaussian noise.

The blocks as shown in Figure B.2 are expanded into separate elements in Figure B.3. Included for purposes of illustration, are noise inputs w_2 , w_3 , and w_4 at various points in the model which would correspond to noise in the neuromuscular system or noise at various points involved with the time delay.

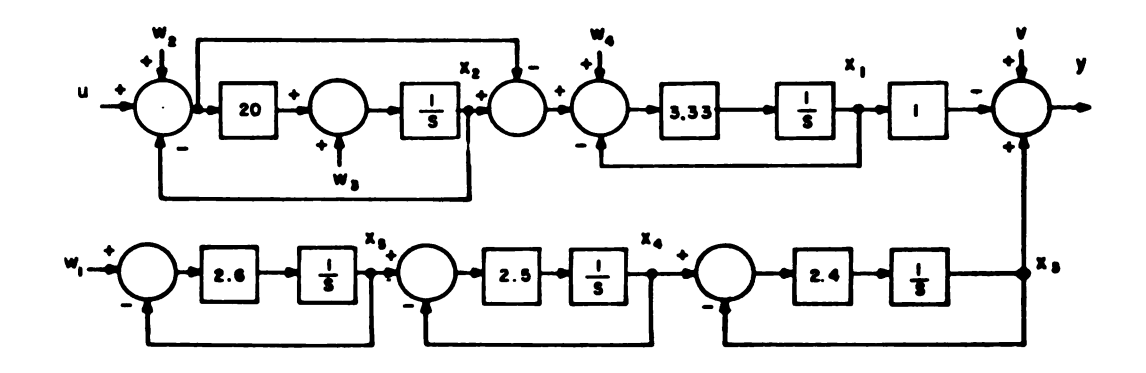


Figure B.3. Expanded example problem block diagram.

Figures B.4 through B.11 show the computer printout for the example problem. Figure B.4 gives the three optional title cards that can be used along with the general form of the system model of the augmented plant, the covariance matrices of the noise inputs, and the cost function. The dimensions of x, u, w, and y and the numerical values for the coefficient matrices A, B, C, and D of the augmented plant are also given in the same general format in Figure B.4.

MANUAL CONTROL STUDY
TRANSFER FUNCTION IN A SINGLE AXIS COMPENSATOR TASK
PLANT IS YC=1
TN=0.3 - TAU=0.1 - WD1=2.4 - WD2=2.5 - WD3=2.6
NI=500 - RI=20 - M22=0.534

JANUARY 5, 1968

SYSTEM MODEL

DXDT = AX + BU + DW

Y = CX + V

COVARIANCE MATRICES

C((UT,WT)T) = M DELTA(TAU)

C(V) = N DELTA(TAU)

COST FUNCTION

E (0 TO TF INT (XTQX + UTRU) DT)

DIMENSION OF X

5.000E+00

DIMENSION OF U

1.000E+00

DIMENSION OF W

4.000E+00

DIMENSION OF Y

1.000F+00

Figure B.4. Input data.

```
-3.330E+00
               6.660E+00
                            0.0
                                         0.0
                                                      0.0
   0.0
               -2.000F+01
                            0.0
                                         0.0
                                                      0.0
                           -2.400E+00
   0.0
               0.0
                                         2.400E+00
                                                      0.0
   0.0
               0.0
                            0.0
                                        -2.500E+00
                                                      2.500E+00
   0.0
                0.0
                            0.0
                                         0.0
                                                     -2.600E+00
  -3.330E+00
   2.000E+01
   0.0
   0.0
   0.0
C
  -1.000E+00
               0.0
                            1.000E+00
                                         0.0
                                                      0.0
D
   0.0
              -3.330E+00
                            0.0
                                         3.330E+00
   0.0
                2.000E+01
                            1.000E+00
                                         0.0
   0.0
               0.0
                            0.0
                                         0.0
   0.0
                0.0
                            0.0
                                         0.0
   2.600E+00
                0.0
                            0.0
                                         0.0
   0.0
               0.0
                            0.0
                                         0.0
                                                      0.0
   0.0
                5.340E-01
                            0.0
                                         0.0
                                                      0.0
   0.0
               0.0
                            0.0
                                         0.0
                                                      0.0
   0.0
                0.0
                            0.0
                                         0.0
                                                      0.0
   0.0
                0.0
                            0.0
                                         0.0
                                                      0.0
NI (INVERSE OF N)
   5.000E+02
Q
               0.0
   1.000E+00
                                         0.0
                           -1.000E+00
                                                      0.0
                                         0.0
   0.7
               0.0
                            0.0
                                                      0.0
  -1.000E+00
              ..0.0
                            1.000E+00
                                         0.0
                                                      0.0
   0.0
               0.0
                            0.0
                                         0.0
                                                      0.0
   0.0
                0.0
                            0.0
                                         0.0
                                                      0.0
RI (INVERSE OF R)
```

Figure B.4. (Con't).

2.000E+01

ADDITIONAL NUMERATOR FACTORS

COEF OF	COEF OF	CONSTANT
S*S	S	TERMS
0.0	-1.000E+00	2.000E+01

ADDITIONAL DENOMINATOR FACTORS

COEF OF	COEF OF	CONSTANT
S*S	S	TERMS
0.0	1.000E+00 3.000E-01	2.000E+01 1.000E+00

Figure B.4. (Con't).

DTMIN = 0.0100 SECONDS

BEGINNING OF SOLUTION FOR STEADY STATE K

	T =	0.0	SECONDS			
K	0					
	0.0		0.0	0.0	0.0	0.0
	0.0		0.0	0.0	0.0	0.0
	0.0		0.0	0.0	0.0	0.0
	0.0		0.0	0.0	0.0	0.0
	0.0		0.0	0.0	0.0	0.0
	T =	0 200	SECONDS			
K	, –	9.200	31011103			
•	9.79	3E-02	2.210E-02	-1.043E-01	-1.726E-02	-2.307F-03
		0E-02	6.010E-03	-2.397E-02	-5.073E-03	-7.395F-04
	-1.04		-2.397E-02	1.114E-01	1.900E-02	2.590F-03
	-1.72		-5.073E-03	1.900E-02	4.732E-03	7.768F-04
	-2.30	7E-03	-7.395E-04	2.590E-03	7.768F-04	1.436E-04
	T =	0.400	SECONDS			
K						
		9F-01	2.320E-02	-1.083E-01	-2.003F-02	-3.343E-03
		0E-02	6.419E-03	-2.543E-02	-6.100E-03	-1.126E-03
	-1.08		-2.543E-02	1.166E-01	2.284F-02	4.089F-03
	-2.00		-6.100E-03	2.284E-02	7.942E-03	2.168F-03
	-3.34	3E-03	-1.126E-03	4.089E-03	2.168F-03	7.912E-04
	T -	0 400	CECONOC			
_	Τ =	0.000	SECONDS			
K	1 01	0E-01	2.321E-02	-1.083E-01	-2.012E-02	-3.416F-03
		1E-02	6.421E-03	-2.544E-02	-6.136F-03	-1.154F-03
	-1.08		-2.544E-02	1.168E-01	2.329E-02	4.460E-03
	-2.01		-6.136E-03	2.329E-02	9.141E-03	3.193F-03
	-3.41		-1.154E-03	4.460E-03	3.193F-03	1.682E-03
	JU		201716 03	77.002 03	301/31 (7.7	
	T =	0.800	SECONDS			
K						
	1.01	0E-01	2.321E-02	-1.083E-01	-2.012E-02	-3.420E-03
		1E-02	6.421E-03	'-2.544E-02	-6.137E-03	-1.156E-03
	-1.08	3E-01	-2.544E-02	1.169E-01	2.344E-02	4.639E-03
	-2.01		-6.137E-03	2.344E-02	9.699E-03	3.867E-03
	-3.42	0E-03	-1.156E-03	4.639F-03	3.867E-03	2.499E-03

Figure B.5. Solution for K.

```
T = 1.000 SECONDS
               2.321E-02
   1.010E-01
                           -1.083E-01
                                        -2.012E-02
                                                    -3.420F-03
   2.321E-02
               6.421E-03
                           -2.544E-02
                                        -6.137F-03
                                                    -1.156F-03
  -1.083E-01
              -2.544E-02
                            1.169E-01
                                         2.350E-02
                                                     4.732F-03
  -2.012E-02
              -6.137E-03
                            2.350E-02
                                         9.959F-03
                                                     4.261E-03
  -3.420E-03
              -1.156E-03
                            4.732E-03
                                         4.261E-03
                                                     3.100E-03
  T =
        1.200 SECONDS
K
   1.010E-01
               2.321E-02
                           -1.083E-01
                                        -2.012E-02
                                                    -3.420E-03
                                                    -1.156F-03
   2.321E-02
               6.421E-03
                           -2.544E-07
                                        -6.137E-03
  -1.083F-01
              -2.544E-02
                            1.169E-01
                                         2.352E-02
                                                     4.778E-03
  -2.012E-02
              -6.137E-03
                            2.352E-02
                                         1.00RE-02
                                                    -4-476F-03
  -3.420E-03
              -1.156E-03
                            4.778E-03
                                         4.476F-03
                                                     3.488E-03
  T =
        1.400 SECONDS
   1.010E-01
               2.321E-02
                           -1.083F-01
                                       -2.012E-02
                                                    -3.420E-03
   2.321E-02
               6.421E-03
                           -2.544E-02
                                        -6.137E-03
                                                    -1.156E-03
  -1.083E-01
              -2.544E-02
                            1.169E-01
                                         2.353E-02
                                                     4.800F-03
                                                     4.586E-03
  -2.012E-02
              -6.137E-03
                            2.353E-02
                                         1.013E-02
  -3.420E-03
               -1.156E-03
                            4.800E-03
                                         4.586E-03
                                                     3.717E-03
  T =
        1.470 SECONDS
   1.010F-01
                2.321E-02
                           -1.083E-01
                                        -2.012E-02
                                                    -3.420E-03
               6.421E-03
   2.321E-02
                           -2.544F-02
                                        -6.137E-03
                                                    -1.156F-03
  -1.083E-01
              -2.544E-02
                            1.169F-01
                                         2.354E-02
                                                     4.805E-03
  -2.012F-02
              -6.137E-03
                            2.354E-02
                                         1.014E-02
                                                     4.610E-03
  -3.420E-03
              -1.156E-03
                            4.805E-03
                                         4.610E-03
                                                     3.771E-03
```

ABOVE MATRIX IS SS SOLUTION FOR K TO WITHIN 0.1%

Figure B.5. (Con't).

DTMIN = 0.0025 SECONDS

BEGINNING OF SOLUTION FOR STEADY STATE P

T =	0.0	SECONOS			
PΠ					
0.0		0.0	0.0	O•O	n. n
0.0		0.0	0.0	0•0	0.0
0.0		0.0	5.000E-01	1.000E-01	1.000E-01
0.1		0.0	1.000E-01	5.000E-01	1.000E-01
0.0		0.0	1.000E-01	1.700E-01	5.000E-01
T =	0.050	SECONDS			
P	00.730	SE COMD.			
0.0		0.0	0.0	0.0	0.0
0.0		0.0	0.0	0.0	0.0
0.0		0.0	3.507F-02	3.248E-02	1.247E-02
0.0		0.0	3.248E-02	3.826E-01	1.131E-01
0.0		0.0	1.247E-02	1.131E-01	5.284F-01
			241: 112 02	101512 1/1	362011 01
T =	0.132	SECONDS			
P					
0.0		0.0	0.0	0.0	0.0
0.0		0.0	0.0	0.0	0.0
0.0		0.0	1.828E-02	4.359F-02	1.848E-02
0.0		0.0	4.359E-02	2.440E-01	1.4765-01
0.0		0.0	1.848E-02	1.476E-01	5.784F-01
T =	0.292	SECONDS			
P					
0.0		0.0	0.0	n.n	0.0
0.0		0.0	0.0	0.0	0.0
0.0		0.0	1.477E-02	3.386F-02	2.976E-02
0.0		0.0	3.386E-02	1.174E-01	1.762E-01
0.0		0.0	2.976E-02	1.762E-01	6.082E-01
T =	0.437	SECONDS			
P	00 1.31	500000			
0.0		0.0	0.0	0.0	0.0
0.0		0.0	0.0	0.0	0.0
0.0		0.0	1.308E-02	2.974E-02	3.603F-02
9.0		0.0	2.974E-02	1.018E-01	1.856F-01
0.0		0.0	3.603E-02	1.856E-01	5.962E-01

Figure B.6. Solution for P.

P	T =	0.542 SECONDS			
,-	0.0	0.0	0.0	0.0	0.0
	0.0	0.0	0.0	0.0	0.0
	0.0	0.0	1.279F-02	2.961F-02	3.794F-02
	0.0	0.0	2.961E-02	9.984E-02	1.833E-01
	0.0	0.0	3.794E-02	1.833E-01	5.812F-01
P	T =	0.652 SECONDS			
	0.0	0.0	0.0	0.0	0.0
	0.0	0.0	0.0	0.0	0.0
	0.0	r.n	1.272F-02	2.943E-02	3.900F-02
	0.0	0.0	2.943F-02		1.781E-01
	0.0	0.0	3.800E-02	1.781E-01	5.697F-01
P	T =	0.972 SECONDS			
	0.0	0.0	0.0	0.0	0.0
	0.0	0.0	0.0	0.0	0.0
	0.0	0.0	1.243F-02	2.840F-02	3.702E-02
	0.0	0.0	2.840F-02	9.258F-02	1.729E-01
	0.0	0.0	3.702E-02	1.7295-01	5.626E-01
P	T =	1.112 SECONDS			
	0.7	0.0	0.0	0.0	0.0
	0.0	0.0	0.0	o.n	0.0
	0.0	0.0	1.239E-02	2.836F-02	3.704F-02
	0.0	0.0	. 2.836E-02	9.248E-02	1.728F-01
	0.0	0.0	3.704E-02	1.728E-01	5.625E-01
P	T =	1.227 SECONDS			
	0.0	0.0	0.0	0.0	0.0
	0.0	0.0	0.0	0.0	0.0
	0.0	0.0	1.238F-02	2.835E-02	3.705E-02
	0.0	0.0	2.835E-02	9.245E-02	1.728E-01
	0.0	0.0	3.705E-02	1.728E-01	5.624F-01
P	T =	1.432 SECONDS			
	0.0	0.0	0.0	0.0	0.0
	0.0	0.0	0.0	0.0	0.0
	0.0	0.0	1.238E-02	2.835E-02	3.704F-02
	0.0	0.0	2.835E-02	9.239E-02	1.727E-01
	0.0	0.0	3.704E-02	1.727E-01	5.623E-01

Figure B.6. (Con't).

T =	1.627 SECONDS			
P		•		
0.0	0.0	0.0	n•n	r•n
0.0	0.0	0.0	0.0	0.0
0.0	0.0	1.238E-02	2.834E-02	3.704F-02
0.7	n• n	2.834E-02	9.237E-02	1.727F-01
0.0	0.0	3.704E-02	1.727E-01	5.623E-01
T =	1.657 SECONDS			
P				
0.0	0.0	0.0	0.0	0.0
0.7	0.0	0.0	0.0	0.0
0.0	0•0	1.238E-02	2.834F-02	3.704E-02
0.0	0.0	2.834E-02	9.237E-02	1.727F-01
0.0	0.0	3.704E-02	1.727F-01	5.623E-01

ABOVE MATRIX IS SS SOLUTION FOR P TO WITHIN 0.017

Figure B.6. (Con't).

AH

```
5.194E+00
             1.007F+01 -9.867F+00 -3.712F+00 -7.812F-01
  -5.120E+01
             -4.045E+01
                         5.976F+01
                                      2.229F+01
                                                 4.692E+00
  6.190F+00
              0.0
                         -8.590F+00
                                      2.400E+00
                                                  0.0
                                                 2.500F+00
   1.417F+01
              0.0
                         -1.417E+01 -2.500E+00
              0.0
   1.852E+01
                         -1.852E+01
                                     0.0
                                                 -2.600F+00
CH
                                    1.115E+00 2.346F-01
  -2.560E+00 -1.023E+00 2.963E+00
KH
   0.0
   0.1
   6.190E+00
   1.417E+01
   1.852E+01
LA(I) -- EIGENVALUES
  -2.304E+00
             1.238E+00
  -2.304F+00 -1.238E+00
  -2.061E+01
            1.536F+01
  -2.061E+01
             -1.536E+01
  -3.112E+00
              0.0
SOLUTION FOR EIGENVALUES CONVERGED
CHARACTERISTIC POLYNOMIAL
   1.000F+00
              4.895E+01
                          1.000E+03
                                      5.996E+03
                                                  1.488F+04
   1.407E+04
```

Figure B.7. Filter and controller model.

	+00 -4.30[F-0] -72 -6.574E-0] +00 -4.548F-0] -01 -7.746E-01	400 4-301E-01 -02 5-575E-01 -01 7-756E-01 -01 1-742E-01	-05 2.346F-07 -07 -7.971F-02 -03 -4.775F-03 -02 -1.133F-07 -07 -1.487F-02	-05 -2.346E-02 -02 7.271F-07 -03 4.775E-03 -02 1.133F-02 -02 1.487E-02	0.000000000000000000000000000000000000
	-1.307F+00 -4.719F+00 -1.314F+00 3.698F-01 3.727F-01	-1.3775+00 -4.7107-02 -1.3145+0 3.6945-01	-7.122E-05 -2.694F-07 4.025E-03 1.045E-02 1.684E-07	-2.122F-05 -2.494E-02 4.025F-03 1.045F-02	2.613F+0n 1.481F-01 2.620E+0n -7.605E-01 2.220F-01
	-4.533F-01 5.714F-07 -4.532F-01 2.607F-01	4.533E-71 -6.714E-02 4.532E-01 -2.607E-01 -1.627E-01	1.511E-01 -4.175E-01 -3.560F-02 -8.562F-02 -1.163E-01	-1.5115-01 4.1755-01 3.5605-07 8.5525-07 1.1636-01	00000
	5.285F-01 2.933F-01 5.400F-01 2.850F-01 -4.076F-02	5.293F-01 2.933F-01 5.400F-01 2.850F-01	2.946F-02 -2.617E-01 1.965E-02 5.237E-02 8.871F-02	2.986F-02 -2.617E-01 1.965F-32 5.737E-02	-1.117F+00 -6.311F-02 -1.119F+00 3.252F-01 -9.590F-02
	1.681E+00 9.968=-01 1.729E+00 1.007E+00	-1.6813+00 -9.6585-01 -1.7205+00 -1.007E+00	6.428E-01 -2.293E+00 -7.440F-02 -1.642F-01	-6.428F-01 2.297E+00 7.440F-02 1.642F-01 1.725F-01	00000
UFS	1.623E+00 -1.664E-01 1.625E+00 -8.169E-01 -5.530E-01	1.623E+01 -1.564E-01 1.625E+01 -8.169E-01 -5.530E-01	-3.262E-01 2.409E-01 1.751E-01 4.399E-01 6.624E-01	-3.262F-01 2.409F-01 1.751F-01 4.399E-01 6.624F-01	-2.594F+0n -1.488E-01 -2.500F+09 7.539E-01 -2.189F-01
AS FIGENVALUES	-4.427F-01 -2.417F-01 -4.518F-01 -2.325F-01 3.623F-02	4.422F-01 2.417F-01 4.518F-01 2.325F-01 -3.623F-02	-2.602E-01 7.627E-01 6.067E-02 1.454E-01	2.6975-01 -7.620F-01 -6.067F-02 -1.454E-01	ccccc
N SAMF ORDER	-3.683E-01 5.912E-02 -3.680E-01 7.191E-01 1.339E-01	-3.683E-01 5.912E-02 -3.680E-01 2.191E-01 1.339E-01	-3.704E-02 4.179F-01 -3.876E-02 -1.010E-01 -1.681E-01	-3.704E-02 -3.826E-01 -1.010E-01 -1.681F-01	8.107F-01 4.595E-02 8.126E-01 -2.361E-01 6.847E-02
DEMPOTENTS I	-1.721F+00 -9.091E-01 -1.757F+00 -8.543E-01 1.538E-01	1.721E+00 9.001E-01 1.757E+00 8.544E-01 -1.538E-01	-5.471E-01 2.140E+00 6.118F-02 1.324E-01 1.292E-01	5.471E-01 -2.140E+00 -6.118E-02 -1.374E-01	
CONSTITUENT INEMPOTENTS IN SAME ORDER AS	-1.341F+00 2.531E-01 -1.339F+00 8.598E-01 5.031E-01	-1,341E+0n 2,531E-01 -1,339E+01 8,589E-01 5,031E-01	3.378F-01 -3.390E-01 -1.640E-01 -4.209E-01 -6.391F-01	3.378F-01 -3.390E-01 -1.590E-01 -4.209F-01 -6.301E-01	3.017F+00 1.719F-01 3.015F+00 -8.758E-01 2.539F-01

Figure B.8. Constituent idempotents.

```
B(I) -- WHERE TE IS SUM OF B(I)/(S - LA(I)) TERMS
   2.311F+00 -4.503E+00
   2.311E+00
             4.503E+00
   1.653F+01
             -1.428F+00
   1.653E+01
              1.428E+00
   7.981E-01
              0.0
THE TF AS A RATIO OF POLYNOMIALS IS AS FOLLOWS:
C(0)(C(1)S(N-1) + C(2)S(N-2) + --- + C(N))
             DIVIDED BY
  (S - LA(1)) (S - LA(2)) --- (S - LA(N))
C(0) -- CONSTANT TERM OF TRANSFER FUNCTION
   3.848E+01
             0-0
C(1) -- NUMERATOR POLYNOMIAL COEFFICIENTS
   1.000E+00
             0.0
   3.233F+01
              1.190E-06
   3.014E+02
              6.344E-06
   1.181E+03
              1.789E-04
   1.660E+03 -9.516E-05
COMPLETE NUM COEF BEGINNING WITH COEF OF S(N-1)
  -3.948E+01 -4.744E+02 1.328E+04 1.865E+05 8.447E+05
   1.278E+06
COMPLETE DENOMINATOR QUADRATIC FACTORS
   1.000E+00
              4.608E+00
                          6.841E+00
   1.000E+00
              4.123F+01
                          6.609E+02
   0.0
              1.000E+00
                          3.112E+00
   0.0
              1.000E+00
                          2.000E+01
                          1.000E+00
   0.0
              3.000E-01
```

Figure B.9. Filter and controller transfer function.

PLANT IS YC=1 TN=0.3 - TAU=0.1 - WD1=2.4 - WD2=2.5 - WD3=2.6 NI=500 - RI=20 - M22=0.534 TRANSFER FUNCTION DATA JANUARY 5, 1968

COEFFICIENTS - FORWARD LOOP NUMERATOR

-3.848E+01 -4.744E+02 1.328F+04 1.865E+05 8.447F+05 1.278E+06

FACTORS - FORWARD LOOP NUMERATOR

1.000E+00	8.995F+00	2.491F+01
1.000F+00	-1.678F-04	-4.000E+07
0.0	1.000E+00	3.332E+00
0.0	0.0	-3.84RE+01

FACTORS - FORWARD LOOP DENOMINATOR

1.000E+00	4.608E+00	6.841E+00
1.000E+00	4.123E+01	6.609F+02
0.0	1.000E+00	3.112E+00
0.0	1.000E+00	2.000E+01
0.0	3.000E-01	1.000E+00

Figure B.10. Man-plant transfer function.

	FORWARD LOOP		
FREQUENCY (RPS)	GAIN(DB)	PHASE (DEG)	
1.0006-03	1.3145+01	-4.275F-01	
1.038F-02	1.314E+01	-4.435F-01	
1.076E-02	1.314E+01	-4.602E-01	
1.117E-02	1.3146+01	-4.774F-01	
1.159E-02	1.314F+01	-4.954F-01	
1.202F-02	1.314F+01	-5.139F-01	
1.247E-02	1.314E+01	-5.332E-01	
1.294E-02 1.343E-02	1.3145+01	-5.533E-01	
1.393E-02	1.314E+01 1.314E+01	-5.740F-01 -5.956F-01	
1.445E-02	1.314F+01	-6.179E-01	
1.5005-02	1.314F+01	-6.411F-01	
1.556F-02	1.314E+01	-6.651E-01	
1.614E-02	1.314F+01	-6.901F-01	
1.675E-02	1.314E+01	-7-160E-01	
1.738E-02	1.314E+01	-7.429F-01	
1.903E-02	1.314F+01	-7.708F-01	
1.9715-02	1.314F+01	-7.997E-01	
1.941E-0?	1.314E+01	-8.297E-01	
2.014E-02	1.314E+01	-8.608E-01	
2.089F-02	1.314E+01	-8.932F-01	
2.168E-02	1.314E+01	-9.267E-01	
2.249E-02	1.314F+01	-9.615F-01	
2.334E-02	1.314E+01	-9.975F-01	
2.421E-02	1.314F+01	-1.035E+00	
2.512F-02	1.314F+01	-1.074F+00	
2.606E-02	1.314F+91	-1.114F+00	
2.704F-02	1.314E+01	-1.1565+00	
2.806E-02 2.911F-02	1.314F+01	-1.199E+00	
3.020E-02	1.314F+01 1.314F+01	-1.244E+00 -1.291E+00	
3.133E-02	1.314E+01	-1.339E+00	
3.251E-02	1.314F+01	-1.390F+00	
3.373E-02	1.314E+01	-1.442F+00	
3.5005-02	1.314F+01	-1.496E+00	
3.631E-02	1.3145+01	-1.552F+00	
3.767E-02	1.314E+01	-1.610F+00	
3.909E-02	1.314E+01	-1.671F+00	
4.055E-02	1.314E+01	-1.734E+00	
4.208E-02	1.314E+01	-1.799F+00	
4.365E-02	1.3148+01	-1.866E+00	
4.529E-02	1.314E+01	-1.936F+00	
4.699F-02	1.314E+01	-2.009E+00	
4.876E-02	1.314F+01	-2.084E+00	
5.059E-02	1.314E+01	-2.162F+00	
5.248F-02	1.314E+01	-2.244F+00	
5.445E-02	1.314E+01	-2.328F+00	
5.650E-02	1.314E+01	-2.415F+00	

Figure B.11. Man-plant frequency response data.

5.962E-02	1.314E+01	-2.506F+00
6.082E-02	1.314E+01	-2.600F+00
6.310F-02	1.314E+01	-2.697F+00
6.547E-02	1.314E+01	-2.799E+00
6.793E-02	1.314E+01	-2.904F+00
7.048E-02	1.314F+01	-3.012F+00
7.312F-02	1.314F+01	-3.126F+00
7.587E-02	1.314E+01	-3.243F+00
7.871E-02	1.314E+01	-3.364E+00
8.167E-02	1.314E+01	-3.491E+00
8.473E-02	1.314E+01	-3.627E+00
8.791F-02	1.313E+01	-3.7585+00
· · · · · ·		-
9.121E-02	1.313E+01	-3.899E+00
9.463E-02	1.313E+01	-4.045E+00
9.919E-02	1.313E+01	-4.197F+00
1.019E-01	1.313F+01	-4.354F+00
1.057F-01	1.313F+01	-4.517F+00
1.097F-01	1.313E+01	-4.687E+00
1.138E-01	1.313F+01	-4.863F+00
1.180E-01	1.313F+01	-5.045F+00
1.225E-01	1.3135+01	-5.234F+00
1.271E-01	1.313E+01	-5.431F+00
1.318E-01	1.313E+01	-5.634F+00
1.368E-01	1.312F+01	-5.846F+00
1.419E-01	1.312E+01	-6.065F+00
1.4725-01	1.312F+01	-6.292E+00
1.528F-01	1.312E+01	-6.528F+00
1.585E-01	1.312E+01	-6.773E+00
1.645E-01	1.312E+01	-7.027E+00
1.706E-01	1.312E+01	-7.290F+00
1.770F-01	1.311E+01	-7.564E+00
1.8376-01	1.311E+01	-7.847E+00
1.906E-01	1.311E+01	-8.141E+00
1.977F-01	1.311E+01	-8.446E+00
2.051E-01	1.310F+01	-8.763E+00
2.128F-01	1.310E+01	-9.091F+00
2.208E-01	1.310F+01	-9.432E+00
2.291E-01	1.309E+01	-9.785F+00
2.377F-01	1.309F+01	-1.015E+01
2.466E-01	1.309E+01	-1.053E+01
2.559E-01	1.308E+01	-1.093E+01
2.655E-01	1.308E+01	-1.133E+01
2.755E-01		
	1.307E+01	-1.176E+01
2.858E-01	1.307E+01	-1.220E+01
2.965F-01	1.306F+01	-1.266F+01
3.076E-01	1.305E+01	-1.313E+01
3.192E-01	1.305E+01	-1.362F+01
3.312E-01	1.304E+01	-1.413E+01
3.436E-01	1.303E+01	-1.466F+01
3.565F-01	1.302E+01	-1.520E+01
3.699E-01	1.302E+01	-1.577F+01
3.837E-01	1.301E+01	-1.636F+01
3.982E-01	1.300E+01	-1.697E+01
4.131E-01	1.298E+01	-1.760E+01

Figure B.11. (Con't).

```
4.286E-01
                1-297E+01
                            -1.826E+01
                1.296E+01
4.447E-01
                             -1.894F+01
4.614E-01
                1.294E+01
                            -1.9656+01
4.787F-01
                1.293E+01
                            -2.038E+01
4.966E-01
                 1.291E+01
                            -2.113E+01
5.153E-01
                1.290F+01
                            -2.192F+01
                1.288F+01
5.346E-01
                            -2.273E+01
5.547F-01
                1.286F+01
                            -2.358E+01
5.755E-01
                1.283E+01
                            -2.445E+01
5.971E-01
                1.281E+01
                            -2.535E+01
6.195F-01
                1.279E+01
                             -2.629E+01
6.428E-01
                1.276F+01
                             -2.726E+01
6.669E-01
                1.273E+01
                            -2.827E+01
6.919F-01
                1.2705+01
                            -2.931E+01
7.179E-01
                1.266F+01
                             -3.039E+01
7.448E-01
                1.263E+01
                            -3.150E+01
7.728E-01
                1.259E+01
                             -3.266E+01
8.018F-01
                1.254F+01
                             -3.385E+01
8.319E-01
                1.250F+01
                            -3.509F+01
8.631E-01
                1.245F+01
                             -3.636F+01
8.955E-01
                1.240E+01
                             -3.768E+01
9.291E-01
                1.234F+01
                             -3.904F+01
9.639E-01
                1.228E+01
                             -4.045E+01
1.000E+00
                1.221F+01
                            -4.190E+01
1.038E+00
                1.214F+01
                            -4.340E+01
1.077E+00
                1.207E+01
                            -4.495E+01
1.117F+00
                1.198E+01
                             -4.654F+01
1.159F+00
               1.190E+01
                             -4.818F+01
                            -4.987E+01
1.202F+00
                1.180F+01
1.249E+00
                1.170F+01
                            -5.161F+01
1.294E+00
                1.159E+01
                             -5.340E+01
1.343E+00
                1.147E+01
                             -5.523E+01
1.393F+00
                ·1.135E+01
                             -5.711E+01
1.446E+00
                1.121E+01
                             -5.904F+01
1.500F+00
                1.107E+01
                            -6.101F+01
1.556E+00
                1.092E+01
                             -6.303F+01
1.615E+01
                1.075E+01
                             -6.509F+01
1.675F+00
                 1.058E+01
                             -6.719E+01
1.738E+00
                1.039E+01
                            -6.932F+01
1.803E+00
                            -7.149F+01
                1.020E+01
1.871E+00
                9.985E+00
                             -7.369F+01
1.941E+00
                9.7625+00
                             -7.592E+01
2.014E+00
                9.527E+00
                             -7.817E+01
2.090E+00
                9.278E+00
                            -8.044E+01
2.158E+00
                9.015E+00
                            -8.272F+01
2.249E+00
                8.739E+00
                            -8.502F+01
2.334E+00
                8.450E+00
                            -8.731E+01
.2.421F+00
                            -8.960F+01
                8.147E+00
2.512E+00
                7.830F.+00
                             -9.189E+01
2.606E+00
                7.500E+00
                            -9.416E+01
2.704F+01
                7.157E+00
                            -9.641E+01
2.804E+00
                6.802E+00
                            -9.864E+01
2.911E+00
                6.435E+00
                            -1.008E+02
3.720F+00
                6.057E+00
                            -1.030F+02
```

Figure B.11. (Con't).

```
3.134E+00
                5.669E+00
                            -1.051E+02
3.251F+00
                5.271F+00
                            -1.072F+02
3.373E+00
                            -1.093E+02
                4.854E+00
3.500F+00
                4.450E+00
                            ~1.113F+02
3.631E+00
                4.029F+00
                            -1.132F+02
3.767F+00
                3.603E+00
                            -1.151F+02
3.909F+00
                3.172F+00
                            -1.170E+02
4.0566+00
                2.738E+00
                            -1.188F+02
4.208E+00
                2.301E+00
                            -1.205E+02
4.366E+00
                1.863E+00
                            -1.222E+02
4.529F+00
                            -1.239F+02
                1.425E+00
4.699F+00
                9.8706-01
                            -1.255F+02
4.876F+00
                5.506F-01
                            -1.271E+02
5.059F+00
                1.164F-01
                            -1.287F+02
5.249F+00
               -3.149E-01
                            -1.303F+02
5.446E+00
               -7.426E-01
                            -1.318E+02
5.650E+00
                            -1.333E+02
               -1.166E+00
5.862E+00
               -1.585E+00
                            -1.348F+02
6.082E+00
               -2.000E+00
                            -1.363F+02
6.310E+00
               -2.409E+00
                            -1.379F+02
6.547E+00
                            -1.394E+02
               -2.812E+00
6.793E+00
               -3.210E+00
                            -1.409E+02
               -3.602E+00
7.048E+00
                            -1.425E+02
7.312F+00
                            -1.441F+02
               -3.989E+00
7.587E+00
               -4.370E+00
                            -1.457E+02
7.871E+00
               -4.746E+00
                            -1.474F+02
8.167F+00
               -5.116F+00
                            -1.491F+02
8.473E+00
               -5.480E+00
                            -1.508E+02
8.791F+00
               -5.840F+00
                            -1.527E+02
9.121E+00
               -6.195E+00
                            -1.545E+02
9.463E+00
              -6.545E+00
                            -1.564F+02
9.919E+00
               -6.891E+00
                            -1.584E+02
1.019E+01
               -7.233E+00
                            -1.605E+02
1.057E+01
               -7.572E+00
                            -1.626E+02
1.097E+01
               -7.907E+00
                            -1.647E+02
1.138E+01
               -8.240E+00
                            -1.670E+02
1.180E+01
               -8.570F+00
                            -1.693E+02
1.225F+01
               -8.899E+00
                            -1.717F+02
1.271E+01
               -9.226E+00
                            -1.742E+02
1.318E+01
               -9.553E+00
                            -1.768E+02
1.368E+01
               -9.879E+00
                            -1.794E+02
1.419E+01
               -1.021E+01
                            -1.821E+02
               -1.053E+01
1.472E+01
                            -1.849E+02
1.528E+01
               -1.086F+01
                            -1.878E+02
1.585E+01
               -1.120E+01
                            -1.908E+02
1.645F+01
               -1.153E+01
                            -1.938F+02
1.706E+01
               -1.187F+01
                            -1.969E+02
               -1.222E+01
1.770F+01
                            -2.001F+02
1.937E+01
               -1.257E+01
                            -2.033F+02
1.906E+01
               -1.293E+01
                            -2.066E+02
1.977E+01
               -1.330E+01
                            -2.100E+02
2.051E+01
               -1.367E+01
                            -2.134F+02
2.128E+01
               -1.406F+01
                            -2.168F+02
2.208E+01
               -1.445E+01
                            -2.203F+02
```

Figure B.11. (Con't).

```
2.291F+01
               -1.485E+01
                            -2.238E+02
2.377E+01
               -1.527F+01
                            -2.274E+02
2.466E+01
               -1.570E+01
                            -2.309F+02
2.559E+01
               -1.614F+01
                            -2.345F+02
2.655F+01
               -1.659E+01
                            -2.389E+02
2.754F+01
               -1.705F.+01
                            -2.416F+02
2.858E+01
               -1.753E+01
                            -2.451F+02
2.965E+01
               -1.802E+01
                            -7.486F+02
3.076F+01
               -1.852E+01
                            -2.520E+02
3.192F+01
               -1.903E+01
                            -2.554F+02
3.312E+01
               -1.956E+01
                            -2.588E+07
3.436F+01
               -2.009F+01
                            -2.621F+02
3.565E+01
               -2.064F+01
                            -2.653F+02
3.699F+01
               -2.119E+01
                            -2.684E+02
3.837F+01
               -2.175E+01
                            -2.715F+02
3.981E+01
               -2.232F+01
                            -2.745F+02
4.131E+01
               -2.290E+01
                            -2.775F+02
4.286E+01
               -2.349E+01
                            -2.803E+02
4.447E+01
               -2.408E+01
                            -2.831F+02
4.614E+01
               -2.467F+01
                            -2.858E+02
4.787E+01
               -2.528E+01
                            -2.884E+02
4.966E+01
                            -2.909E+02
               -2.5885+01
5.153E+01
               -2.649E+01
                            -2.934F+02
5.346E+01
               -2.711E+01
                            -2.958E+02
5.547F+01
               -2.773E+01
                            -2.981F+02
5.755E+01
               -2.835F+01
                            -3.003F+02
5.971E+01
               -2.897E+01
                            -3.024F+02
6.195E+01
               -2.960E+01
                            -3.045E+02
6.427E+01
               -3.022E+01
                            -3.065F+02
6.669F+01
               -3.085E+01
                            -3.084F+02
6.919E+01
               -3.148E+01
                            -3.103E+02
7.179E+01
               -3.212E+01
                            -3.121F+02
7.448E+01
               -3.275E+01
                            -3.139E+02
                            -3.155E+02
7.727E+01
               -3.338E+01
8.017F+01
               -3.402E+01
                            -3.171F+02
               -3.465E+01
8.318E+01
                            -3.186F+C2
               -3.529E+01
8.630E+01
                            -3.201F+02
               -3.593E+01
8.954E+01
                            -3.216F+02
9.290E+01
               -3.657E+01
                            -3.230F+02
9.639E+01
               -3.720E+01
                            -3.243E+02
1.000E+02
               -3.784E+01
                            -3.256E+02
```

Figure B.11. (Con't).

The matrix M that must be read into the program is defined by

$$E\left\{\begin{bmatrix} u(t+\tau) \\ w(t+\tau) \end{bmatrix} \begin{bmatrix} u(t) \\ w(t) \end{bmatrix}^{T}\right\} = M\delta(\tau)$$
(B.1)

Since u is known, the covariance terms involving u are zero, and since u is single dimensional, the first row and column of M in (B.1) are zero. For simplicity all components of w are assumed to be zero except for the forcing function w_1 . As given by (3.27), the variance of w_1 is 0.534, yielding the complete matrix M as shown in Figure B.4.

Since v is a scalar, the covariance of v is of dimension one with

$$N^{-1} = \frac{1}{n}$$
 (B.2)

As shown in Figure B.4, the value chosen for n^{-1} is

$$n^{-1} = 500$$
 (B.3)

With the assumption that the operator simply minimizes the integral-squared error between the forcing function \mathbf{x}_3 and the plant output \mathbf{x}_1 , and that he also minimizes the integral-squared value of the control \mathbf{u} , the cost function matrices \mathbf{Q} and \mathbf{R} become those shown in Figure B.4. The value selected for the single dimensional \mathbf{R}^{-1} is

$$R^{-1} = \frac{1}{r} = 20$$

Finally, given in Figure B.4, is the s-domain transfer function representing the physiological characteristics of the man and the plant, as required in Appendix A.

Figure B.5 shows the printouts of the time solution for K where (2.12) is solved backwards starting with $K(t_f) = 0$. The solution is continued until

$$\frac{\left|\sum_{i,j} k_{ij}(t)\right| - \sum_{i,j} k_{ij}(t-0.2)}{\sum_{i,j} k_{ij}(t)} \leq 0.001$$
(B.4)

or

$$\sum_{i,j} |k_{ij}(t)| \le 0.0000001$$
 (B.5)

Figure B.6 shows the printouts of the time solution for P with an arbitrarily selected initial condition of

The solution is assumed to have converged when

$$\frac{\left|\sum_{\mathbf{i},\mathbf{j}} \left| P_{\mathbf{i}\mathbf{j}}(\mathbf{t}) \right| - \sum_{\mathbf{i},\mathbf{j}} \left| P_{\mathbf{i}\mathbf{j}}(\mathbf{t}-0.2) \right|}{\sum_{\mathbf{i},\mathbf{j}} \left| P_{\mathbf{i}\mathbf{j}}(\mathbf{t}) \right|} \leq 0.0001$$
(B.7)

or

$$\sum_{i,j} |P_{ij}(t)| \le 0.0000001$$
 (B.8)

In both the solution for K and P, the Runge-Kutta integration technique is used (36).

Figure B.7 shows the solutions for the matrices \hat{A} , \hat{C} , and \hat{K} for the state model of the filter and controller as given by (3.7), (3.8), and (2.8). Also shown are the eigenvalues and characteristic polynomial of \hat{A} .

Figure B.8 shows the constituent idempotents corresponding to the solution $e^{\hat{A}t}$. The characteristic polynomial and the constituent idempotents are found using the conjoint algorithm (37) and the eigenvalues of the characteristic polynomial are obtained using Barstow's method (38).

Figure B.9 shows the transfer function for the filter and controller in two forms and then shows the numerator and denominator of the complete transfer function including the physiological characteristics and the plant. The first form for the filter and controller is

$$G(s) = \frac{B_1}{s-LA_1} + \frac{B_2}{s-LA_2} + --- + \frac{B_n}{s-LA_n}$$
 (B.9)

and the second is

$$G(s) = \frac{C_0(C_1 s^{n-1} + C_2 s^{n-2} + --- + C_n)}{(s-LA_1)(s-LA_2) --- (s-LA_n)}$$
(B.10)

The eigenvalues LA_i are given in Figure B.7 and the B_i and C_i are given in Figure B.9. (The first columns are real parts and the second columns are imaginary parts.) The complete transfer function including the physiological characteristics and the plant is shown next where the numerator is given as a polynomial and the denominator is given as quadratic factors. The first column of the quadratic factors is the coefficient of s^2 , the second the coefficient of s, and the third the constant term.

Figure B.10 shows the input data to the Bode plot subroutine. The first three lines are the titles as given in Figure
B.4. The forward loop numerator coefficients correspond to the
complete system numerator in polynomial form as given in Figure
B.9. Shown next are the quadratic factors for this numerator, again
starting with the coefficient of s², followed by a repeat of the
complete denominator quadratic factors as given in Figure B.9.
Figure B.11 shows the frequency, gain, and phase angle of the complete man-plant transfer function. Since the feedback is unity, the
forward loop response that is printed out is the complete open loop
response. A plot of this data as provided by the Calcomp plotter is
given in Figure B.12. The match of this result with experimental
data is discussed in Chapter 3 in connection with Figure 3.3.

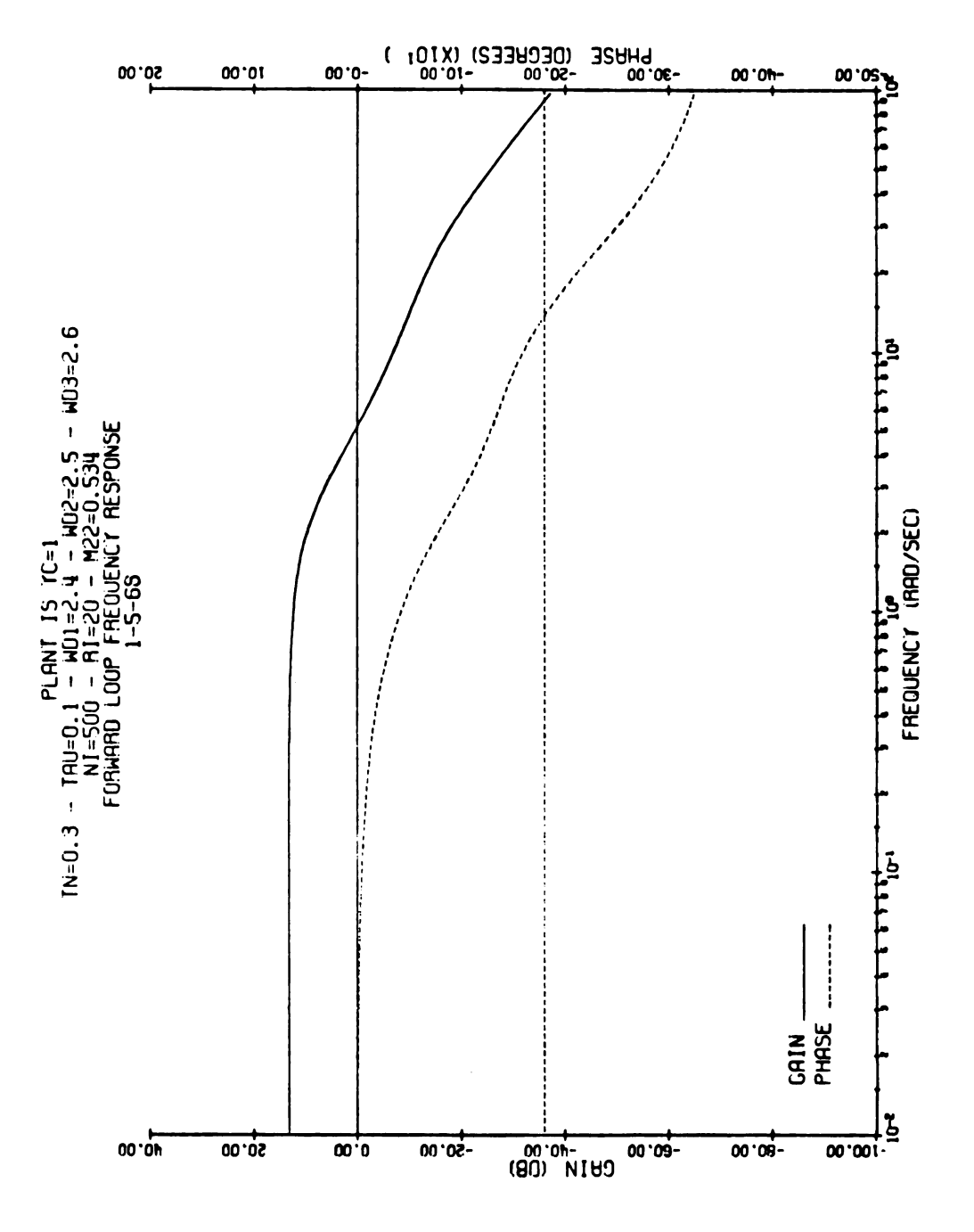


Figure B.12. Example problem Bode plot.

APPENDIX C

EFFECTS OF $\frac{M}{n}$ AND $\frac{Q}{r}$ ON THE MODEL

If N, as defined by the covariance of the measurement noise v given by (2.4), can be written as

$$N = nI \tag{C.1}$$

where n is a constant scalar and I is the unit matrix, then the time solution for the man-plant combination depends only on the ratio M/n, where M is a matrix, and not on M and N individually.

Upon examination of the equations given by (2.1) through (2.13) that define the complete man-plant combination, it is observed that M and N appear in the matrix Riccati equation for P as given in (2.9), N and P appear in the Kalman gain matrix for \hat{K} given in (2.8), and \hat{K} appears in the model for the estimated state vector given in (2.7). Thus, if \hat{K} depends on the ratio M/n only, then the complete model depends on the ratio only.

The dependence of \hat{K} on the ratio M/n can be shown by first substituting the inverse of (C.1) into (2.8) and (2.9), and dividing (2.9) through by n. Thus

$$\frac{P}{n} = A \frac{P}{n} + \frac{P}{n} A^{T} - \frac{P}{n} C^{T} I C \frac{P}{n} + D \frac{M}{n} D^{T}$$
 (C.2)

$$\hat{K} = \frac{P}{n} C^{T}$$
 (C.3)

Next, let

$$P^* = \frac{P}{n} \tag{C.4}$$

and since n is a constant

$$P^* = \frac{P}{n} \tag{C.5}$$

By substitution

$$\dot{P}^* = AP^* + P^*A^T - P^*C^TICP^* + D\frac{M}{n}D^T$$
 (C.6)

$$\hat{K} = P * C^{T}$$
 (C.7)

The solution for P* depends on the ratio $\frac{M}{n}$ only and therefore so does \hat{K} and the complete solution for the man-plant combination.

A similar argument can be applied to the solution for the optimal control gain matrix $\, K \,$ where with $\, R \,$ of the form

$$R = rI \tag{C.8}$$

the solution for K depends on the ratio Q/r only, and therefore, so does the solution for the complete man-plant combination.

APPENDIX D

CROSS-SPECTRAL ANALYZER

As described in detail in [5, 19, 43, 45, and 46], the techniques for finding the cross-spectral density of two stationary random functions of time are well known. The detailed analysis of the accuracies involved when the techniques are mechanized with realizable components, however, is extremely complex. The fundamental basis and the methods used in the display study in Chapter 5 are briefly outlined here.

The basic operations for finding the cross-spectral density at the frequency ω_n are performed as shown in Figure D.1. The two stationary random time functions x(t) and y(t) are frequency shifted using the sine and cosine of ω_n , filtered with a very narrow bandwidth filter, multiplied, and averaged over a long period of time.

Consider the operations performed on x(t) in Figure D.1. The multiplications by $\cos \omega_n t$ and $\sin \omega_n t$ provide the real and imaginary parts, respectively, of a frequency shift where in the time domain

$$x_2(t) = x(t) \left[\cos \omega_n t - j \sin \omega_n t \right]$$

$$= x(t) e^{-j\omega_n t}$$
(D.1)

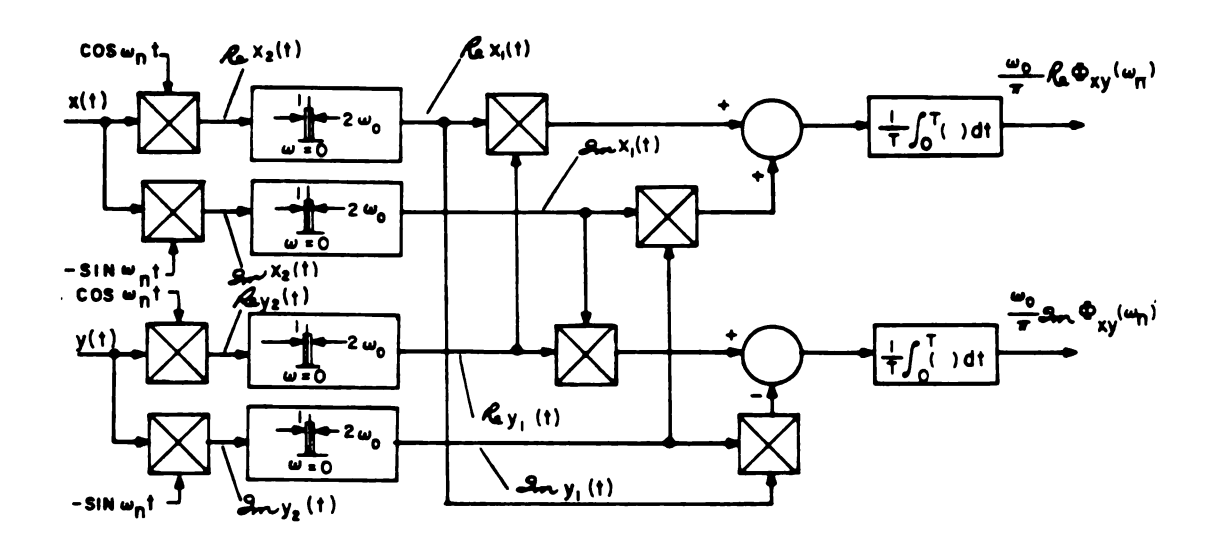


Figure D.1. The basic operations to find the cross-spectral density at $\omega_{\rm n}$.

and the frequency shift is

$$X_{2}(\omega) = \int_{-\infty}^{\infty} \left[x(t) e^{-j\omega_{n}t} \right] e^{-j\omega t} dt$$

$$= X(\omega + \omega_{n})$$
(D.2)

The complete frequency domain representation is shifted to the "left" by $\ensuremath{\omega_n}.$

The narrow bandwidth filter, centered around $\,\omega\,$ = 0, that follows the frequency shift in Figure D.1 yields

$$X_1(\omega) = X_2(\omega)$$
 for $-\omega_0 < \omega < \omega_0$
= 0 elsewhere

and

$$X_1(\omega) = X(\omega + \omega_n)$$
 for $-\omega_0 < \omega < \omega_0$
= 0 elsewhere

By a change of variables

$$X_1(\omega - \omega_n) = X(\omega) \text{ for } -\omega_0 + \omega_n < \omega < \omega_0 + \omega_n$$

$$= 0 \qquad \text{elsewhere}$$
(D.4)

For ω_0 sufficiently small, both (D.3) and (D.4) give

$$X_1(0) = X(\omega_n)$$
 (D.5)
 $X_1(\omega) = 0$ for $\omega \neq \omega_n$

The operation in (D.4) is a bandpass filtering of $X(\omega)$ over the interval $(-\omega_0+\omega_n^{}, \omega_0+\omega_n^{})$ as indicated in Figure D.2. Since both (D.3) and (D.4) give (D.5), the shift of the narrow-band filter to the right is equivalent to shifting $X(\omega)$ to the left and filtering with a filter centered at $\omega=0$.

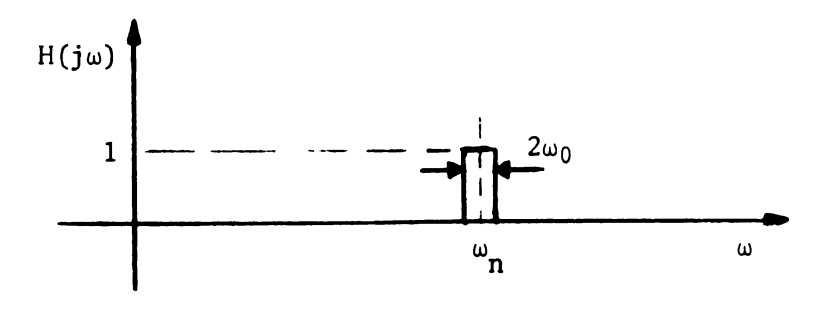


Figure D.2. Frequency shift and filter combined.

If h(t) represent the impulse response of the combined operations shown in Figure D.2, convolution gives

$$x_1(t) = \int_{-\infty}^{\infty} h(\tau)x(t-\tau)d\tau$$
 (D.6)

$$y_1(t) = \int_{-\infty}^{\infty} h(\tau)y(t-\tau)d\tau$$
 (D.7)

The cross-correlation of the complex quantities $x_1(t)$ and $y_1(t)$ [42] is

$$R_{X_1Y_1}(\sigma) = E\left\{x_1(t+\sigma)y_1^*(t)\right\} \tag{D.8}$$

$$= E \left\{ \int_{-\infty}^{\infty} h(\tau) x(t+\sigma-\tau) d\tau \int_{-\infty}^{\infty} h^{*}(\alpha) y(t-\alpha) d\alpha \right\}$$
 (D.9)

Since the integrands are square integrable, the order of integration can be interchanged [42] giving

$$R_{x_1y_1}(\sigma) = \int_{-\infty}^{\infty} h(\tau) \int_{-\infty}^{\infty} h^*(\alpha) R_{xy}(\sigma + \alpha - \tau) d\alpha d\tau$$
 (D.10)

The cross-spectral density is

$$\Phi_{\mathbf{x}_{1}\mathbf{y}_{1}}(\sigma) = \int_{-\infty}^{\infty} e^{-\mathbf{j}\omega\sigma} R_{\mathbf{x}_{1}\mathbf{y}_{1}}(\sigma)d\sigma \qquad (D.11)$$

which, by substitution of (D.10) yields

$$\Phi_{\mathbf{x}_{1}\mathbf{y}_{1}}(\omega) = \int_{-\infty}^{\infty} e^{-\mathbf{j}\omega\sigma} \int_{-\infty}^{\infty} h(\tau) \int_{-\infty}^{\infty} h^{*}(\alpha) R_{\mathbf{x}\mathbf{y}}(\sigma + \alpha - \tau) d\alpha d\tau d\sigma \quad (D.12)$$

$$= \int_{-\infty}^{\infty} h(\tau) e^{-j\omega\tau} \int_{-\infty}^{\infty} h(-\alpha) e^{j\omega\alpha} \int_{-\infty}^{\infty} e^{-j\omega(\sigma+\alpha-\tau)} R_{xy}(\sigma+\alpha-\tau) d\sigma d\alpha d\tau \qquad (D.13)$$

$$\Phi_{\mathbf{x}_1 \mathbf{y}_1}(\omega) = \mathbf{H}(\mathbf{j}\omega)\mathbf{H}(-\mathbf{j}\omega)\Phi_{\mathbf{x}\mathbf{y}}(\omega)$$
 (D.14)

$$= \left| H(j\omega) \right|^2 \Phi_{xy}(\omega) \tag{D.15}$$

The expected value of the complex quantities $x_1(t)$ and $y_1(t)$ at the same time t is

$$E \{x_1(t)y_1^*(t)\} = \frac{1}{2\pi} \int_{-\infty}^{\infty} \Phi_{x_1y_1}(\omega) d\omega$$
 (D.16)

Substitution of (D.15) gives

$$E \left\{ x_1(t) y_1^*(t) \right\} = \frac{1}{2\pi} \int_{-\infty}^{\infty} \left| H(j\omega) \right|^2 \Phi_{xy}(\omega) d\omega \qquad (D.17)$$

With ω_0 in Figure (D.2) sufficiently small, application of the mean value theorem yields

$$E \{x_1(t)y_1^*(t)\} = \frac{\omega_0}{\pi} \Phi_{xy}(\omega_n)$$
 (D.18)

The time average in Figure D.1, with the assumption that the functions are ergodic, corresponds to the ensemble average on the left side of (D.18). In expanded form, (D.18) becomes

$$E\left\{\left[\operatorname{Re} x_{1}(t) + j \operatorname{Im} x_{1}(t)\right] \left[\operatorname{Re} y_{1}(t) - j \operatorname{Im} y_{1}(t)\right]\right\}$$

$$= \frac{\omega_{0}}{\pi} \left[\operatorname{Re} \phi_{xy}(\omega_{n}) + j \operatorname{Im} \phi_{xy}(\omega_{n})\right] \qquad (D.19)$$

giving

$$\frac{\omega_0}{\pi} \operatorname{Re} \Phi_{xy}(\omega_n) = E \left(\operatorname{Re} x_1(t) \operatorname{Re} y_1(t) + \operatorname{Im} x_1(t) \operatorname{Im} y_1(t) \right)$$

$$\frac{\omega_{0}}{\pi} \operatorname{Im} \, \phi_{xy}(\omega_{n}) = E \left(\operatorname{Im} \, x_{1}(t) \operatorname{Re} \, y_{1}(t) - \operatorname{Re} \, x_{1}(t) \operatorname{Im} \, y_{1}(t) \right)$$
(D.21)

It is desired to have a running time that is not too long a time for a human operator to properly perform his task. This places a lower bound on the filter bandwidth and an upper bound on the averaging time. As stated by Blackman and Tukey in [45], the filter bandpass should be "several to many times" wider than the reciprocal of the run time. Also, to obtain a good average, the run time should include several periods of each ω_n . A second-order lag with a corner frequency of 0.0707 rad/sec and a damping ratio of 0.707 were selected for the filter. A four minute run time was used. Thus, the filter bandpass of 0.184 [=2(0.0707)(1.3)] rad/sec is many times larger than 0.0042(=1/240). Based on Table 5.1, the number of cycles per run, for the 10 frequencies, ranges from 6 to 527 allowing a reasonable number of periods at each frequency for averaging. The frequency spacing between the sine-waves in i(t) from Table 5.1 ranges from 0.105 to 6.23 rad/sec. With the filter selected, the main lobes of power [19] centered around each ω_n are within $\omega_n \pm 0.041$. Since 2(0.041) is less than the minimum separation of 0.105, there is no overlapping of these main lobes of power.

The cross-spectral densities $\phi_{ie}(\omega_n)$ and $\phi_{ic}(\omega_n)$ are required in (5.4). Since the forcing function i(t) is composed of the sum of sine-waves, the same sine-waves can be used for the frequency shifting. Consequently, setting

$$x(t) = i(t) \tag{D.22}$$

the steady-state real and imaginary parts of $x_1(t)$ can be computed for the ten forcing function frequencies. In the time domain, the impulse response of the ideal low-pass filter is

$$h_{p}(t) = \frac{\sin \omega_{0}t}{\pi t}$$
 (D.23)

giving by convolution

Re
$$x_1(t) = \int_{-\infty}^{\infty} \frac{\sin \omega_0(t-\tau)}{\pi(t-\tau)} \left[\cos \omega_n \tau\right] i(\tau) d\tau$$
 (D.24)

$$= \int_{-\infty}^{\infty} \frac{\sin \omega_0(\mathbf{t} - \tau)}{\pi(\mathbf{t} - \tau)} \left[a_1 \cos \omega_n \tau \cos \omega_1 \tau + \cdots + a_n \cos^2 \omega_n \tau + \cdots + a_1 \cos \omega_n \tau \cos \omega_1 \sigma \tau \right] d\tau$$

$$+ a_{10} \cos \omega_n \tau \cos \omega_1 \sigma \tau \right] d\tau$$
(D.25)

The constants a_n are the half amplitudes of the sine-waves in i(t). Since ω_0 is chosen smaller than the sums and differences of ω_n and ω_i for $\omega_n \neq \omega_i$, the terms involving $\cos \omega_n \tau \cos \omega_i \tau$, $\omega_n \neq \omega_i$ are zero. The term containing $\cos^2 \omega_n \tau$ yields

Re
$$x_1(t) = \frac{a_n}{\pi} \int_{-\infty}^{\infty} \frac{\sin \omega_0(t-\tau)}{(t-\tau)} \cos^2 \omega_n \tau d\tau$$
 (D.26)

$$= \frac{a_n}{\pi} \int_{-\infty}^{\infty} \frac{\sin \omega_0 \tau}{\tau} \left[\frac{1}{2} + \cos^2 \omega_n (t - \tau) \right] d\tau \qquad (D.27)$$

$$= \frac{a}{\pi} (\pi) \left[\frac{1}{2} \right] = \frac{a}{2}$$
 (D.28)

In a similar manner, the imaginary part of $x_1(t)$ is found with the $\cos \omega_n \tau$ term in (D.24) replaced by $\sin \omega_n \tau$. In this case also, all terms containing $\sin \omega_n \tau \cos \omega_i \tau$ for $\omega_n \neq \omega_i$, are zero. The remaining term gives the result,

$$\operatorname{Im} x_{1}(t) = \int_{-\infty}^{\infty} -\frac{\sin \omega_{0}(t-\tau)}{\pi(t-\tau)} a_{n} \sin \omega_{n} \tau \cos \omega_{n} \tau d\tau \qquad (D.29)$$

$$= \frac{a_n}{\pi} \int_{-\infty}^{\infty} \frac{\sin \omega_0 \tau}{\tau} \left[\frac{1}{2} \right] (\sin^2 \omega_n \tau) d\tau$$
 (D.30)

$$= 0$$
 (D.31)

The block diagram at one frequency, after the above simplifications and assumptions are made, is shown in Figure D.3. The

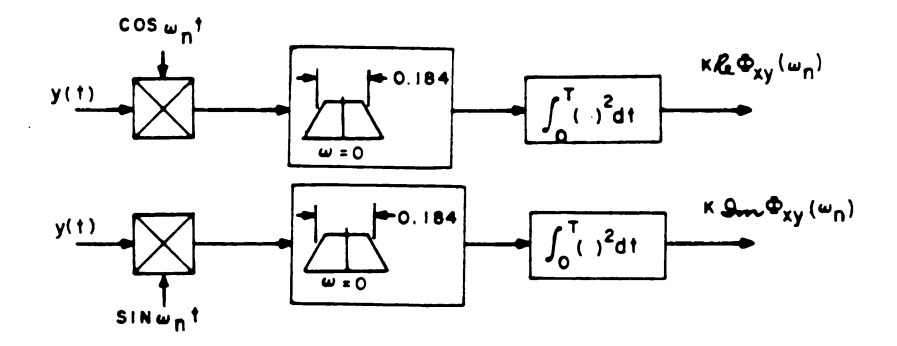


Figure D.3. Simplified block diagram for $\Phi_{xy}(\omega_n)$.

input is either

$$y(t) = e(t) (D.32)$$

or

$$y(t) = c(t) \tag{D.33}$$

which give, respectively, $\phi_{ie}(\omega_n)$ and $\phi_{ic}(\omega_n)$.

As indicated in [46], prewhitening of y(t) can be used to improve the scaling of the analyzer -- particularly at high frequencies. Given the ratio

$$Y_{p} = \frac{\Phi_{ic}(\omega_{n})}{\Phi_{ie}(\omega_{n})}$$
 (D.34)

prewhitening in both e(t) and c(t) cancel, leaving the transfer function unchanged. Prewhitening with a transfer function

$$G_{\mathbf{w}}(j\omega) = 20 \left[\frac{j\omega + 1}{j\omega + 20} \right]$$
 (D.35)

was used.

LIST OF REFERENCES

- 1. Bliss, J., "Human Operator Describing Functions with Visual and Tactile Displays," Paper presented at the <u>Third Annual NASA</u>

 <u>University Conference on Manual Control</u>, <u>University of Southern California</u>, <u>Los Angeles</u>, <u>California</u>, <u>March 1-3</u>, 1967.
- 2. McRuer, D. T., R. E. Magdaleno, and G. P. Moore, "A Neuromuscular Actuation System Model," Third Annual NASA University Conference on Manual Control, University of Southern California, Los Angeles, California, March 1-3, 1967.
- 3. Moore, G. P., "Physiological Bases for Tracking Behavior,"
 Short Course: Modern Man-Machine Systems Theory, UCLA, August 1967.
- 4. McRuer, D., and E. Krendel, <u>Dynamic Response of Human Operators</u>, WADC-TR-56-524, October 1957.
- 5. McRuer, D., D. Graham, E. Krendel, and W. Reisener, Jr., Human Pilot Dynamics in Compensatory Systems: Theory, Models, and Experiments with Controlled Element and Forcing Function Variations, AFFDL TR-65-15, July 1965.
- 6. Leonard, T., "Optimizing Linear Dynamics for Human-Operated Systems by Minimizing the Mean Square Tracking Error," <u>IRE WESCON</u> Convention Record, Volume 4, Part 4, 1960, pp. 57-62.
- 7. McRuer, D. T., and H. R. Jex, "A Review of Quasi-Linear Pilot Models," IEEE Transactions, Volume HFE-8, No. 3, September 1967.
- 8. Pew, R. W., J. C. Duffendack, and L. K. Fensch, "Sine-Wave Tracking Revisited," Second Annual NASA University Conference on Manual Control, M.I.T., Cambridge, Mass., February 28 March 2, 1966.
- 9. Obermayer, R. W., F. A. Muckler, On the Inverse Optimal Control Problem in Manual Control Systems, NASA CR-208, April 1965.
- 10. Young, L. R., and L. Stark, <u>Biological Control Systems -- A</u>

 <u>Critical Review and Evaluation</u>, <u>Developments in Manual Control</u>,

 <u>NASA CR-190</u>, <u>March 1965</u>.
- 11. Muckler, F. A., Man as a Controller: Theory and Applications, Paper presented at Ninth Annual Meeting Human Factors Society, Dayton, Ohio, 19 October 1965.

- 12. Mitchell, M. B., "Systems Analysis The Human Element," Electro-Technology, April 1966.
- 13. Shinners, S. M., "Man-Machine Control Systems," Electro-Technology, pp. 59-76, April 1967.
- 14. Bekey, G. A., "Description of the Human Operator in Control Systems," Modern Control Systems Theory, pp. 431-462, McGraw-Hill Book Co., New York, 1965.
- 15. Mehr, M. H., "Bibliography on Tracking Controls," Measurement Systems, Inc., Norwalk, Conn., July 1967.
- 16. Costello, R. G., and T. J. Higgins, "An Inclusive Classified Bibliography Pertaining to Modeling the Human Operator as an Element in an Automatic Control System," 7th IEEE Symposium on Human Factors in Electronics, Minneapolis, Minn., May 5-6, 1966.
- 17. Diamantedes, N. D., "Information Feedback in Jet-Pilot Control Stick Motion," AIEE Applications and Industry, November 1957.
- 18. Diamantedes, N. D., "A Pilot Analog for Airplane Pitch Control," Journal of Aero. Sciences, Volume 25, pp. 361-371, June 1958.
- 19. Bekey, G. A., An Investigation of Sampled Data Models of the Human Operator in a Control System, Ph.D. Thesis, E.E. Department, UCLA, 1962.
- 20. Thomas, R. E., <u>Development of New Techniques for Analysis of Human Controller Dynamics</u>, USAF, MRL, TDR-62-65, 1962.
- 21. Obermayer, R. W., and F. A. Muckler, Modern Control System Theory and Human Control Functions, NASA CR-256, 1965.
- 22. Koenig, H. E., Y. Tokad, and H. K. Kesavan, <u>Analysis of Discrete</u> Physical Systems, McGraw-Hill Book Co., 1967.
- 23. Bryson, A. E., and D. E. Johansen, "Linear Filtering for Time-Varying Systems Using Measurements Containing Colored Noise,"

 IEEE Transactions on Automatic Control, Volume AC-10, No. 1,
 pp. 4-10, January 1965.
- 24. Kovatch, G., "Optimal Guidance and Control Synthesis for Maneuverable Lifting Space Vehicles," Presented at the 9th Symposium of Ballistic Missile and Space Technology, San Diego, California, Volume 1, pp. 328-379, 1964.
- 25. Joseph, P. D., and J. T. Tou, "On Linear Control Theory," AIEE Trans., Volume 80, pp. 193-196, 1961.
- 26. Lee, R. C. K., Optimal Estimation, Identification, and Control, Research Monograph No. 28, The M.I.T. Press, Cambridge, Mass., 1964.

- 27. Kalman, R. E., "A New Approach to Linear Filtering and Prediction Problems," <u>Journal of Basic Engineering Transactions</u>
 ASME, Series D, Volume 82, pp. 35-45, March 1960.
- 28. Kalman, R. E., T. S. Englar, and R. S. Busy, <u>Fundamental Study</u> of Adaptive Control Systems, USAF, ASD-TRD-61-27, Volume 1, 1961.
- Richman, J., and F. Thau, "Elements of Kalman Filtering Techniques: Part I -- Theory," General Precision Aerospace
 Technical News Bulletin, Volume 9, No. 3, 3rd Quarter, 1966.
- 30. Richman, J., and F. Thau, "Elements of Kalman Filtering Techniques: Part II -- Applications," General Precision Aerospace Technical News Bulletin, Volume 9, No. 4, 4th Quarter 1966.
- 31. Deutsch, R., Estimation Theory, Prentice-Hall, Englewood Cliffs, New Jersey, 1965.
- 32. Athans, M., and P. L. Falb, Optimal Control, McGraw-Hill Book Co., 1966.
- 33. DeRusso, P. M., R. J. Roy, and C. M. Close, State Variables for Engineers, John Wiley and Sons, New York 1966.
- 34. McRuer, D. T., and R. E. Magdaleno, <u>Human Pilot Dynamics with</u> Various Manipulations, USAF, AFFDL-TR-66-138, December 1966.
- 35. Truxal, J. G., Automatic Feedback Control System Synthesis, McGraw-Hill Book Co., New York, 1955.
- 36. Henrici, P., Elements of Numerical Analysis, John Wiley and Sons, New York, 1964.
- 37. Frame, J. S., "Matrix Functions and Constituent Matrices," IEEE Spectrum, June 1964.
- 38. Hildebrand, F. B., <u>Introduction to Numerical Analysis</u>, McGraw-Hill Book Co., 1956.
- 39. Slack, M., "The Probability Distribution of Sinusoidal Oscillations Combined in Random Noise," <u>Journal IEE</u> (London), Volume 93, Part III, 1945.
- 40. Elkind, J., Characteristics of Simple Manual Control Systems, MIT, Lincoln Laboratory, TR-111, April 1956.
- 41. Wasicko, R. J., D. T. McRuer, and R. E. Magdaleno, <u>Human Pilot</u>
 Dynamic Response in Single-Loop Systems with Compensatory and
 Pursuit Displays, USAF, AFFDL-TR-66-137, December 1966.
- 42. Papoulis, A., The Fourier Integral and Its Applications, McGraw-Hill Book Co., New York, 1962.

- 43. Graham, D., and D. McRuer, Analysis of Nonlinear Control Systems, John Wiley, New York, 1961.
- 44. Bearne, A. C., and A. Kahn, "Describing Functions for Compensatory Tracking of Sine-Waves Plus Noise," Third Annual NASA-University Conference on Manual Control, University of Southern California, Los Angeles, California, March 1-3, 1967.
- 45. Blackman, R. B., and J. W. Tukey, The Measurement of Power Spectra, Dover Publications, New York, 1959.
- 46. Korn, G. A., Random-Process Simulation and Measurements, McGraw-Hill Book Co., New York, 1966.
- 47. Friedland, B., and I. Bernstein, "Estimation of the State of a Nonlinear Process in the Presence of Nongaussian Noise and Disturbances," <u>Journal of the Franklin Institute</u>, Volume 281, No. 6, June 1966.

